Mechanical aspects of biological and biomedical systems

Politecnico di Bari

Department of Mechanics, Mathematics and Management

MECHANICAL AND MANAGEMENT ENGINEERING PH.D. PROGRAM

SSD: ING-IND/14– MECHANICAL DESIGN AND MACHINE CONSTRUCTION

Final Dissertation

Mechanical aspects of biological and biomedical systems

by

Cianci Claudia:

Supervisor:

Prof. Carmine Pappalettere

Coordinator of Ph.D. Program:

Prof. Giuseppe P. Demelio

Course n°32, 12/01/2017-12/01/2020

(*) - Department of Mechanics, Matemathics and Management
(**) - MECHANICAL AND MANAGEMENT ENGINEERING Ph.D. Program
(***) – SSD ING-IND/14 MECHANICAL DESIGN AND MACHINE CONSTRUCTION

Politecnico di Bari

MECHANICAL AND MANAGEMENT ENGINEERING PH.D. PROGRAM

SSD: ING-IND/14– MECHANICAL DESIGN AND MACHINE CONSTRUCTION

Final Dissertation

Mechanical aspects of biological and biomedical systems

---

by

Cianci Claudia :

_____

Referees:

Prof. Andrea Corvi

Prof. Mario Guagliano

Supervisor:

Prof. Carmine Pappalettere

_____

Coordinator of Ph.D Program:

Prof. Giuseppe P. Demelio

_____

Course n°32, 12/01/2017-12/01/2020

(*) - Department of Mechanics, Matemathics and Management
(**) - MECHANICAL AND MANAGEMENT ENGINEERING Ph.D. Program
(***) – SSD ING-IND/14 MECHANICAL DESIGN AND MACHINE CONSTRUCTION

INDEX

INTRODUCTION

The present work of doctoral thesis describes the studies and researches conducted on two different mechanical aspects of biological and biomedical systems, one related to ultrasound therapy effects on cancer cells and the other related to the mechanical properties of orthodontic aligners.

In the first part of this work, the effects of low-intensity ultrasound on cancer cells are presented. Different studies demonstrate that heat, cavitation and hyperthermia induced by ultrasounds can produce antitumor effects. Moreover, several studies report that low-intensity ultrasound therapy has antitumor effects via the induction of apoptosis in several type of cancer cells. Low-intensity ultrasound can play a positive role in cancer therapy by causing membrane damage, affecting the Ca2+/mitochondrial pathway, inducing apoptosis and enhancing the effect of anticancer drugs on cancer cells. In this work, the effects of low intensity ultrasound on two particular cancer cell line are presented: osteosarcoma MG63 and lymphoma U937. MG63 osteosarcoma cells were sonicated at frequencies ranging between 400 and 1.000 kHz for 180 s, using 10 Hz pulse repetition frequency, 50% duty cycle and a constant voltage of 60 V. Results showed that MG-63 cell mortality tends to increase with sonication frequency. Cell behaviour monitoring after sonication showed that the treatment produces some effects on cell proliferation when the ultrasound frequency is equal to 800 kHz. Moreover, cells detached during ultrasound treatment, both for 800 kHz and 1,000 kHz, have a cell proliferation equal to 0 and they are therefore irreversibly damaged or killed by the ultrasound waves. Experiments on U937 cells were performed on the basis of the results obtained from previous tests on this cell line, which were performed by Polytechnic of Bari researchers in collaboration with Fukuoka University. These results showed that sonication at decreasing frequency in a range between 620 and 400 kHz, duty cycle 50%, burst rate 10 Hz, induced 80% cell killing rate after 180 s duration and another 13% apoptosis and 11% late apoptosis after 6-h incubation. Further tests were carried out to evaluate the effects of ultrasound at several fixed frequency. It was found that U937 cells sonication for 180 s at frequency of 1 MHz, duty cycle 50%, burst rate 10 Hz, induces 84% cell killing.

In the second part of this work, the mechanical behaviour of the orthodontic aligners has been investigated. Orthodontic aligners are medical devices able to produce the movement of one or more teeth through a number of steps decided by the orthodontist. In particular, two different aspects of the mechanical behaviour of these devices were considered First, the specific pressures exerted by invisible aligners on teeth, and the precise areas at which these are applied were considered. The

analysis of forces, moments and pressure points has long been of great interest in orthodontics. Hence, a method for measuring the pressure exerted by aligners on the teeth was defined. Intraoral scans were performed on a patient with optimal alignment and levelling before and after 2º vestibularisation of the upper central incisor. Pressure sensor film was placed in a dedicated housing between the aligner and teeth in order to record the pressure exerted after 15 s of aligner application. The images captured by the film were scanned, digitised, and subsequently analysed. Areas and amounts of pressure generated by the aligners were evaluated, and the net force of each area was calculated. The method revealed the areas of contact by which the aligner transmits force on the teeth, and the pressures at which it does so. The pressure exerted by an aligner is not evenly distributed across the entire surface of the tooth during lingual tipping of an upper incisor. The areas of force concentration were not identical, as these are influenced by factors resulting from the manufacturing and casting processes. A second study was conducted to evaluate the dimensional stability of clear aligners after the application of in vivo dynamic stress and in-vitro static stress. Three different aligners made by different materials (PET-G; PET; SmartTrack®) were tested. For each material, three aligner samples were manufactured: one to be used in-vivo, one to be tested in-vitro, and one to be used as a control. To evaluate the effects of the dynamic stress produced in-vivo, each aligner was worn by a single patient 22 hours per day, followed by a wash-out period of two weeks. To evaluate the effects of static stress, each aligner was exposed to the in-vitro continuous force of 50N. The tested and control aligners were scanned, then linear measurements were taken to evaluate their dimensional stability after different types of stresses. PET aligners seem to have the lowest percentage of deformation, while PET-G and SmartTrack® aligners show a reduced deformation going from the posterior to the anterior area. Finally, it was demonstrated that the contact with human saliva induces a greater deformation.

PART 1

ULTRASOUND THERAPY EFFECTS ON CANCER CELLS

1.1 CELL PHYSIOLOGY, DIFFERENTIATED AND TUMOR CELLS

1.1.1 Cell Physiology

Cells are the elementary morphological and physiological unit of all animal and plant organisms. They were observed with a microscope for the first time in 1665 by Hooke, but only in 1839 Schwann announced in his famous publication that all tissues of animal body are composed of cells: "That there is one universal principle of development for the elementary part of organisms, however different, and that this principle is the formation of cells" [1].

Their diameter is generally between 7 and 50 μm, so that only with an optical microscope it is possible to study cells and identify many intracellular organelles. A more accurate study of the fundamental intracellular structures is instead possible with the use of an electron microscope.

It is possible to distinguish between eukaryotic cells, in which the DNA is inside the nucleus enclosed in a membrane, and prokaryotic cells, in which the DNA is free in the cytoplasm, in a region called nucleoid. Moreover, prokaryotic cells are characteristic of unicellular organisms, such as bacteria and archaea, and they have a very simple internal structure compared to eukaryotic cells.

1.1.1.1 Cell structure

Eukaryotic cells present a binary structure: a nucleus surrounded by the cytoplasm. Different types of cells can have different volumes and different shapes, from spherical to polygonal, with or without prolongations. Despite this, eukaryotic cells have many common features.

First, a continuous membrane, called plasma membrane, which controls interactions with the extracellular environment and defends its specificity. Plasma membrane is composed of lipids and proteins. Lipids are principally phospholipids, which present a hydrophilic pole called “head” and a hydrophobic pole called “tail”. In the membrane, the phospholipids are arranged to form a bilayer, in which the heads face outwards while the hydrophobic tails are arranged towards the inside. This layer, at body temperature, is liquid, allowing the movement of phospholipid molecules and membrane

protein. The other principal lipid component, cholesterol, regulates the degree of the fluidity of the different membranes. About proteins, they are partly integral proteins, which penetrate and cross the whole membrane, and partly peripheral proteins, which are adherent to the surface. Generally, the integral protein molecules protrude with respect to the two surfaces of the membrane and, as they are usually hydrophilic and electrically charged, they allow binding of peripheral proteins. Other fundamental properties of membranes are the asymmetry, due to the diversity of the phospholipids and the portions of the membrane proteins in the two surfaces, and the electric charge, which is negative on the inner side.

The plasma membrane allows signals exchange, so that cells can operate in a coordinated manner. Cells can respond to stimulations and transfer signals along the membrane in a very short time, even at a considerable distance from the stimulus site. This is possible thanks to the variations of the electrical potential, which activate signal and allow the ionic flows through temporary protein pores. In addition to these channels and receptors, the plasma membrane presents pumps and transporters. The coordinated action of all these proteins allows the cell to establish an appropriate microenvironment in the cytosol and to acquire important metabolites, such as glucose, amino acids, etc. Another important feature of the plasma membrane is its ability to integrate into a tissue and establish interactions with the extracellular matrix. This is possible thanks to the presence in the plasma membrane of various families of binding proteins, such as integrin.

Cells develop different junction systems at the level of their plasma membrane according to specific functional needs. The gap junctions are composed of numerous channels of high permeability, which allow the intercellular passage of ions and other messengers directly from one cell to another. The tight junctions are made of protein molecules exposed to the surface and welded between two adjacent cells in order to form the walls of the lumen of the hollow organs. Finally, the desmosomes, or adherent junctions, allow to establish a functional continuity between the cytoskeleton of adjacent cells, in order to realize intercellular mechanical connections.

The plasma membrane presents structures assigned to the movement, such as cilia and flagella, which protrude on the surface of the cell and are closely connected with the cytoskeleton.

Another important characteristic of eukaryotic cells is the presence of a nucleus. This is often located towards the centre of the cell and presents a nuclear envelope, consisting of two membranes: the first is covered with ribosomes and in continuity with the endoplasmic reticulum; the second adheres closely to the nuclear lamina, a structure of filamentous proteins disposed all around the nuclear content. The nuclear envelope is covered by pores, which allow the passage of macromolecules.

In each species, the number of DNA molecules present in the nucleus is fixed and it corresponds to the number of chromosomes. Inside the nucleus, DNA molecules interact closely with specific basic proteins, histones, giving rise to a structure composed of nucleosomes. This structure, folding in on itself, forms the chromatin.

Inside the nucleus, there is also a filamentous and granular area, called nucleolus and rich of RNA, where the ribosomes are synthesized and assembled.
The fundamental activities that take place in the nucleus are two: the duplication of DNA before the mitosis, and the transcription of the genetic information from the DNA to the RNA, used outside the nucleus for protein synthesis. The transcription process is regulated by specific factors, which can be modulated by messages generated at the level of the receptors in the plasma membrane. The intra-nuclear environment shares with the cytosol different characteristics, such as pH, ion distribution, small metabolites and proteins, while other characteristic may differ in certain phases of cellular life.

Inside the plasma membrane, there is the cytosol, in which the nucleus, endocellular organelles and the cytoskeleton are immersed. The cytosol represents the operative compartment of cellular life. For example, signals of growth or differentiation, which originate from specific receptors of the membrane, are transferred along chains of intracellular enzymes, in order to reach the nucleus and modify the functioning of specific transcription systems.
The coordination between various cell functions is guaranteed and it can be modified according to the physiological conditions. Phosphorylation is the reaction that regulates the functioning of innumerable cytosolic enzymes and substrates. Many protein-kinases and protein-phosphatases are regulated by messengers received at the level of plasma membrane. Another fundamental role is recognized to the Ca2+ ion, which acts both through the activation of protein-kinase and protein-phosphatase Ca2 +-dependent, binding itself directly to specific proteins.
In particular conditions, cytosolic micro areas with a high concentration of Ca2 + can be generated locally. These conditions make it possible to carry out processes that require high concentrations of Ca2 + and also rhythmic processes (oscillations) or oriented processes (waves) with a high concentration of Ca2 +.
Finally, another characteristic of the cytosol is the presence of ribosome complexes (polyribosomes) deputed to the synthesis of proteins, which are destined to cytosol, nucleus and, partly, also to the organelles.

Cells presents also a cytoskeleton, made up of filamentous structures and organized according to the specialization, the area and the functional moment of the cell. The three components of the cytoskeleton are:

- Contractile cytoskeleton, which represents the main property of muscular cells, but it is also present in different non-muscular cells. In order to have a contraction, the co-expression of actin and myosin, both filamentous, is required. The characteristic of this cytoskeleton is their organization, in which the actin forms thin filaments that surround the thick filament of myosin. The basic process of contraction is the filament slippage, which takes energy from the ATP released by myosin, which has ATPase activity. This activity is induced by the increase of Ca2 + in the cytosol caused by cellular stimulation.
- Microtubules are structures made from the polymerization of globular proteins, the tubulins. Microtubules radiate in an orderly way starting from the perinuclear site, called centrosome. The microtubules are similar to rails on which the organelles are quickly transported. The role of microtubules is fundamental also for the functioning of surface structures that ensure motility to the cell.
- Intermediate filaments, which are, rom a structural and functional point of view, simpler than the other components of the cytoskeleton. The basic protein of intermediate filaments is not always the same: depending on the cell type, there are four types, all filamentous and resistant both mechanically and metabolic. The most well-known constituent of intermediate filaments is keratin, specific for epithelial cells.

The various components of the cytoskeleton described above do not function independently but in a coordinated manner. It is possible to think to the cytoplasm as a complex three-dimensional network of protein filaments, whose general organization depends on microtubules. In this context, actin filaments have a particularly dynamic role and intermediate filaments play a mechanical role. The interaction between the various cytoskeletal components determine the cell shape and its plasticity.

The cytoplasm contains different organelles, which works in coordination, giving rise to functional pathways, such as the exocytic and endocytic pathways.

Mitochondria are a different type of organelles, also called “semi-autonomous organelles”, as they possess a whole genetic heritage, complete of a system of expression. A double membrane surrounds them: the external one, of presumed cellular origin, delimits a first compartment; the inner one, of bacterial origin, delimits the wider internal compartment called matrix. Mitochondria employs, for its functioning, substances that come from the cytosol. The enzymes of the matrix are able to subtract electrons from these substances, transferring them to other enzymes, responsible for the electron

transport chain. The energy loss that occurs through four stages of “electron leap” is used to expel H+ from the mitochondria. In this way, an electrochemical gradient is created between the inner membrane and the cytosol. For the loss of H+ the membrane becomes electronegative and the matrix becomes alkaline. These conditions allow the return of H+, making energy available for the functioning of an ATP-synthesise. The system is extraordinarily well built and only a little part of the energy is dispersed in heat. Through mitochondria, cell synthesizes large amounts of ATP, which represents the main sources of energy for them.

There is also a group of organelles which takes part to the exocytotic pathway, first of all the Endoplasmic Reticulum (ER). It consists of a large endomembrane system composed by cisterns and tubules. The cisterns are covered with ribosome complexes and tubules, which realize the granular and smooth reticulum respectively. The presence of polysomes clearly indicates that protein synthesis take place in this reticulum. The endoplasmic reticulum also performs other important functions: among these, the phospholipid synthesis and the rapid exchange Ca2+ accumulation.

The exocytic path continues with the Golgi apparatus. It is composed by 3 or 5 tanks, connected by the transgolgian network, composed of tubules. The role of the Golgi apparatus is to modify the proteins coming from the reticulum through conjugation with sugars (glycosylation), or with phosphate residues (phosphorylation) or sulphate. The multiplicity of tanks allows the development of numerous events connected, for example, with glycosylation. At this point lysosomal enzymes are transported to vesicles and finally reach lysosomes, while the remaining material is divided between granules and vesicles responsible for regulated and not regulated secretion. In the transgolgian network of many cells, moreover, the pH of the lumen becomes more acidic, thus leading to the aggregation of proteins secreted. This mechanism allows the cell to accumulate the products of its own secretion, while it is possible to interrupt the exocytosis with an external signal. Other non-condensed proteins travel in vesicles, which merge through the plasma membrane in an unregulated way. The secretion of these proteins occurs continuously and not in pulses, as it happens instead for the hormones or other enzymes.

The endocytosis is the formation of vesicles that detach from the plasma membrane and then return to the cytoplasm. A very complex membrane path allow the formation of vesicles, whose purpose is not only to preserve the appropriate size of the plasma membrane, but also to maintain its original composition. For this reason, receptors activated by the specific ligands are subjected to the “acid washing” of the membranes, which determines the detachment of the stimulators from the receptors, which are internalized in the endosomes. After the formation of endosomes, these can follow two

pathways: some vesicles merge with the tubules of the Transgolgian network and therefore fall into the exocytotic path; others become even more acidic and merge with lysosomes.
Lysosomes are the organelles responsible for intracellular digestion thanks to fifty different enzymes capable of attacking proteins, lipids, sugars, etc. The digestive activity of lysosomes maintains the right dimension in terms of volume, surface ratio, and composition.

1.1.1.2 Cell Proliferation

Cell cycle begins with a phase called G0, defined as a quiescence phase. After stimulation by growing factors, cell moves to G1 phase, during which it prepares to double its DNA (phase S). After a further preparatory period (G2), cell starts the redistribution of one cell's living material into two cells (phase M, Mitosis). The purpose of this last phase is a precisely and egalitarian redistribution, which allows both resulting cells to be alive and active.
Traditionally, mitosis consists of six phases, detectable by microscopic investigation. Before the mitosis, the DNA is scattered in the nucleus and the microtubules are arranged geometrically in the cell starting from the centrosome. In the prophase, the chromatin condenses to start chromosome formation, each containing its single doubled DNA molecule. At the same time, in the cytoplasm there is a doubling of the centrosome and migration of the two resulting centrosomes to the cell poles, forming the spindle.
The following phases consists first in the disintegration of the nuclear envelope, accompanied by those of the endoplasmic reticulum and the Golgi apparatus, and the formation of numerous groups of vesicles dispersed throughout the whole cell (prometaphase). Subsequently, each chromosome attaches itself to a group of microtubules of the spindle. In this phase (metaphase), the chromosomes migrates to the cell's equator and are arranged so that the chromatids produced by the doubling of the DNA are oriented towards a pole. The loss of the bond between the chromatids initiates their migration towards the two centrosomes (anaphase). Finally, when all chromatids reach the two centrosomes, a nuclear envelope begins to reform around the two clusters of DNA, while the cytoplasmic organelles begin to reorganize themselves in the cytoplasm (telophase). These processes are followed by the separation of the two cells (cytodieresis), which generally occurs at the level of the equatorial zone, where an actin ring is formed just below the plasma membrane. The regulation of the processes described seems to depend on protein synthesis, which are able to control the functioning of specific protein-kinases and therefore the phosphorylation of important substrates.

1.1.1.3 Cell death: apoptosis and lysis

Cell death can be classified into two distinct categories, accidental cell death (ACD) and regulated cell death (RCD). Accidental cell death can be caused by severe mechanical, physical, or chemical factors such as high temperature. Regulated cell death, on the other hand, refers to multiple genetically encoded pathways, which starts to maintain cell homeostasis. It includes a subtype called programmed cell death (PCD).

In the past, apoptosis was classified as a programmed cell death, while necrosis was classified as an occasional death, based on morphologic changes. Modern classifications also include molecular and biochemical measures to determine the functional aspects of cell death.
Apoptosis depends on the activation of several cysteine proteases belonging to the caspase family [2]. There are several pathways to apoptosis-associated caspase activation, while some proteins, such as BCL-2 proto-oncogene, can inhibit apoptotic process. When the apoptosis process starts, the cell passes through a series of modifications. The condensation and extensive hydrolysis of DNA and the condensation and progressive fragmentation of the cytoplasm take place. Fragments are rapidly phagocytosed by adjacent cells, with rapid lysosomal digestion of the molecules and reuse of the basic components for synthetic purposes. The process is rapid and ends up leaving no trace.
Necrosis is characterized by cytoplasmic granulation, cellular swelling plasma membrane rupture and cytosol leakage. Necrosis has long been described as a process which starts when lesions of any kind (physical, chemical, traumatic, etc.) take place. Nowadays it is known that necrosis can exist as a highly regulated and genetically directed process. Over the past 10 years, a number of regulated necrosis pathways have been described. One of the most important is necroptosis, a caspase-independent form of regulated necrosis that is dependent on receptor-interacting protein 1 (RIPK1) and RIPK3 activity. It can be triggered by the ligation of death receptors in the presence of caspase inhibition, as well as by members of the PRR family, which are expressed by cells of the innate immune system to sense pathogen associated molecular patterns (PAMPs). Other forms of regulated necrosis occur independently of RIPK1 or RIPK3 or occur in the presence of RIPK1 or RIPK3 inhibitors. They represent various forms of genetically controlled cell death, which presents a period of oncosis, occurring in different physiologic conditions or cell types.

A damaged cell can repair itself, first by stopping the loss of cytoplasm, and then regenerate by rebuilding structures that were damaged or lost. Knowledge of how single cells repair and regenerate themselves could guide treatments for conditions involving cellular damage.

Tang et al. [3] distinguish wound healing from regeneration as two aspects of self-repair that serve distinct purposes. Regeneration is the process by which the cell specifically rebuilds and replaces the missing components (organelles, plasma membrane, cytoplasm, etc.) after the wound has been stabilized. as two aspects of self-repair that serve distinct purposes. Wound healing is the process that stops loss of material, while regeneration is the process by which the cell specifically rebuilds and replaces the missing components after the wound has been stabilized. Some cells can heal wounds but cannot regenerate. Dividing cells might not need an active regeneration mechanism, because as the cells proliferate, they will build new structures during normal growth.

Ca2+ is necessary to trigger a wound response, composed by two complementary mechanisms:

- the fusion of vesicles with the membrane to patch the wound, induced through a range of processes, including exocytosis, endocytosis.
- actomyosin purse string around the wound creates a contraction, which brings intact membrane and underlying cortical cytoskeleton to close the wound.

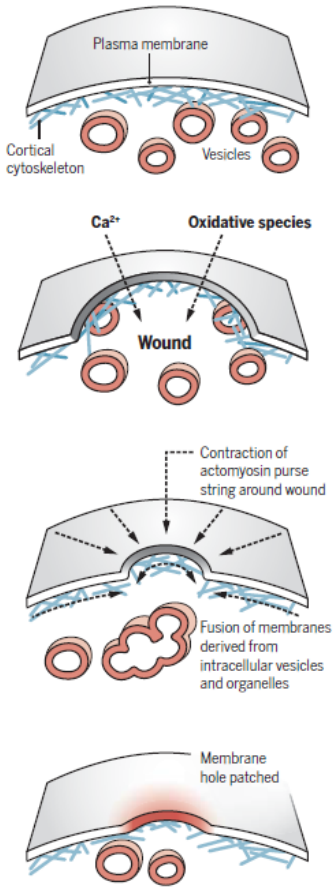

Figure 1.1.1. Representation of wound repair process.

1.1.2 Cell differentiation and neoplastic transformation

Cell differentiation consists of a large number of closely coordinated phenomena, controlled at molecular level by gene expression processes, through which a specialized phenotype is acquired by a cell. Streuli [4] found that the process is regulated by signals from the extracellular environment. Cell behaviour is affected not only by growth factors, but also by other signals such as locally acting molecules within the ExtraCellular Matrix (ECM), as well as molecules in adjacent cells. The ECM can affect cell behaviour in two different way: harbouring growth factors or growth factor-binding proteins; through receptor-mediated signalling or by modulating the cellular response to growth factors. For example, ligation of integrin affects cellular response to mitogenic signals, indicating that cell–matrix interactions are an important determinant in the regulation of cell cycle entry. Different ECM components can affect many types of signal transduction pathways, including those leading to suppression of apoptosis and to differentiation. For this reason, every event altering the composition or structure of the ECM, for example through remodelling enzymes, can have profound effects on cellular differentiation. ECM remodelling is a process in which a large number of enzymes are involved. These include tissue serine proteases and the large family of matrix metalloproteinase (MMPs). These enzymes act as broad-spectrum proteases for major ECM degradation events that occur during tissue remodelling. In addition, these enzymes cleave specific ECM proteins at unique sites, altering interactions either with sequestered growth factors or with cell surface signalling receptors.

In this context, the ECM become a powerful resource for controlling cell phenotype. The positional data contained within ECM is vital for differentiate decisions and normal cellular homeostasis, while inappropriate alterations in both its structure and information content lead to disease states such as neoplasia.

Tumorigenesis in humans is a multistep process, where each step reflects genetic alterations that drive the progressive transformation of normal human cells into highly malignant derivatives. In particular, oncogene is a gene that can induce cell transformation [4]. When DNA from transformed cells is introduced into normal cells, the recipient cells could be induced to undergo transformation. Pathological analyses reveal that lesions on organs represent the intermediate steps in a process through which cells evolve from normalcy via a series of pre- and malignant states into invasive cancers. Moreover, there are more than 100 different types of cancer, and subtypes of tumours can be found within specific organs.

Hanahan et al. [6] suggests that the vast catalogue of cancer cell genotypes is a manifestation of six essential alterations in cell physiology that collectively dictate malignant growth: self-sufficiency in growth signals, insensitivity to growth-inhibitory (antigrowth) signals, evasion of programmed cell death (apoptosis), limitless replicative potential, sustained angiogenesis, and tissue invasion and metastasis.

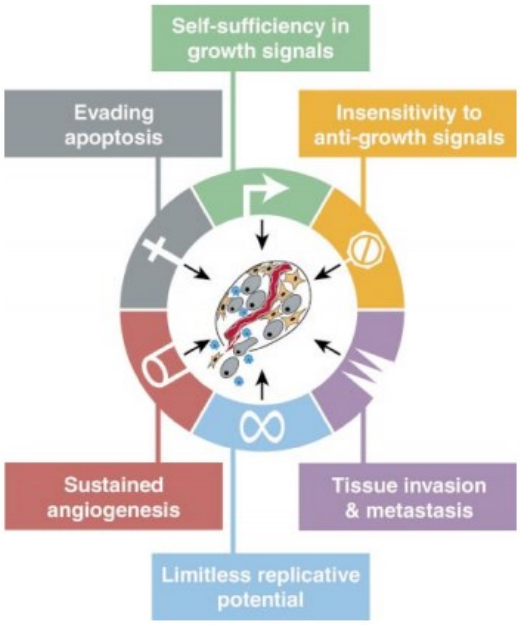

Figure 1.1.2. Representation of the alterations in cell physiology.

Tumors can be classified, according to their origin, in 4 different types:

1. Epithelial tumors (carcinomas) are the most common forms of human cancer that originate in the layer of cells (the epithelium) lining a cavity or a duct. Cancers occurring in epithelia that form protective cell layers are squamous cell carcinomas (which occur in different types of organs, including the skin, esophagus, prostate, lungs and cervix), and those originating in secretory epithelia (e.g. in glands) are adenocarcinomas;
2. Mesenchymal tumors (sarcomas) originate in mesenchymal cells. Sarcomas occur in connective or supportive tissue (bone, cartilage, muscle, and fat) and soft tissue;
3. Hematopoietic tumors originate in the immune and circulatory systems. They involve myeloid and lymphatic tissues that comprise blood-forming cells;
4. Neuroectodermal tumors are found in components of the nervous system.

As all tumors take place from a genetic alteration, the precise nature of these mutations and the cell types in which they take place must be the determinants of each individual type of cancer. Luzzatto [7] suggests considering three different aspects:

- the number of mutations required to convert a normal cell into a cancer cell. There are cells belonging to lesions who have undergone one or more somatic mutations, but short of the total number required to give cancer. Luzzatto suggests that the number of mutations (n) could be the same for all tumours and it may range from 2 to 5.
- the specific genes in which the mutations occur. if we attempt to classify the kinds of genes which, when mutated, contribute to cause cancer, we find the following list: (a) genes encoding growth factors and growth factor receptors; (b) genes participating in signal transduction and otherwise in the cell cycle; (c) transcription-controlling genes and other genes encoding nuclear proteins; (d) genes involved in DNA repair and in chromosomal replication, mitotic segregation and telomere maintenance; (e) genes responsible for triggering apoptosis of abnormal cells; (f) genes involved in interactions of cells with the extracellular matrix and blood vessels
- the nature of the mutations themselves. Mutation could be associated with a failure of differentiation, which can be regarded as a loss of function, a failure of controls on proliferation and a loss of function of a tumour suppressor gene.

An important topic to study is that malignant transformation in cells changes their mechanical properties. The mechanical properties of cells, such as stiffness, nonlinearity, anisotropy, the dynamic reorganization of the cytoskeleton and changes in cell morphology, motility, adhesion and invasion have been extensively studied in the last few decades, providing insight into the biological characteristics of cells.

In particular, cell stiffness can be determined by micropipette aspiration, optical tweezers, particle-tracking micro rheology, and atomic force microscopy (AFM). AFM is an instrument with a flexible cantilever that behaves like a spring, so that any force acting on the AFM causes the cantilever to deflect. For the detection of stiffness, the tip of the cantilever is pushed into the cell surface, recording the indentation depth and the deflection of the cantilever.

Cross et al. [8] studied changes in cell elasticity, using these changes as an indication of disease. They found a reduction in stiffness with increasing metastatic efficiency in human cancer cell lines using several different in vitro biomechanical assays. They measured stiffness using an atomic force microscopy (AFM). In particular, Cross et al. measured the nanomechanical of metastatic

adenocarcinoma cells and benign mesothelial cells in pleural effusions obtained from body cavity fluid samples collected from patients with suspected metastatic adenocarcinoma, using standard protocols. Data clearly showed that cell stiffness of metastatic cancer cells is > 70% lower than normal reactive mesothelial cells in the same sample, when compared to other pleural effusions, or even for patients with different clinical histories.

Xu et al. [9] studied the mechanical properties of cells from several different ovarian cancer cell lines and non-malignant immortalized ovarian surface epithelial cells (IOSE). They demonstrated that cell stiffness allows to distinguish ovarian cancer cells from non-malignant cells, but also to distinguish more tumorigenic/invasive cancer cells from less tumorigenic/invasive types.
The reduction of stiffness, when a cell transforms from non-malignant to cancerous state, is explained by the change in cytoskeletal structure from an organized to an irregular network.
It is important to notice that AFM-determined Young's modulus is greatly affected by the characteristics of the cytoskeleton, as well as the procedures and parameters used in detection. Luo et al. [10] investigated the role of cytoskeleton in determining cell motility and stiffness, analysing the contribution made by the polymerization of actin filaments, and by the microtubules, the stiffest polymers of the cytoskeleton.

1.1.3 Cancer treatment

It is possible to distinguish between traditional cancer treatment and innovative cancer treatment [11]. Both will be briefly described in the following paragraphs.

1.1.3.1 Traditional cancer treatments

There are different types of cancer treatment, each of them is chosen based on the type of tumour to be treated. Moreover, a treatment can be used alone or combined with others. The most used cancer treatments are:

- Surgery, the procedure in which a surgeon physically removes cancer.
- Radiation therapy, a type of cancer treatment that uses high doses of radiation to kill cancer cells and shrink tumours.
- Chemotherapy, which uses drugs to kill cancer cells.
- Immunotherapy, a type of cancer treatment that helps your immune system fight cancer.

- Targeted therapy, which targets the changes in cancer cells that help them grow, divide, and spread.
- Hormone therapy, a treatment that slows or stops the growth of breast and prostate cancers that use hormones to grow.
- Precision medicine, which helps doctors to select treatments that are most likely to help patients based on a genetic understanding of their disease.

1.1.3.2 Innovative cancer treatments

There are also different types of cancer treatments, which use non-invasive approaches. These treatments can potentially avoid infections and scar formation associated with surgery, as well as minimizes effects of chemotherapeutic drugs.

Non-invasive cancer treatments typically use various physical stimuli such as light, heat, magnetic field, electrical field, ultrasound [12]. Between these, some of the most interesting treatment are indicated below.

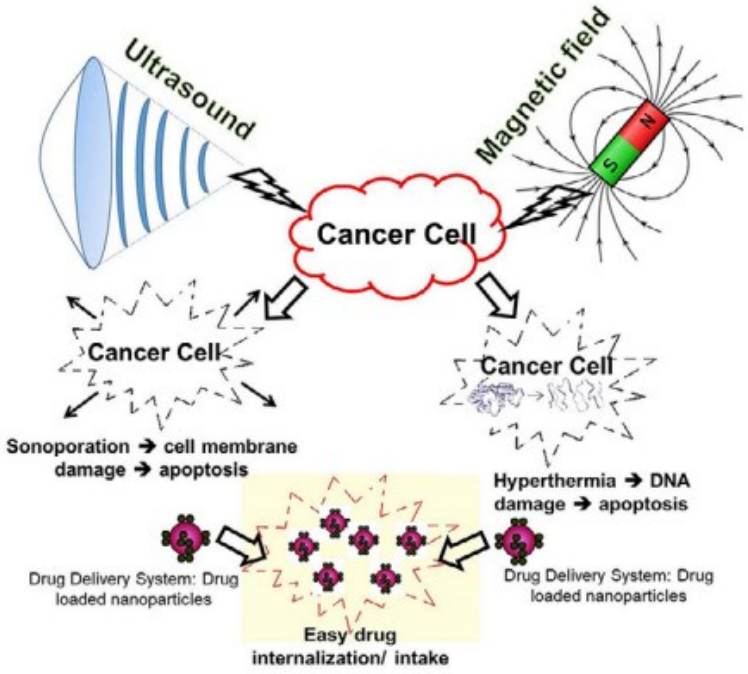

Figure 1.1.3. Representation of the major non-invasive cancer treatments.

Sound therapy

Sound Therapy is the treatment based on the theory that cells respond to sound frequencies by changing their physical characteristics, and the hypothesis that sick cells can be healed or harmonized by sound. This therapy was developed by French musician Fabien Maman. He conducted some biology experiments in the early 80s at the University of Jussieu in Paris, showing the impacts of acoustic sound on human cells and their energy fields. He found that through a series of acoustic sounds, cancer cells would explode and healthy cells would become energized and empowered.

In his book "Music heals" Maman [13] reported the experiments he carried out on HeLa cells. He subjected these cells to different sounds and to human voice. Sound was produced at a distance of 30 cm with an amplitude between 30 and 40 decibels.

The effects determined on the cell structure were monitored with electrophotography (Kirlian photography) to record changes in electromagnetic fields. Cells were photographed each minute for 21 minutes with and without sound.

In the following figure it is possible to see a sequence of photographs respectively of cells without sound stimulation and cells subjected to a gong sound. While cells, in absence of sound, tend to expand in an attempt to adhere, in presence of the sound of the gong their plasma membrane begins to lose its own structure.

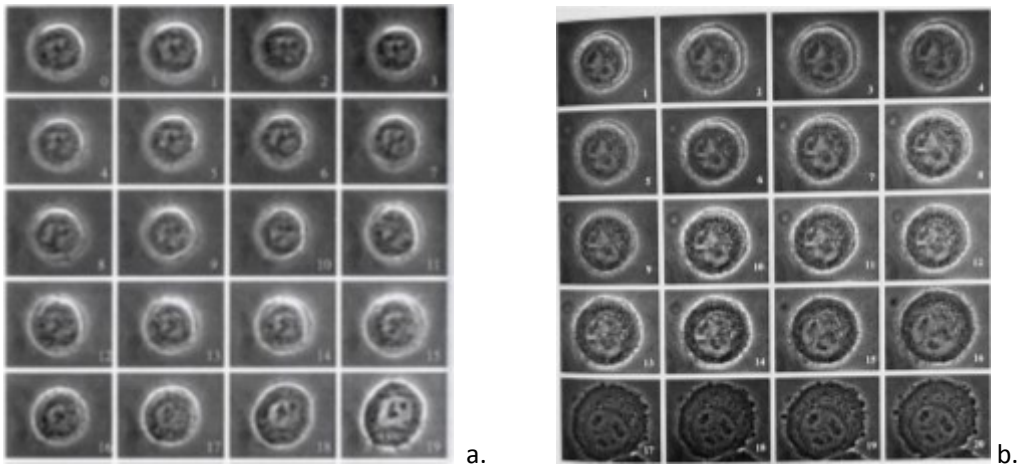

Figure 1.1.4. Sequence of photographs of cells without sound stimulation (a) and cells subjected to a gong sound (b).

Maman also observed that, when two cells are exposed to notes "La" and "Si", produced by an acoustic guitar, the oldest one is the most affected by the effect of the sound. In particular the oldest cell progressive increase in size and, at the end of the experiment, has a surface equal to about twice the youngest cell, being close to explosion induced by the sound.

Figure 1.1.5. Sequence of photographs of two cells are exposed to notes "La" and "Si", produced by an acoustic guitar

After these experiments, Maman discoverded that it is possible to completely destroy the cell structure by applying an harmonic scale of sounds and increasing the exposure time.

Finally, he found that, after a time of sound exposure which depends on the phase of cell mitosis and which can vary between 9 and 21 minutes, cell structure becomes destabilizing and it progressively disintegrate. At the end of the treatment, cells resonate until they explode.

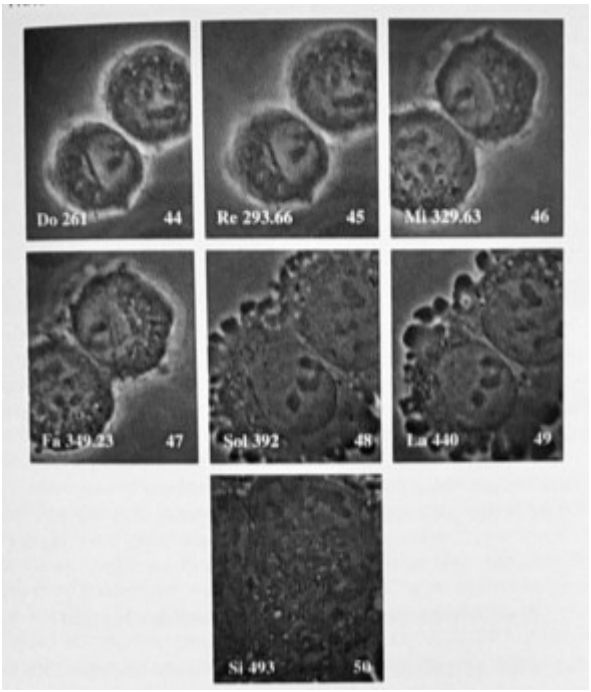

Figure 1.1.6. Sequence of photographs of two cells subjected to a harmonic scale of sounds.

Magnetic fields

Magnetic fields are widely being used to induce detoxification effect, enhanced metabolism, to promote repair and healing, to stimulate collagen density in and around the joints, and help to trigger Ca2+ flow to the defect site resulting in faster bone healing.

In particular, Static Magnetic Field (SMF) seems to have anti-inflammatory effects at molecular level, controlling secretion of pro-inflammatory cytokines (IL-6, IL8, and TNF-a) and enhanced anti-inflammatory cytokines production (IL-10). Since inflammation is closely linked to cancer, the SMF exposure could be a potential cancer therapy. It is possible to induce small electric currents by Alternating Magnetic Fields (AMF)/Pulsed Magnetic Fields (PMF) in conducting tissues. These currents can generate excessive heat in the tissues and cause thermal damage at very high frequencies or amplitudes, while at extremely low frequencies (0–300 Hz) and very low frequencies (300–100,000 Hz) the tissue heating is negligible, and the induced currents can stimulate electrically excitable cells for their treatment.

The effects of magnetic fields on cancer cells depends on thermic effect, cavitation effect, and non-thermic/non-cavitation effect.

Magnetic fields can also decrease Vascular Endothelial Growth Factor (VEGF) level and therefore reduces the growth and migration of cancer cells to other parts of the body.

PMF can provoke localized hyperthermia in the tissues where magnetic nanoparticles have been accumulated. Extremely low frequency PMF also inhibit murine malignant tumour growth by arresting neoangiogenesis.

Also SMF induces the damage of cancer cellular membrane ion channels followed by apoptosis and the production of reactive oxygen species (ROS), which inhibit cells growth and proliferation. In particular, the use of SMF between 200 and 2000 mT on various cancer cells increases apoptotic rate via altering gene expression of bcl-2, bax, p53 and hsp70 in isolated human lymphocytes. These altered gene expressions control the influx of Ca2+ towards cellular compartment by altering membrane permeability. Moderate intensity of SMF (8.8 mT exposed for 12 h) on K562 cells (human chronic myelogenous leukaemia) affect their metabolic activity, cell cycle distribution, and it induce DNA damage and P-glycoprotein (P-gp) expression.

Hyperthermia generated by alternating magnetic fields (AMF) also inhibits cancer cell proliferation and enhances the treatment efficiency by easy internalization of drugs.

Pulsed electromagnetic field (PEMF) treatment also appears to have strong application potential. An interesting in vitro study realised by Crocetti et al. [14] evaluated selectivity of ultra-low intensity and frequency pulsed electromagnetic fields (PEMF) treatment on human breast adenocarcinoma cells (MCF7). MCF7 cells and normal breast epithelial cells (MCF10) were treated with 20 Hz PMF having 3 mT intensity for 30, 60, and 90 min/day up to 3 days. In vitro analysis showed that MCF7 cells are highly reactive to 3 mT flux density in terms of apoptosis and cell electrical properties, while normal cells (MCF10) are unaffected.

Ultrasound

Ultrasound are widely used for diagnostics and for different types of treatments. Their effects depend on the interaction of acoustic waves with biological soft tissues through thermal and non-thermal physical mechanisms. Thermal effects originate from conversion of acoustic energy into heat. When US interacts with biological tissue starts to oscillate and rise its temperature, which can be used to achieve hyperthermia and treat cancer as in the case of HIFU.

Recently, low-intensity ultrasound has been studied with the aim of identifying a new cancer treatment. The sonication parameters are 1.0–2.0 MHz frequency and 0.5–3.0Wcm2 intensity. With these parameters it is possible to generate inertial cavitation inside the tumour: the rapid production and collapse of microbubbles produce mechanical shock waves, free radicals and apoptotic initiators, which inhibit cancer cell growth.

The effects of high and low intensity ultrasounds will be discussed in more detail in the next chapter.

1.1.4 Laboratory treatment of cell cultures

In the 1950s the first cell line, HeLa, was successfully cultured from a human cervical cancer and in the mid-1980s a reproducible culture of mammalian cells has been achieved. The development of cell culture led to new experimental approaches and allowed direct manipulations of the environment and measurement of the resulting changes in the function of a single cell type [15].

It is possible to initiate a culture from cells, tissues, or organs taken directly from an animal and treated as an explant culture known as primary culture. These cultures can passage for a finite number of population doublings before senescence occurs, but usually the number of doublings is limited. After a certain number of doublings, a cell line can die out or it can transform to become a continuous cell line.

Cell cultures in vitro can grow in suspension or attached to the surface of the flask. as an adherent monolayer. Cell culture medium must mimic the physiological conditions within tissues. Moreover, in vitro growth of cell lines requires a sterile environment in which all the nutrients for cellular metabolism can be provided in a readily accessible form at the optimal pH and temperature for growth.

Cell culture media essentially consist of several factors required for cells growing, including amino acids, lipids, vitamins, and cofactors. Other essential components include inorganic salts, which provide buffering capacity and osmotic balance to counteract the effects of carbon dioxide and lactic acid produced during cellular metabolism. Media formulations vary in complexity and have been developed to support different cell types, including Eagle's minimum essential medium (MEM), Dulbecco's modified Eagle's medium (DMEM), RPMI 1640, and Ham's F12. Cell lines may require the addition of serum to the culture medium to stimulate growth and cell division. The most common source is bovine and this may be of adult, new born, or foetal origin.

A cell culture laboratory needs the following instruments:

- Class II downflow recirculating laminar flow cabinet;
- CO2 incubator;
- Inverted microscope with phase-contrast capabilities;
- Low-speed biological centrifuge;

- Refrigeration and freezing facilities;
- Cell storage (liquid nitrogen) facilities.

Prevention of contamination by bacteria, fungi (especially yeast), mycoplasma, or viruses is necessary in cell culture.

1.2 MEDICAL APPLICATION OF ULTRASOUND

1.2.1 Ultrasound description

Ultrasounds are sound waves with frequencies higher than 20 kHz, which represents the audibility limit. As they cover an extensive range of frequencies (from 20 kHz up to several gigahertz), they present diversified phenomena and effects which affect various disciplinary areas [16]. The most important parameters to define ultrasound are:

- Frequency (f), the number of times the wave oscillates through a cycle each second (sec) (Hertz: Hz or cycles/sec);
- Period (t), the time duration of one wave cycle (t = 1/f);
- Speed of sound (c), the distance travelled by the wave per unit time and is equal to the wavelength divided by the period. Speed of sound is dependent on the propagation medium and varies widely in different materials. A highly compressible medium, such as air, has a low speed of sound, while a less compressible medium such as bone has a higher speed of sound. It turns out that interface between two media causes a change in speed of sound and so in wavelength.
- Amplitude of a wave, which is the size of the wave displacement. Larger amplitudes of vibration produce denser compression bands and, hence, higher intensities of sound.
- Intensity of ultrasound is the amount of power (energy per unit time) per unit area proportional to the square of the pressure amplitude (milliwatts/cm2).

Ultrasound interactions are determined by the acoustic properties of matter. As ultrasound energy propagates through a medium, interactions that occur include reflection, refraction, scattering and absorption (attenuation) [17]. Acoustic Impedance (Z) is equal to the product of density of the material, measured in kg/m^3, and the speed of sound of the material in which ultrasound travels, measured in m/sec. Air has a low value of Z, while bone and metal have high values. Large differences in Z at the interface between two materials cause reflection, while small differences allow transmission of sound energy. The differences of acoustic impedance values at an interface determines the amount of energy reflected at the interface. Refraction is the change in direction of an ultrasound beam when passing from one medium to another with a different acoustic velocity.

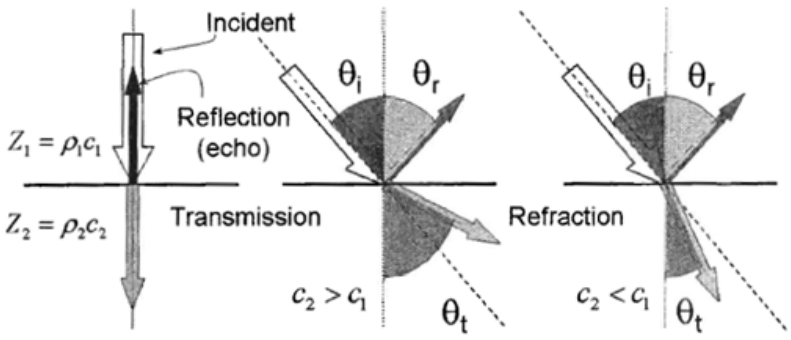

Figure 1.2.1. Reflection, transmission and refraction of an ultrasound wave.

Acoustic scattering happens when materials are about the size of the wavelength of the incident beam, and it represents a non-specular reflector surface. As frequency increases, the non-specular (diffuse scatter) interactions increase, resulting in an increased attenuation and loss of intensity.

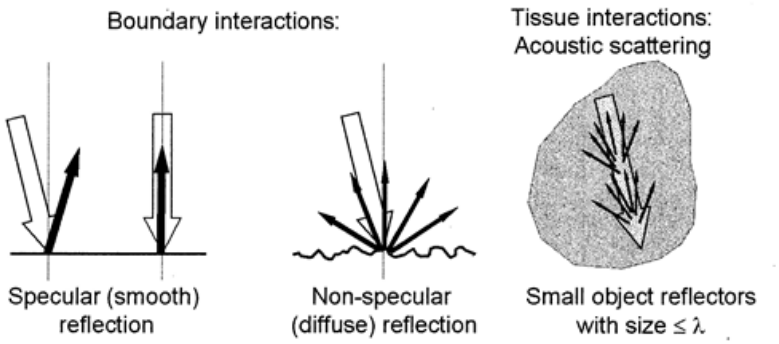

Figure 1.2.2 Representation of different interaction of an ultrasound wave.

Finally, ultrasound attenuation represents the loss of energy with distance travelled and it is caused principally by scattering and material absorption of the incident beam. The intensity loss per unit distance (dB/cm) is the attenuation coefficient, which is directly proportional to the frequency and also dependent from the medium.

A transducer is a device which can convert one form of energy into another. Piezoelectric transducers convert electrical energy into ultrasonic energy and vice versa. It is composed by different parts, as shown in the following figure.

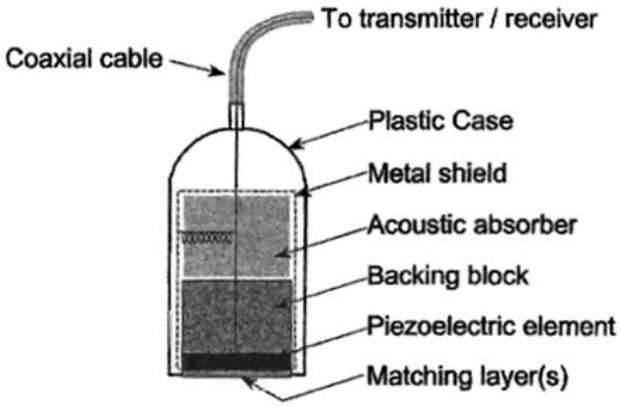

Figure 1.2.3 Schematic representation of a transducer.

The electrical energy, produced by a pulse generator and sent to the ultrasound transducer by a transmitter, causes the piezoelectric crystal to momentarily change of shape (expand and contract depending on current direction). This change in shape of the crystal increases and decreases the pressure in front of the transducer, thus producing ultrasound waves. When the crystal is subjected to pressure changes by the returning ultrasound echoes, the pressure changes are converted back into electrical energy signals. Return voltage signals are transferred from the receiver to a computer to create an ultrasound image.

Transducers are made of piezoelectric materials, chosen to have a particular type of propagation in the materials. After an initial period in which quartz was the most used material for the generation and reception of ultrasound, the use of piezoelectric ceramics has gradually spread, together with the use of other piezoelectric materials with high transduction efficiency, such as lithium niobite, aluminium nitride and some oxides, tellurium and zinc.

The thickness of a piezoelectric crystal determines the resonant frequency of the transducer, which is equal to half the wavelength of emitted sound in the crystal compound.

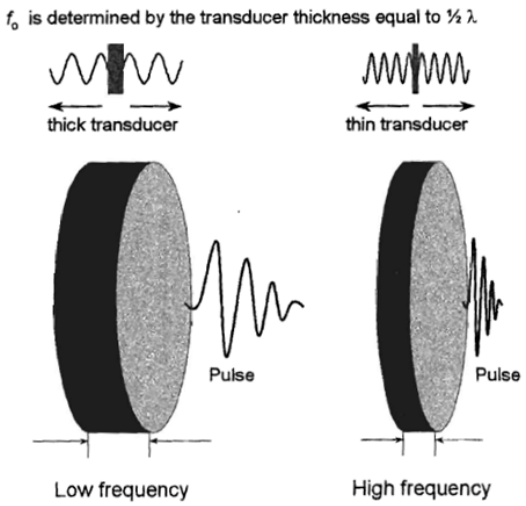

Figure 1.2.4. Influence of the transducer thickness on frequency.

Another important element of a transducer is the damping block, which absorbs the backward directed ultrasound energy and dampens the transducer vibration to create an ultrasound pulse with a short spatial pulse length, which is necessary to preserve detail along the beam axial resolution.

The Q factor determines the purity of the sound and length of time the sound persists. It is equal to the ratio between the operating frequency (f_0) and the width of the frequency distribution (bandwidth). High-Q transducers produce a relatively pure frequency spectrum, while Low-Q transducers produce a wider range of frequencies.

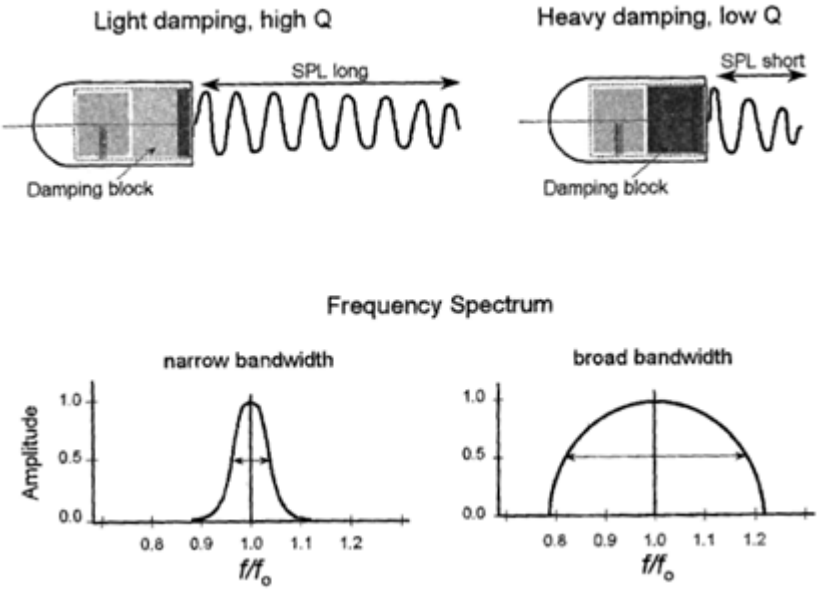

Figure 1.2.5. Representation of the influence of the damping block.

A matching layer of material is placed on the front surface of the transducer to improve the efficiency of energy transmission. Acoustic coupling gel is used to eliminate air pockets that could attenuate and reflect the ultrasound beam.

The intensity of the ultrasonic waves inside the beam generated by the transducer is not constant, but it varies due to diffraction phenomena caused by the finite size of the ultrasound source. It is possible to distinguish between the near field and a far field.

Near Field is adjacent to the transducer face and has a converging beam profile. Convergence occurs because of multiple constructive and destructive interference patterns of the ultrasound waves (pebble dropped in a quiet pond). Inside the next field, the distance corresponding to the duration time of the impulse is defined as “dead zone"

The far field or Fraunhofer zone is where the beam diverges. This beam divergence is reduced with high-frequency or large-diameter transducers.

The ultrasonic beam, overcome the next field, tends to have characteristics of greater stability and, from a geometric point of view, the tendency to diverge becomes evident.

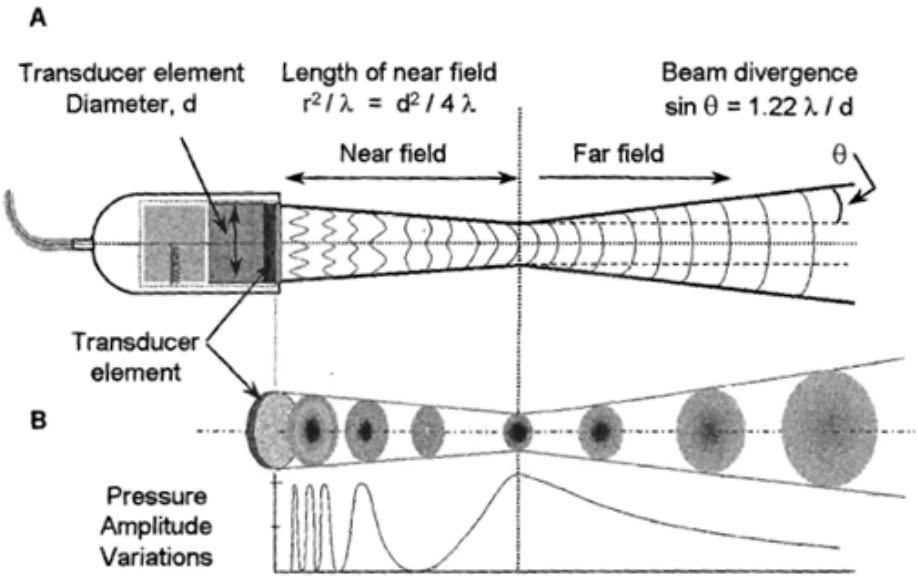

Figure 1.2.6. Representation of the pressure amplitude variations in the ultrasonic beam.

Ultrasound has a wide range of applications, which can be divided, depending on the amplitude of the ultrasonic waves used, in high intensity applications (intensity greater than 1 W/cm2, which can reach up to 104 W/cm2 in metal welding) and in applications of small intensity. Examples of the first

type are welding of plastic materials, ultrasonic cleaning, manipulation of animal and plant cells. Examples of the second type are the non-destructive inspection of welded or stressed materials, the characterization of materials, acoustic microscopy and diagnostic.

1.2.2 Mechanisms of interaction between biological tissues and ultrasound

Ultrasound can propagate through tissue as an oscillating wave of alternating pressure. The elements of the tissue move in response to the applied pressure and this forms the mechanism by which US interacts with tissue.

Ultrasound interaction with biological tissues are widely used in the diagnostic field, with equipment able to generate pressures ranging between 0.5 and 5 MPa. The characteristics of ultrasonic images are determined by the acoustic properties of tissues. Diagnostic US examinations are generally performed in 3 different modes:

- B-mode or grey scale imaging: in this technique the transducer is energized by a short pulse and echoes from acoustic impedance discontinuities in tissues are displayed on a trace that represents the line of sight of the transducer;
- Spectral Doppler Analysis: the major difference is that in B-mode the ultrasonic beam is scanned to form the image, whereas, in spectral Doppler, the beam is kept stationary and the signal is processed to determine the amplitude and the range of frequencies present. When an interface is moving with respect to the transducer, the frequency content in the pulse is shifted by the Doppler effect. The Doppler frequency shift is proportional to the examination frequency, the velocity of propagation in tissue, and the velocity of the interface relative to the transducer.
- Color Doppler Imaging: in this technique the transducer is energized by a relatively short pulse and the Doppler information obtained along the line of sight of the transducer is displayed in color rather than in gray scale as used in B-mode imaging. A cross-sectional image is formed by scanning the line of sight of the transducer and making the trace follow the same scan pattern. The technological requirements are much more complex than those used in B-mode.

In order to verify the effects of ultrasound used for diagnostic purposes on tissues, the American Institute of Ultrasound in Medicine (AIUM) examines the literature on ultrasound bioeffects and develops conclusions and recommendations related to diagnostic ultrasound [18].

It is possible to analyse these different ultrasound bioeffects:

- Thermal effects: this type of effects depend on many factors, such as the exposure duration, the type of tissue exposed, its cellular proliferation rate, and its potential for regeneration. Temperature increases of several degrees above normal (i.e., 37°C) can occur naturally; there have been no significant biological effects observed resulting from such temperature increases except when they were sustained for extended periods.
- Fetal considerations: diagnostic ultrasound devices can cause temperature elevation infetal tissue. Temperature elevation becomes progressively greater from B-mode to color Doppler to spectral Doppler applications. Even if an adverse fetal outcome is possible at any time during gestation, most severe and detectable effects of thermal exposure in animals have been observed during the period of organogenesis. For identical exposure conditions, the potential for thermal bioeffects increases with the dwell time during examination.
- Non-thermal effects: It is important to distinguish between tissues containing stabilized gas bodies and tissues without gas. The former are more susceptible to nonthermal damage by diagnostic ultrasound than tissues that do not contain undissolved gas. For these tissues, there are no confirmed reports of adverse biological effects in animals produced by a nonthermal mechanism from exposure to pulsed ultrasound when $pr/\sqrt{f} < 0.4$ MPa/MHz½, where pr and f are the in situ values of the rarefactional acoustic pressure and frequency, respectively. In tissues that are not known to contain gas bodies, the requisite amplitude of the ultrasound field for inducing bioeffects is relatively high. For example, 10-microsecond pulses of 1 MHz ultrasound up to a peak rarefactional acoustic pressure of 4 MPa would not produce such an effect.

Studies on the interaction of ultrasound and biological tissue focused on diagnostic nonthermal, noncavitational (<100 mWcm-2) and therapeutic potentially cavitational (>100 mWcm-2) spatial peak temporal average intensity levels. Krasoviski et al. [19] introduced a new model of direct interaction between the oscillating acoustic pressure and the cellular bilayer membranes able to explain both cavitational and noncavitational ultrasound bioeffects. They supposed that the intramembrane hydrophobic space between the two lipid monolayer, when exposed to ultrasound, inflates and deflates periodically. In this model, the two monolayers are pulled apart when the acoustic negative pressure overcomes the molecular attractive forces and pushed back together by the positive pressure. They introduced the term "bilayer sonophore" (BLS) to emphasize that the bilayer membrane is able of transforming the millimeter wavelength of the acoustic pressure wave into

nanometric intracellular deformations. This cyclic behaviuor could stimulate cycles of stretch and release in cell membranes and in the cytoskeleton, which could activate mechano-sensitive proteins and/or increase membrane permeability.

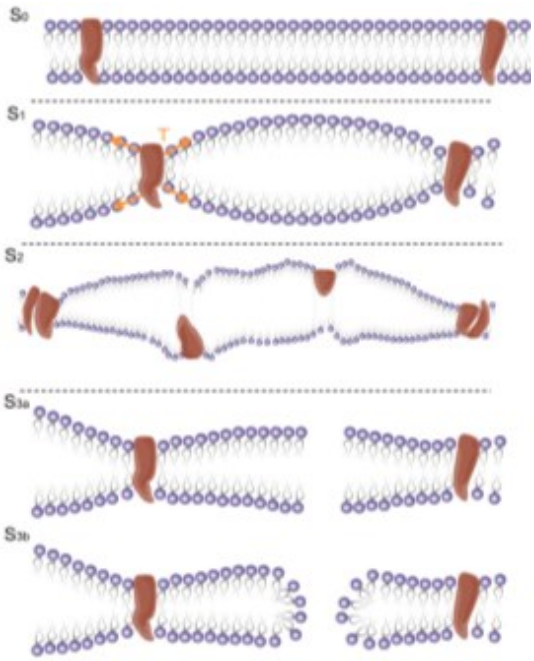

Figure1.2.7. From stage (So), as tension gradually increases, the stretched leaflets might at first activate mechano sensitive proteins (S1); growing tension might damage membrane proteins (S2) and then might induce pore formation (S3a/ S3b) or cause membrane rupture at high levels of stretching.

Krasoviski [19] constructed three physical models to evaluate dynamical response to ultrasound for multiple parameter: the size of the free membrane when the BLS is surrounded by water (model I); the combined effect of acoustic pressure amplitude and frequency for a BLS bounded by a thin layer of tissue (model II); the amplification of the pressure amplitude by a nearby microbubble (model III).

With these models they predict that the maximum area strain is proportional to the acoustic pressure amplitude and inversely proportional to the square root of the frequency and is intensified by proximity to free surfaces, the presence of nearby microbubbles in free medium, and the flexibility of the surrounding tissue

1.2.3 Therapeutic techniques based on the use of ultrasound

The interaction of ultrasound with tissue can induce mechanical effects, chemical effects and thermal effects, depending on the ultrasound setting, which in turn can lead to several bio-effects. A tissue stressed with high-intensity ultrasound absorbs acoustic energy and the local temperature rises leading to tissue irreversible damage, while at low-intensity ultrasound mechanical effects occur and biological signals are activated as a consequence of the stress induced by stable or inertial cavitation.

One of the best-known therapeutic techniques based on the use of ultrasound is certainly the High-intensity focused ultrasound (HIFU) [20]. This technique uses high-intensity ultrasound efficiently targeted on tumour masses to induce protein degeneration and coagulation necrosis.

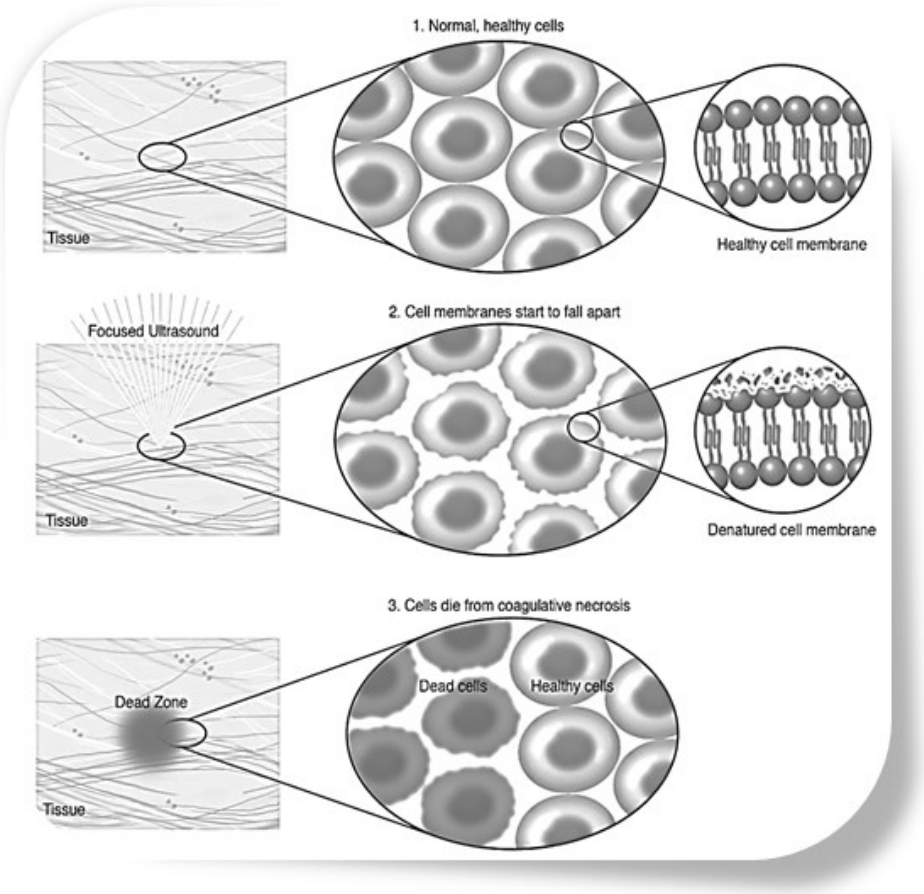

Figure1.2.8. Representation of US-induced thermal ablation.

HIFU has been used to treat different solid tumours without damaging healthy tissues. In breast cancer, HIFU treatment decreased the expressions of proliferating cell nuclear antigen and cell adhesion molecule. Good results were also obtained for pancreatic cancer, especially when HIFU is

used in combination with gemcitabine. Generally, HIFU could enhance chemotherapeutic drug delivery into tumor tissue by permeabilizing cell membrane. In cervical cancer and bladder cancer, HIFU ablation combined with DDP was found to reduce tumor volume and increase tumor necrosis. However, the response of chemoresistant cells to insonation usually differs from that of chemosensitive cells. Zhang et al. investigated the response of DDP-resistant LA cells to HIFU and its underlying molecular mechanisms using molecular biology techniques both in vitro and in vivo. They found that exposure to HIFU determines a significant decrease of cell viability and proliferation. In particular the expressions of CDK2, CDK4, Cyclin D1, and Cyclin E were remarkably decreased by HIFU treatment. Furthermore, HIFU exposure significantly enhanced the expressions of pro-apoptotic proteins, cleaved caspase-3 and PARP, and decreased the expression of anti-apoptotic protein Bcl-2. A similar result was also observed in vivo: xenograft mice in which a tumor growth was induced, after HIFU treatment, showed a drastic reduction of solid tumor size accompanied with a drastic reduction of cyclin D1 and CDK4 protein levels.

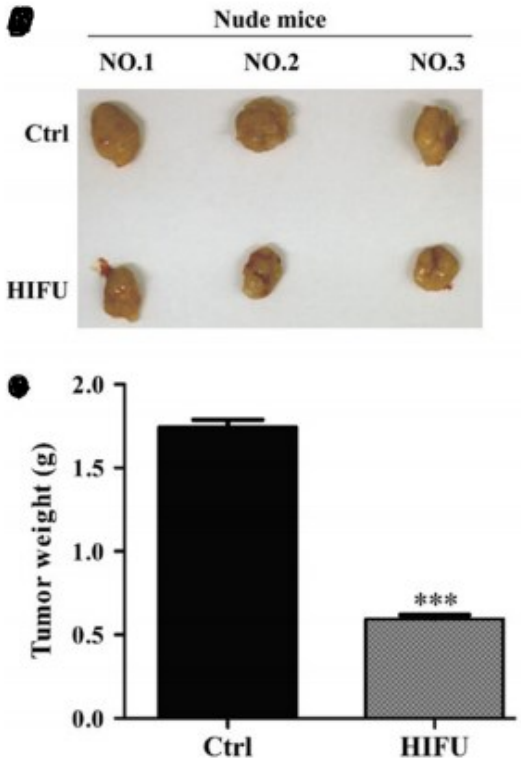

Figure 1.2.9. Images of the effect of HIFU on tumors from mice. In the graph is represented the tumor weight before (Ctrl) and after (HIFU) ***P < 0.001.

Ultrasound has also been widely used to enhance drug delivery. Sonoporation is the formation of temporary pores in the cell membrane, through which it is possible to realize drug delivery. Lentacker et al. [21] categorized the mechanisms contributing to sonoporation according to three ultrasound settings:

i) low intensity ultrasound leading to stable cavitation of microbubbles;

ii) high intensity ultrasound leading to inertial cavitation with microbubble collapse;

iii) ultrasound application in the absence of microbubbles.

Stable oscillations of microbubbles may stimulate the intracellular delivery of macromolecular drugs and nanoparticles. Two mechanisms have been postulated to contribute to the uptake of cell impermeable molecules: the formation of small pores and endocytosis. Pore formation in the cell membrane allows molecules to enter the cell via passive diffusion. Moreover, during microbubble cavitation, reactive oxygen species (ROS) are produced. These ROS can modulate ion channels or can lead to membrane disruption via lipid peroxidation. The calcium influx is overcompensated by potassium efflux via BKCa channels and it seems to stimulate also endocytosis.

The microstreaming generated by stably cavitating bubbles and the corresponding shear stresses can deform the cell membrane. This leads to cytoskeletal rearrangements and differences in membrane tension, which is sensed by mechanosensors. These sensors can initiate a signalling cascade that influences endocytosis/exocytosis processes.

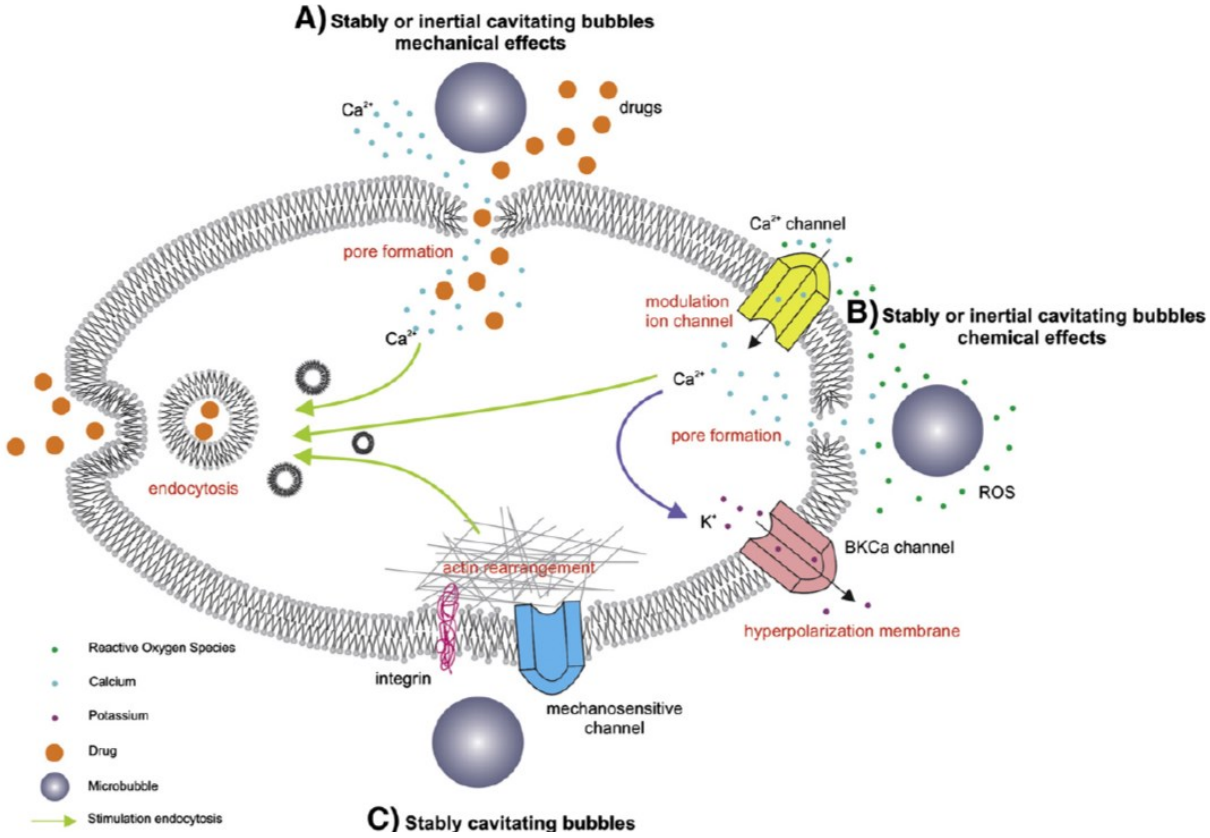

Figure1.2.10. Biological effects of stably and inertial cavitating microbubbles.

At higher ultrasound intensities, the oscillation amplitude of the microbubbles grows rapidly until the microbubbles collapse and the fragmentation of the microbubbles into many smaller microbubbles occur. This type of cavitation is called inertial cavitation. During the collapse of the microbubbles, shock waves can be generated in the fluid and jet formation can occur. These two phenomena create very high forces that can perforate cell membranes. In this case, direct cytoplasmic uptake of drugs becomes possible.

Zhao et al. [22] investigated the role of mitochondrial dysfunction in tumour cell apoptosis induced by acoustic cavitation of microbubbles. They studied the effects of low-intensity pulsed ultrasound (1 MHz frequency and 0.3-MPa peak negative pressure) used in combination with 10% (v/v) SonoVue microbubbles to K562 chronic myelogenous leukaemia cells. They found that this treatment increases cellular apoptosis, mitochondrial depolarization and cytochrome c release in K562 cells. The increase in calcium concentration plays an important role in these processes. In fact, ultrasound stimulated calcium increase regulates the transcription of genes coding calcium-dependent enzymes and endonucleases, resulting in the activation of apoptosis. Moreover, calcium enhances the activity

of proteases, endonucleases and transglutaminases that are involved in the degradation of cell structures and macromolecules, activating specifics biochemical patterns of apoptosis. The increased cytoplasmatic calcium concentration determine a rise of the ion level also in mitochondria, which undergo swelling and mitochondrial permeability transition pore (mPTP) opening. The mPTP opening provoke the release of the cytochrome c molecule, which start the apoptosis process irreversibly. These evidences demonstrate that mitochondrial dysfunction induced by acoustic cavitation and can be used as a basis for therapy.

Other important studies on ultrasound in the therapeutic field concern the possibility of using low-intensity ultrasound, capable of acting selectively on cancer cells without damaging healthy cells. Different studies have shown that low intensity ultrasound can provoke cell kiling also without significant temperature rise. The studies conducted by Feril et al. [23] have made an important contribution to this research by investigating various aspects of low intensity ultrasound and cellular conditions, with particular attention to factors that enhance cell killing and factor that inhibit it.

A first factor to consider is that low-intensity ultrasound, in combination with hyperthermia, synergistically induce apoptosis, as verified for human lymphoblastoma cell line. A possible explanation could be that temperature rise inhibit membrane reparation caused by sonication, or that hyperthermia-stimulated apoptosis is enhanced by ultrasound.

Another interesting factor is that hypotonia also enhanced cell killing, even for ultrasound intensities far below the usual threshold for bioeffects, by inducing a physiologic cell swelling. In fact, water molecules are transported into the cell depending on the osmotic gradient between the extracellular and intracellular compartment, thus increasing the pressure inside the cell. As a result, the cellular membrane is strained, and the tension grows as a function of the internal and external pressure. In these conditions, cells are more susceptible to the mechanical effects of ultrasound, delaying or inhibiting the repair of membrane.

The ultrasound ability to kill cells could be also augmented by using echo-contrast agents (ECA). These agents can maximize the effects of delivered antitumoral drugs in a specific target area. In particular, Feril performed an in vitro study on human lymphoma U937 cell line, founding that cytolysis as well as apoptosis are strongly boosted when ECAs are present in the medium during ultrasound treatment. Also another class of molecules, named thermal sensitizers, are able to potentiate the apoptotic cell death induced by ultrasounds.

Mizrahi et al. [24] investigated aspects related to cytoskeleton deformation, which occurs when cells are subjected to low-intensity ultrasound. They report that low-intensity ultrasound acts as a mechanical stimulus in a manner similar to a transient physiological stretch, fluidizing cells and a rapid accelerating their remodelling dynamics. This fluidization is slowly followed by recovery, which is interpreted as a form of physical rejuvenation followed by aging.

Louw et al. [25] also investigated the effects of low-intensity ultrasound on cells, focusing on effects on nuclear processes. They sonicated isolated primary bovine chondrocytes with different values of ultrasound frequencies (from 2 MHz to 8 MHz), finding that this stress induced phosphorylation of focal adhesion kinase, Src, p130-Crk-associated substrate (p130Cas), Crk-II and extracellular-regulated kinases (ERK), activating an ultrasound-mediated signalling pathway. ERK regulates proliferation, differentiation and many other cell processes in response to extracellular signals. Louw found that the expression of genes regulated by ERK kinase, such as c-Myc, c-Fos and c-Jun resulted highly modulated and dependent on the ultrasound frequencies used, as shown in the following histograms. It is possible to see that the frequency which mostly affected gene expression is 5 MHz.

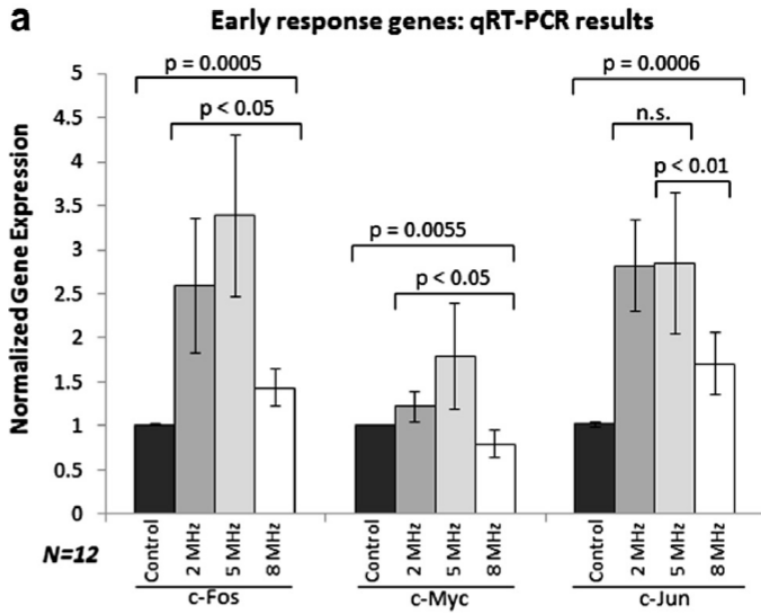

Figure1.2.11. Histograms showing the dependence between c-Fos, c-Myc and c-Jun expression and the frequency.

A possible interpretation of these results is that the pathways activated depend on both the energy transferred from acoustic waves and cell's characteristics. Louw considers in particular three characteristics: cell radius, solid bulk modulus, which could change during stimulation through cytoskeleton dynamics, and cell porosity.

Another important contribution to the study on mechanotrasduction pathway activated by ultrasound is the one provided by Sato et al. [26], who particularly examined how low-intensity pulsed ultrasound activates integrin-mediated mechanotransduction pathway in synovial cells. They demonstrated a significant increase of phosphorylated/activated integrin, as shown in the following fluorescent microscopy images: the red fluorescent signal, referred to the activated beta-1 integrin subunit, is progressively increased during ultrasound exposure.

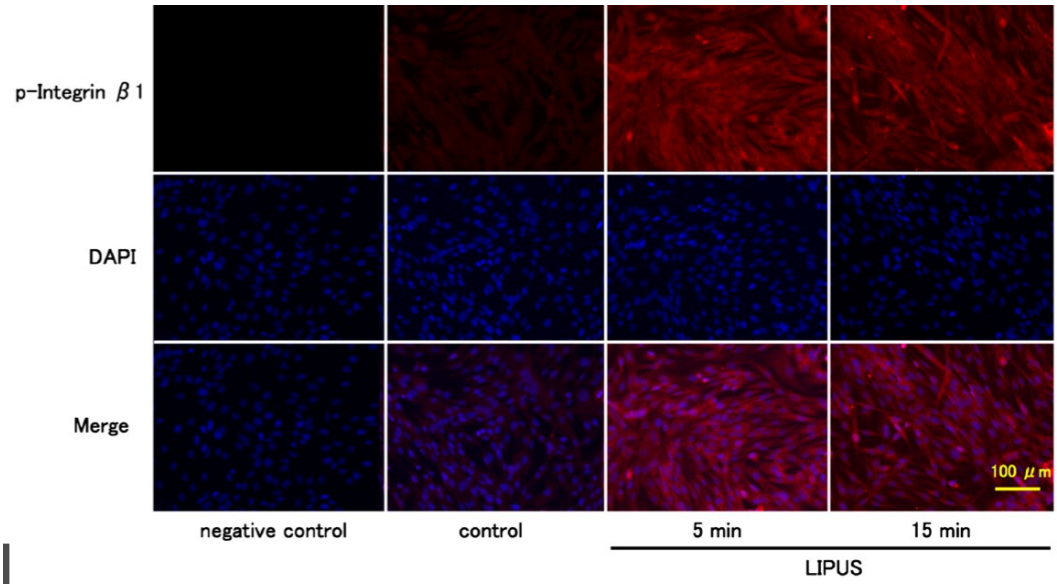

Figure 1.2.12. Immunofluorescence of phosphorylated Integrin b1 in the synovial cells after LIPUS exposure.

Ultrasound-mediated activation of integrin stimulates activation cascade of several other downstream proteins such as FAK (Focal Adhesion Kinase), the most important enzyme involved in the activation of pathways that regulate cell proliferation, cell cycle arrest and apoptosis. A significant increase of the activation (phosphorylation) of ERK 1-2, P38 and JNK 1-2-3 proteins, well-known effectors of the signal cascades, was also demonstrated. Depending on the cell type and on the integration of these

different activated pathways, the bioeffect determined by ultrasound could alternatively result in a stimulated proliferation or in a hyperproliferation arrest.

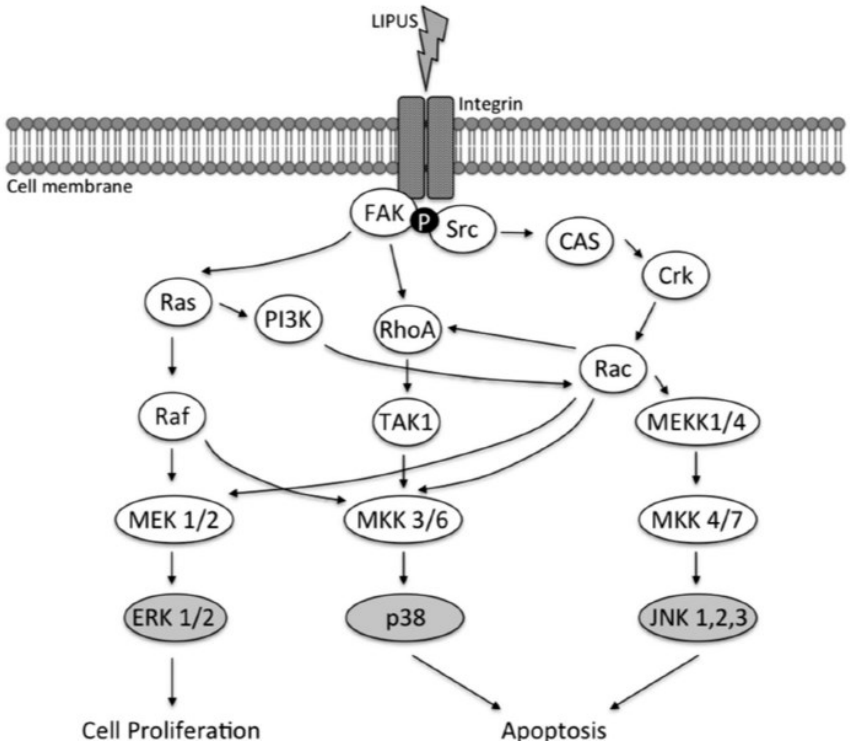

Figure1.2.13. Schematic illustration of mechanisms of signal transduction pathways enhanced by ultrasound. Ultrasound may regulate synovial cell metabolism via integrin/FAK/MAPK pathway.

In 2017 Miller et al. [27] explained how ultrasound stimulation of anchored chondrocytes, at resonant frequency, maximized the expression of genes which are regulatory markers for cellular response to external stimuli. To understand what the underlying mechanisms are, they realized a model which showed that the mechanical energy storage is maximized at the chondrocyte's resonant frequency, which is, for the chondrocytes, about 5 MHz. Moreover, they found that the energy density in the nucleus is almost twice than in the cytoplasm.

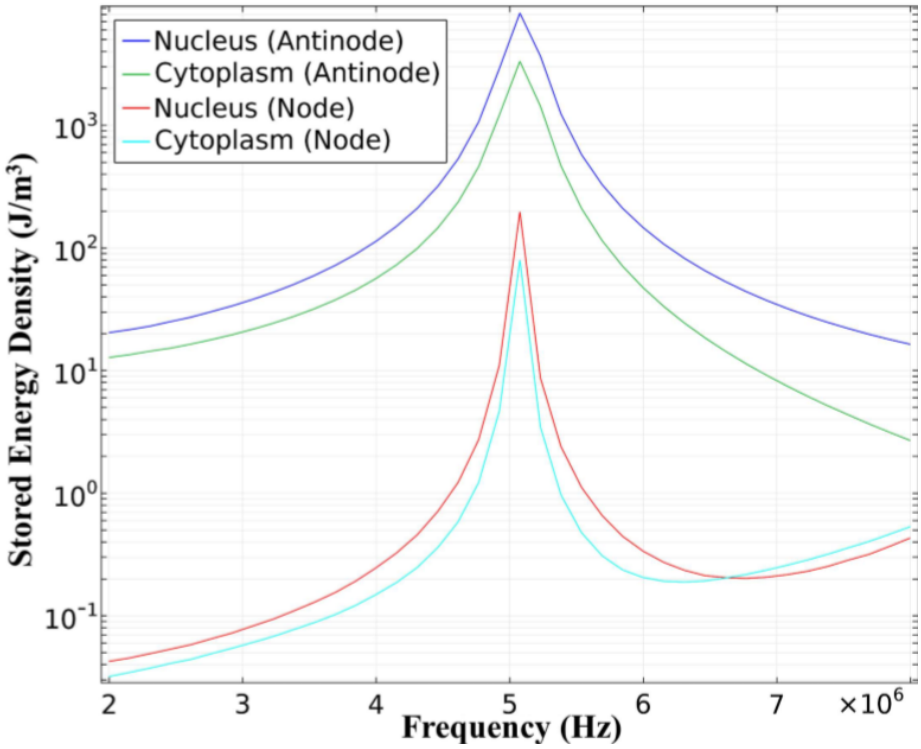

Figure1.2.14. Total mechanical energy density in the cytoplasm and nucleus for cells attached to a plane located at a pressure anti-node and node.

They also realised a mechanochemical model to link this increased mechanical energy density in the nucleus to the downstream targets of the ERK pathway, finding that ultrasound stimulation induces frequency dependent gene expression as a result of altered rates of transcription factors binding to chromatin.

Moreover, Furusawa et al. [28], demonstrated that in two leukaemia cell line, after ultrasound treatment, the activation of stress response led to the phosphorylation/activation of ATR protein and check-point kinase (Chk1); these proteins are both involved in stimulating the cell cycle arrest in G1 and G2 phases.

Generally, cells treated with ultrasounds accumulates DNA mutations. When cells are able to implement DNA repair mechanisms, the cell survives and meets the mitosis and cytokinesis. Otherwise, when the DNA repair fails, cells arrest in G1 phase and the apoptosis is triggered.

Furusawa et al. [28] demonstrated that leukemia cell lines treated with ultrasounds, if compared to untreated control cells, express at higher level the activated form of caspase-3, a well-known apoptotic marker. Moreover, the expression of this protein is progressively increased during the time of incubation (1, 3 and 6 hours after ultrasounds stress). In this case, the apoptosis induced by ultrasounds is activated upstream by the ATR pathway and is strictly dependent from the activation of the check-point kinase 1 (Chk1). In accordance with western blot analysis, the evaluation of DNA content confirmed that cells are blocked in subG1 phase and in G2/M phase of cell cycle thus suggesting that ultrasound-injured cells have a less tendency to replicate and a remarkable protention to trigger the apoptosis.

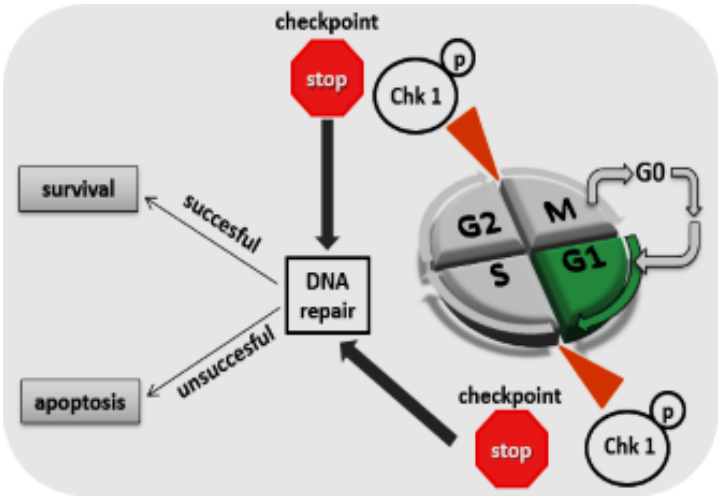

Figure 1.2.15. Representation of the activation of the check-point kinase 1 (Chk1).

1.2.4 Factors influencing the ability of ultrasound to induce cell mortality

The effects of ultrasounds on tumour cells can be improved under certain conditions. Several researchers have investigated these aspects in their studies.

In 2003 Feril et al. [29] demonstrated that, if cells are suspended in a medium saturated with CO2, cell killing induced by ultrasound and free-radical production are inhibited. They used NaHCO3 and HCl to produce a predictable concentration of CO2 within the culture medium. They sonicated U937 cells suspension for 1 min, using 1 MHz continuous wave ultrasound and 4 W/cm2 intensity. Results showed that cell killing decreased with increasing CO2 concentration until no effect production at 20

mM CO2 concentration. Also free-radical production induced by ultrasound significantly decreased at 1 mM and became undetectable at 2 mM CO2.

Another important factor that influences ultrasound-induced cell killing is cell density, indicated as the number of cells present in one millilitre of medium. As cell density increases, the viscosity of medium grows, and ultrasound transmission is drastic reduced. Feril et al. [30] demonstrated in 2005 this particular effect, conducting some experiments on U937 cells. They correlated different cell density with the production of ROS, which are considered as a cavitation indicator. Results show that when cell density increase, ROS production is reduced.

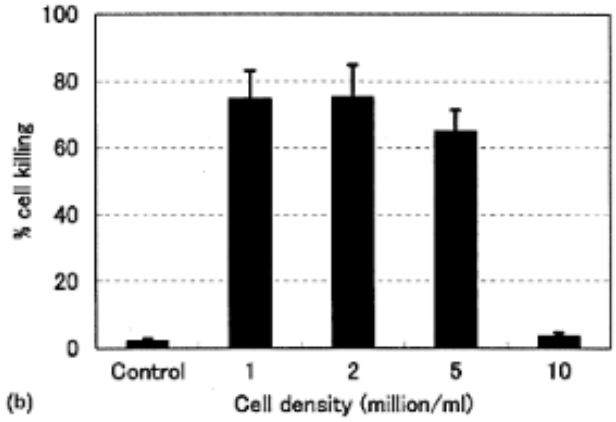

Figure1.2.16. Cell killing trend as a function of cell density.

In the in vitro study on the effects of ultrasound on tumour cell cultures, it is also important to consider how the ultrasound propagate inside the dish, which contains the cell culture. In fact, these studies require well-defined and reproducible experimental conditions. Kinoshita et al. [31] experimentally verified the importance of the exact distance between cells and a reflective interface in a sound field. Hensel et al. [32] conducted an analysis of ultrasound fields in cell culture dishes to verify the real sonication conditions.

To perform the measurements of the various parameters, one-element planar transducers with central frequencies of 3.5 MHz (C380, Olympus NDT, USA) were used. The transducers were excited by a programmable ultrasound system (1 cycle at 1 MHz, PCM100, Inoson, St. Ingbert, Germany) and scanned by a calibrated hydrophone (0.2 mm needle diameter, Precision Acoustics, Dorchester, UK) positioned by a 3D positioning device (M-IMS400CC / M-IMS600CC and XPS, Newport, Irvine, CA, USA). A 12-bit digitizer (100 MHz sampling rate, U1070A-002 Acqiris, Agilent, Santa Clara,

CA, USA) recorded the data. For all the setups polystyrene wells were used with an internal diameter of 33.7 mm, a height of 15 mm and a wall having a thickness of 1.25 mm less.

They studied four different sonication setups, both through the analysis of the finite elements, with PZflex simulation software, and through experimental measurements: well on transducer, well on water surface, sealed well and transducer in well.

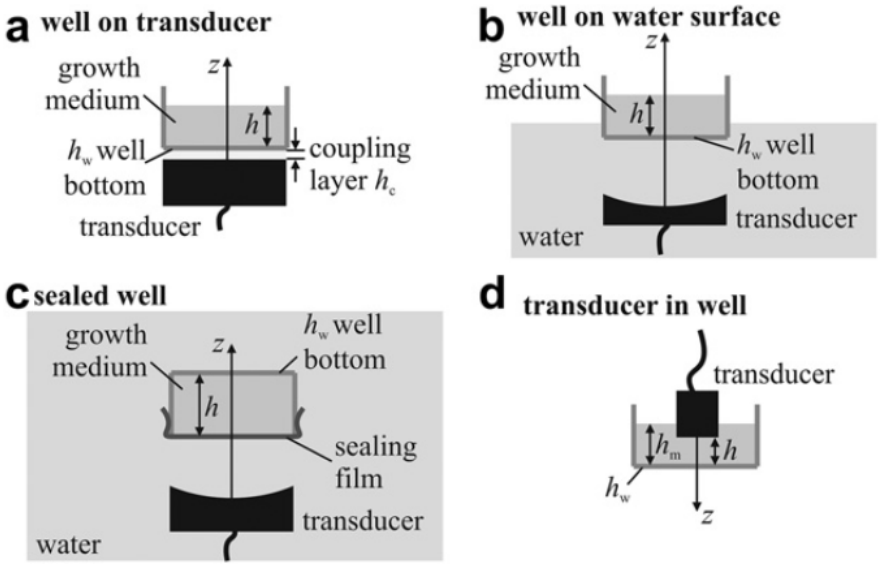

Figure1.2.17. Representation of the four sonication setups tested.

A) **Well on transducer**: this configuration consists of a polystyrene plate filled with DMEM, positioned on a planar transducer (38 mm diameter), where the acoustic «matching» is guaranteed by the presence of a layer of gel or water interposed between the probe and the base of the plate. The figures show the distribution of the "peak rarefaction pressure" in the +z direction in the xz (a) plane, and in the xy plane passing through the cell layer (b). The different materials are outlined in white. The results of the simulation, verified by the measurements, show a ring distribution of pressures, with a high pressure in the center of the well. Pressure distribution across the cellular layer is not homogeneous, so the therapy is governed by the average pressure amplitude.

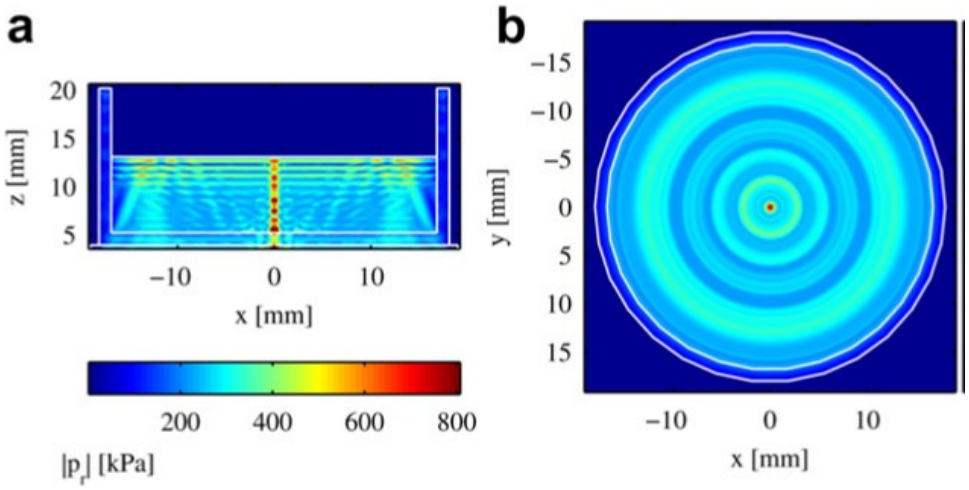

Figure 1.2.18. Pressure distribution in a well on transducer simulated sonication.

The following graphs show the "peak rarefaction pressure" in absolute value and the "temporal average intensity" along the z axis. These results were obtained both from the measurements and from the simulations (pressure wave with 40Pa peak-to-peak amplitude, burst length 5 cycles). Five antinodes are visible in the distribution of pressure and intensity. Depending on the number of cycles (burst length), nodes and antinodes can affect the cell layers at the bottom of the well. This happens when the height h of the volume of the growth medium, the number of cycles n and the wavelength in the medium λ correspond to $2h < n\lambda$. Height h is a dominant parameter, and this indicates the importance of the exact distance between cell layer and air interface.

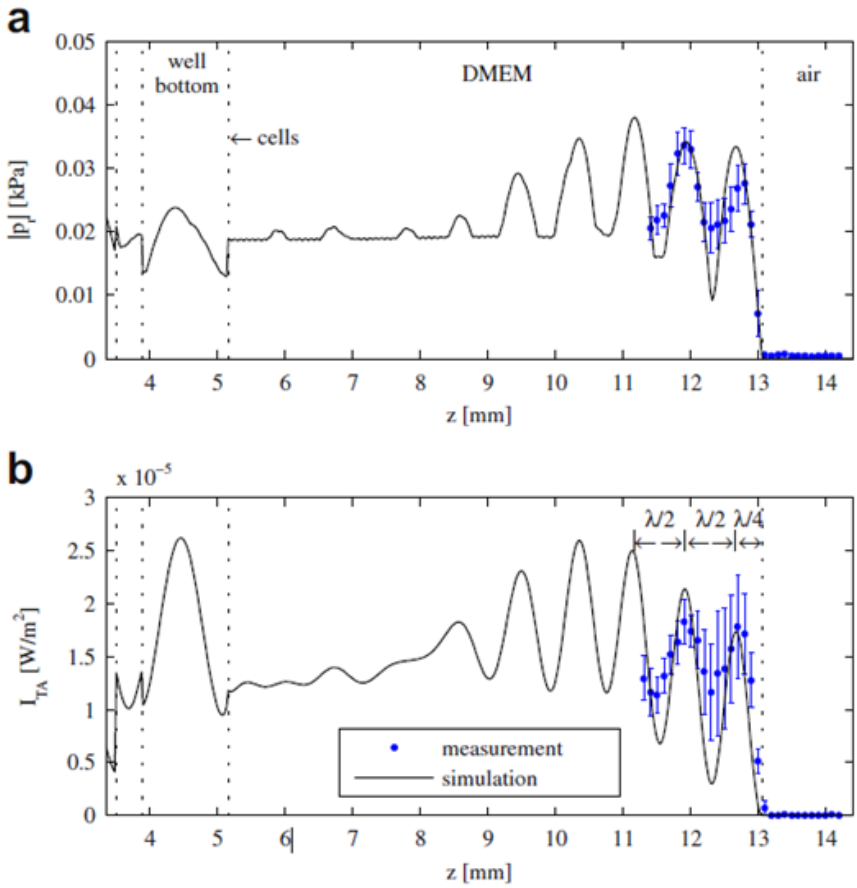

Figure 1.2.19. "Peak rarefaction pressure" in absolute value and the "temporal average intensity" along the z axis.

B) **Well on water surface**: in this case the well is placed on the surface of the water contained in a tank, all inside which the transducer is located, placed at a known distance from the bottom of the well. Supposing the distance between the transducer and the well > 50λ, it is possible to ignore multiple reflections between the well and the transducer. In the following picture are represented the pressure distributions for h = 7 / 4λ (a, b) and the pressure and intensity distribution for h = 7 / 4λ and 2λ. The interference pattern caused by the liquid-air interface influences results for the cellular layer (2h < nλ).

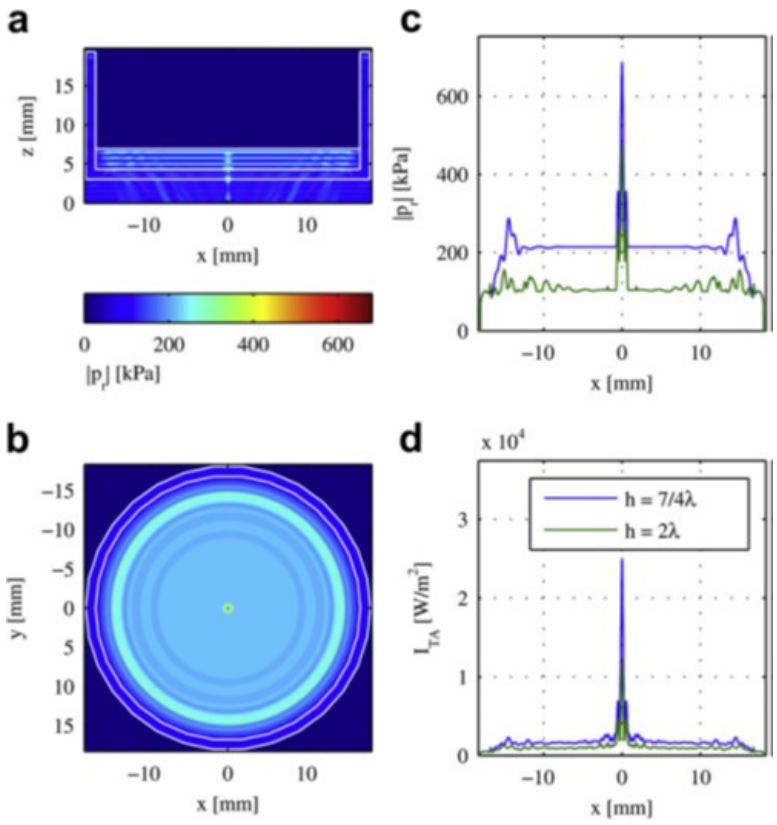

Figure1.2.20. Pressure distributions for h = 7 / 4λ (a, b) and the pressure (c) and intensity (d) distribution for h = 7 / 4λ and 2λ.

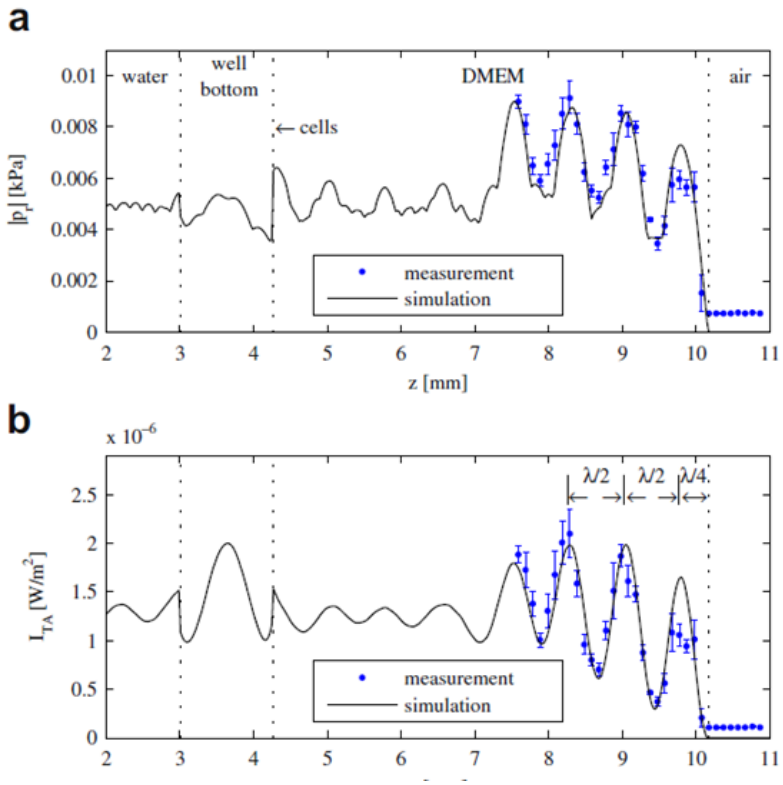

Figure1.2.21. Distribution of pressures (a) and intensity (b) along the z axis obtained by simulation and measurement (h = 5.9 mm, hw = 1.25 mm).

C) **Sealed well**: in this case the well and the transducer are both immersed in a tank full of water (h = 15 mm, hw = 1.25 mm). Reflection phenomena occur at the bottom of the well, so hw is an important parameter for pressure superposition.

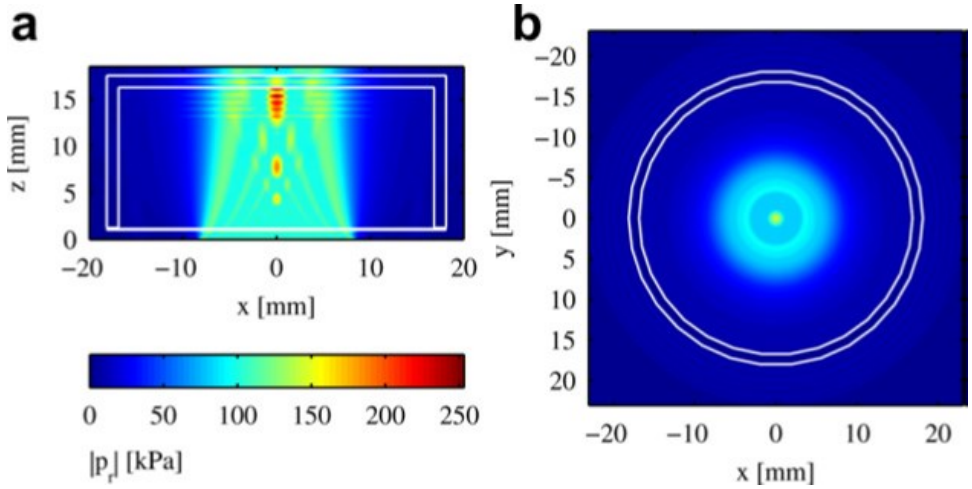

Figure 1.2.22. Pressure distribution in a sealed well simulated sonication.

The following graphs show pressure and intensity respectively all along the z azis and at the level of the cellular layer (hw). There is constructive overlap on the cellular layer for hw = λ / 4 and hw = 3λ / 4. The common value of hw = 1.25mm corresponds to 0.52λ for a frequency of 1MHz, a situation that leads to destructive overlap on the cellular layer.

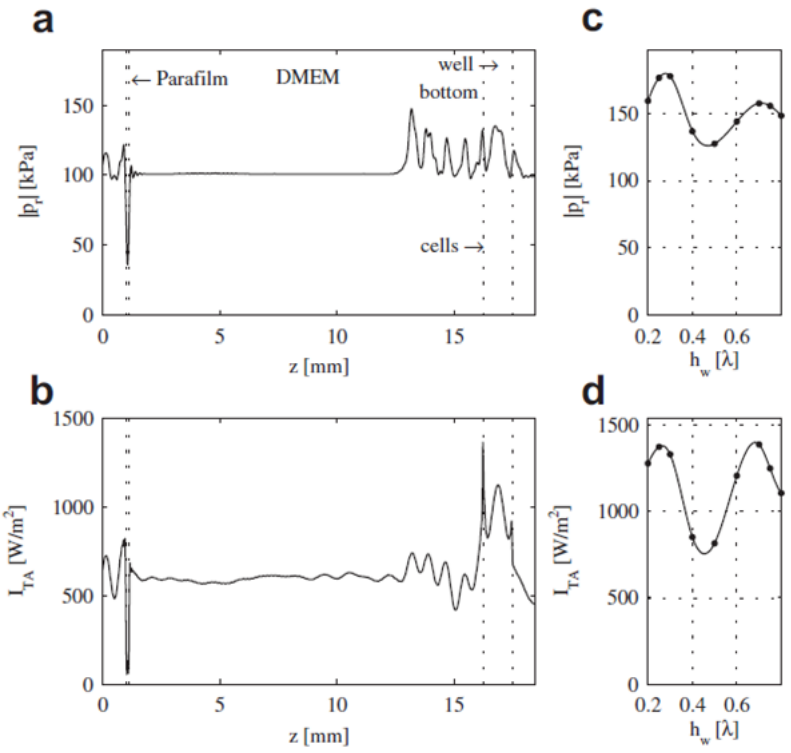

Figure 1.2.23. Pressure (a, c) and intensity (b, d) all along the z axis and at the level of the cellular layer.

D) Transducer in well: in this case the waves propagate from the transducer in the DMEM with a distance h = 9λ / 4 from the bottom of the plate (hw = 1.25 mm, height DMEM hm = 2h). There is no pressure on the walls of the well, so the pressure distribution is not related to the geometry of the plate. The interface with the air and the transducer can create a situation similar to a resonator. However, the thickness of the bottom plate (hw) is the dominant parameter in this configuration. The most reproducible results are obtained for high distances between the transducer and the bottom of the well.

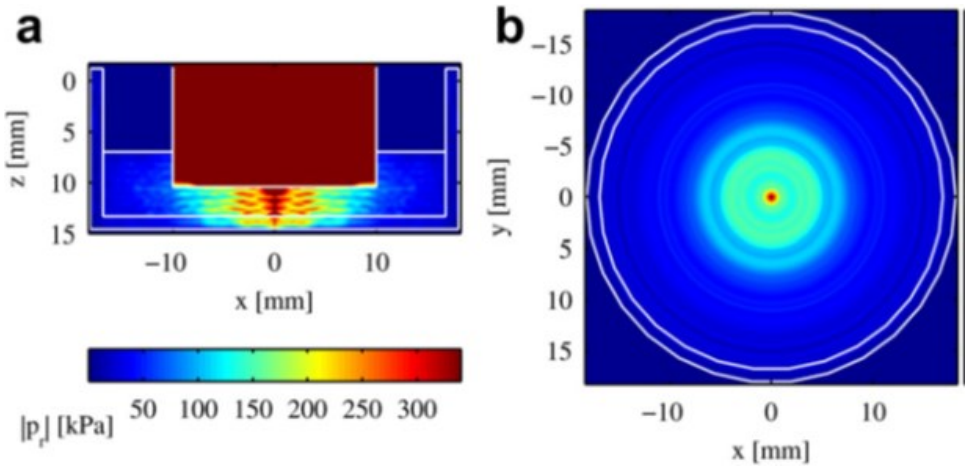

Figure 1.2.24. Simulation of the sound field distribution in the xz plane and in the xy plane through the cell layer.

Hensel found that in configurations where reflective interfaces are present, such as liquid-air interfaces, it is difficult to obtain reproducible results. Moreover, small variations in liquid volume can cause the increase or decrease of pressure amplitude by a factor of 2.

1.3 EXPERIMENTAL STUDY ON THE EFFECTS OF ULTRASOUND ON DIFFERENT CELL LINES

1.3.1 Introduction

In this chapter the studies conducted by the Experimental Mechanics research group of the Polytechnic of Bari on two tumour cell lines, the MG63 osteosarcoma cell line and the U937 lymphoma cell line, are described. In particular, the experiments on MG63 cell line were performed in collaboration with the researchers of the Dental Clinic of the University of Foggia, while the experiments on U937 cell line were performed at the cell culture laboratory of the Polytechnic of Bari. The aim of these studies was to identify specific frequencies able to induce cell death for each of the two cell lines considered. To achieve this, the two cell cultures were subjected to ultrasounds at different frequencies and intensities, finding for some conditions up to 80% of cell killing.

As already reported in the previous chapter, low-intensity pulsed ultrasound is a non-invasive technology used in different medical fields, for example to trigger bone formation and accelerate bone maturation in bone fractures or delayed fracture healing. There have been several studies reporting that low-intensity ultrasound has antitumor effects via the induction of apoptosis in several type of cancer cells. Different studies demonstrate that heat, cavitation and hyperthermia induced by ultrasounds can produce antitumor effects. Hrazdira et al. [33] treated HeLa cells with ultrasound at a frequency of 0.8 MHz, intensity of 50, 100 and 500 mW/cm2, for 5 or 10 minutes. These treatments affected cell proliferation and acted on cytoskeleton. The latter is probably due to the immediate action of mechanical forces of the ultrasound field on cellular structures. Feril et al. [23, 29, 30] investigated how low intensity ultrasounds can induce cell mortality and synergistic effects between ultrasounds and other agents. Ivone et al. [34] analysed mechanical and biological effects of US on floating (U937) and attached (MCF-7) cancer cells. The author used fixed and variable frequencies finding frequency values that yield the highest cell mortality. Another interesting study was showed by Lagneaux et al. [35], who treated human leukaemia cell lines with 1.8 MHz frequency ultrasound and different exposure times. They observed cell damage associated with the apoptotic process.

Several studies have demonstrated the positive role of low-intensity ultrasound in cancer therapy by causing membrane damage in human leukaemia cells, affecting the Ca2+/mitochondrial pathway in human hepatocellular carcinoma cells and in enhancing the effect of an anticancer drug on lymphoma and liver cancer cells. Other studies investigated the effects of low-intensity ultrasound combined with chemotherapy in osteosarcoma cell lines. The results suggest an antitumor effect, probably due to mechanical force.

1.3.2 Ultrasonic generator device: the K-TAC 4000

Ultrasound waves were generated by a SonoPore K-TAC 4000 device (NEPA GENE, Chiba, Japan). This equipment allow setting seven basic parameters directly from the dial: Frequency, Voltage, Duty Cycle, Burst Rate, Duration, Wave pattern type, sweep on/off.

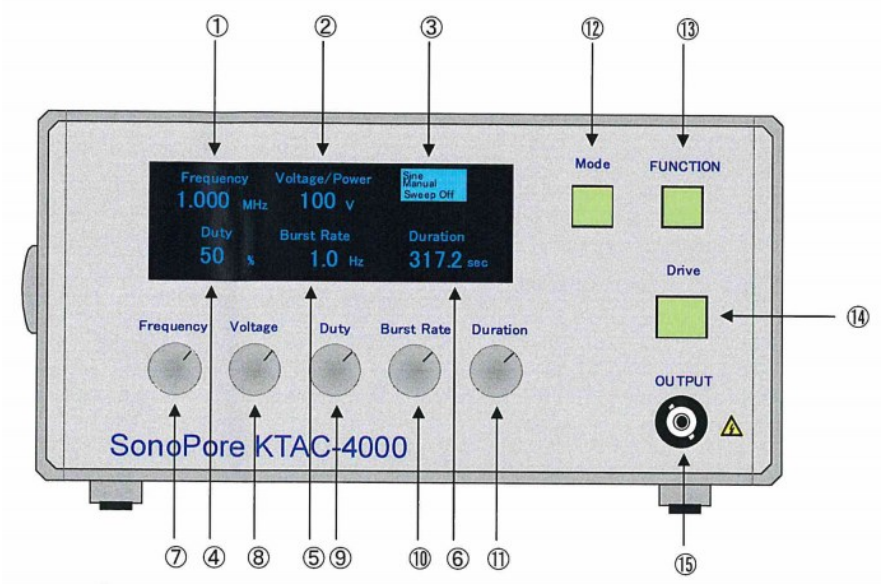

Figure 1.3.1 Representation of the K-TAC control panel: (1) Frequency display. (2) Voltage/Power (selected voltage is displayed, while the power reading is displayed during "drive" switch on. (3) Display of the current status (top line indicates pulse type (rectangular or sin), middle line indicates timer status mode (auto or manual), bottom line indicates frequency sweep status mode (on or off)) (4) Duty cycle display. (5) Burst rate display. (6) Duration display. (7) Frequency dial/Pulse type dial. (8) Voltage dial. (9) Duty selection dial. (10) Burst rate dial. (11)Duration dial. (12) Mode switch. (13) Function switch. (14) Drive switch. (15) Output connecter.

Frequency can be selected ranging 0.200 MHz – 5 MHz. Voltage range is 0 V- 60 V, while the output power may range from 0 to several Watt, depending on the ultrasound probe used in the experiments. The duration can be set between 0.1 s – 999.9 s. The output burst rate parameter, which represent the frequency of pulses, range from 0.5 Hz to 100 Hz. Duty rate is the percentage of "on" period of output burst. It range between 0% - 100%. For example, burst rate parameter 10 Hz, duty rate parameter 10% will result in 10 ms output burst for each 100 ms duration.

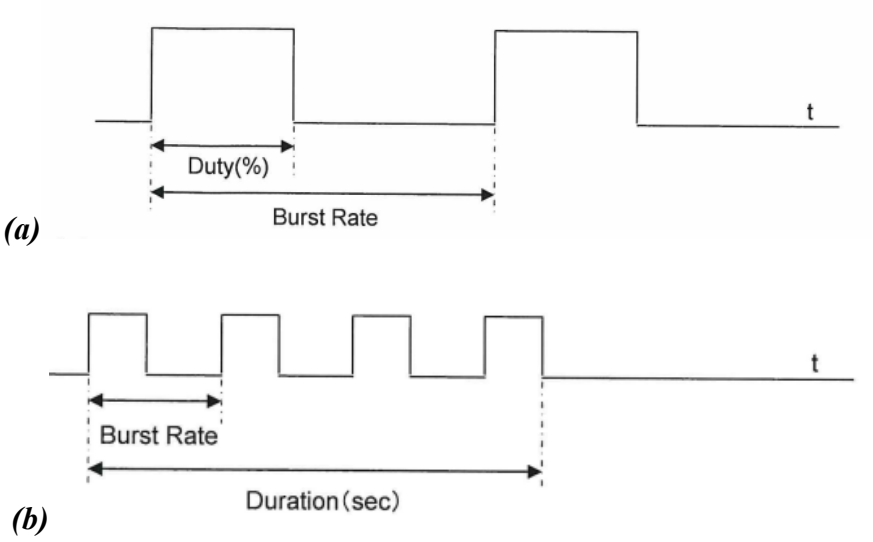

1.3.2 Representation of the burst rate parameter, duty rate parameter (a) and output duration parameter (b).

It is also possible to operate at increasing frequency (sweep 1) and decreasing frequency (sweep 2).

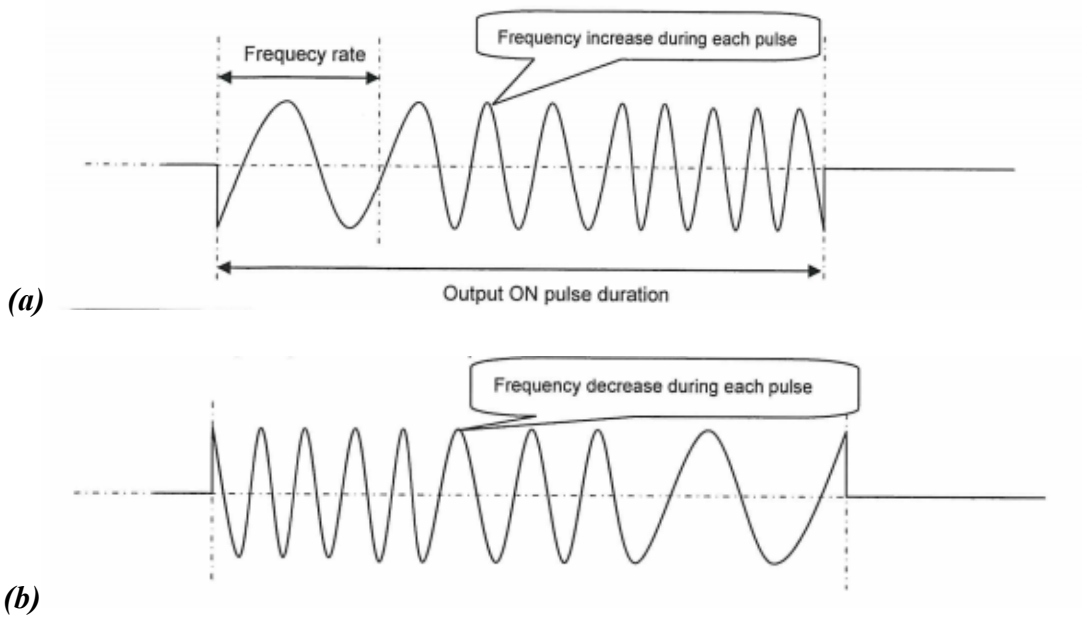

Figure 1.3.3 Representation of Frequency increase sweep (a) and Frequency decrease sweep (b)

The probe used to transfer ultrasounds to the specimens was the KP-S20, with a 20 mm diameter transducer.

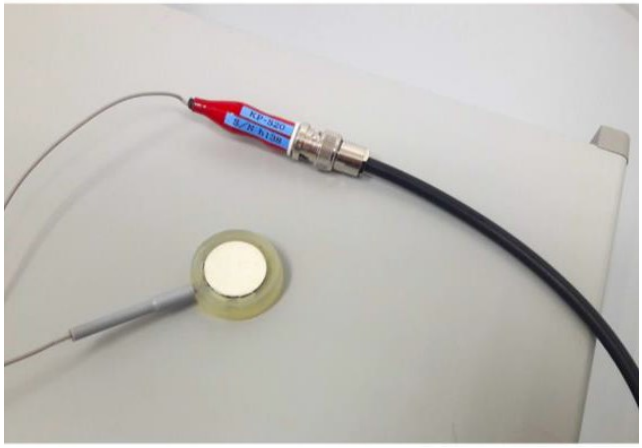

Figure 1.3.4. The KP-S20 probe.

In order to verify the correct functioning of the probe, various tests have been carried out using an ultrasound measurement system recorded by PAC PCI – 2 Acoustic Emission system. The system was composed by band pass filters (1 kHz – 10 MHz) and a 2/4/6 Preamplifier. The signals were pre-amplified by 40 dB. The waveforms of the signals were recorded at a high sampling rate of 10 MSPS (Mega Samples Per Second). We used also two different transducer to take measurements of KP-S20 probe emission:

- Pico sensor, which has high sensitivity and bandwidth and an operating frequency range of 200-750 kHz;
- R30a sensor, a narrow band resonant sensor with a high sensitivity and a 300 kHz central frequency.

The K-TAC 4000 has been set with different ultrasound emission parameters, measuring what was emitted and recorded through the two acoustic emission transducers. For each measurement, the Amplitude = U_{max} / U_{ref} was recorded, where U_{max} is the maximum energy registered and U_{ref} is the threshold we chose. U_{ref} was always set at 35 dB, except for tests conducted with the PICO-SENSOR on the top of the well full of liquid, where the threshold was 60 dB.

First, we performed tests with the R30a transducer put in direct contact with KP-S20 probe. Test were performed for 60 seconds, 20 V voltage, and two frequency values, 400 kHz and 1,000 kHz.

Table 1.3.1. Parameters set for the sent signal.

Signal Sent	
Voltage	20 V
Frequency	400 kHz
Duration of Pulsing	60 seconds
Burst Rate	10 Hz
Duration of Waveform Recorded	150000

We observed that amplitude values were bigger when we used a gel for coupling probe and transducer than for tests performed with adhesive tape for coupling (10 mV versus 1.5 mV).

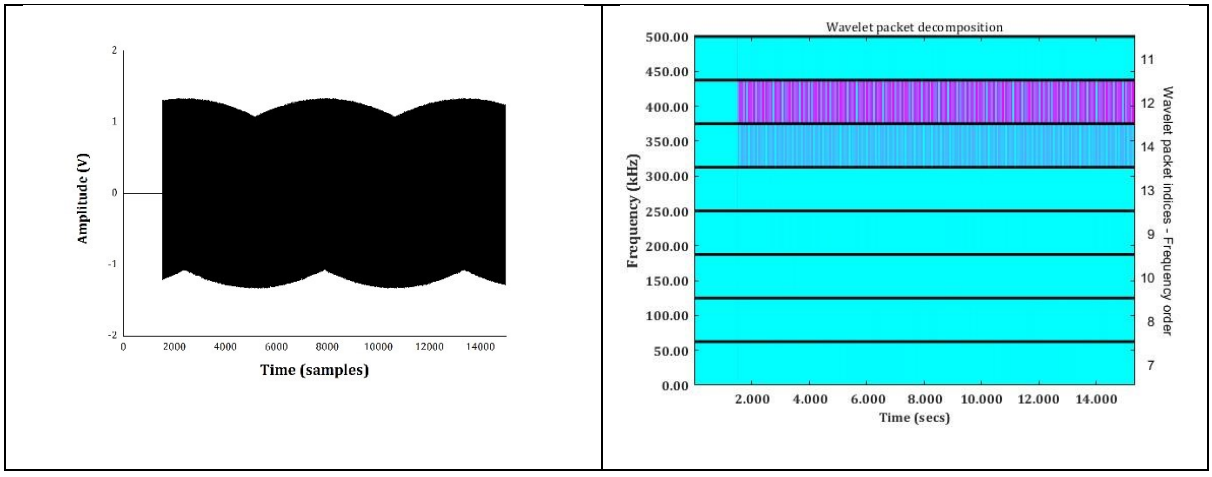

Figure1.3.5. Waveform recorded when sensor is coupled with Kapton tape.

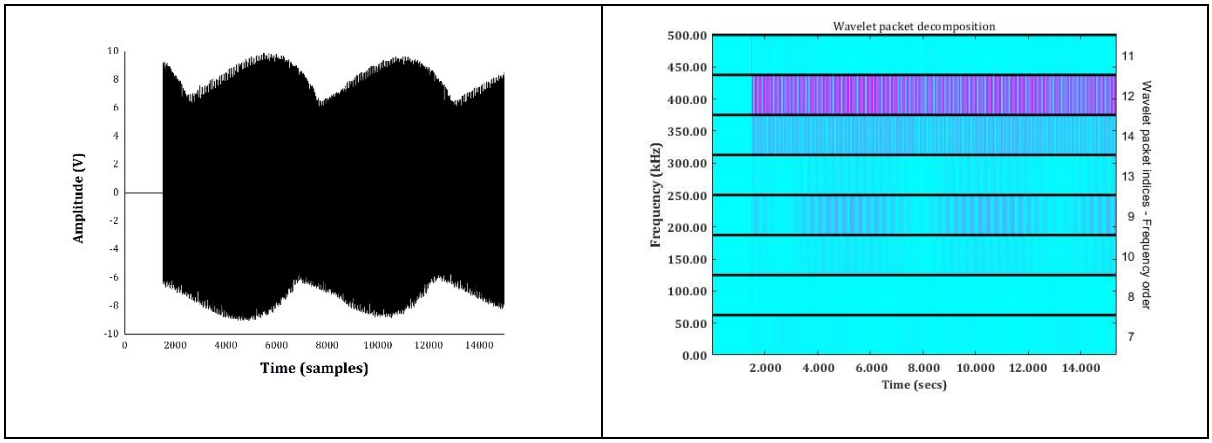

Figure 1.3.6. Waveform recorded when sensor is coupled with gel.

We performed also different tests with the Pico transducer put in direct contact with KP-S20 probe, using a 20 V voltage and, duration of 60 seconds and different frequency values: 400 kHz, 700 kHz, 800 kHz and 1,000 kHz. We verified that the KP-S20 probe presents 4 emission points.

Having verified the correct functioning of the probe, we evaluated how much the interposition of the base of the well interferes in the ultrasound transmission. We put a 60 mm diameter dish on the KP-S20 probe, and then we put the two different transducers inside the dish coupled with adhesive tape.

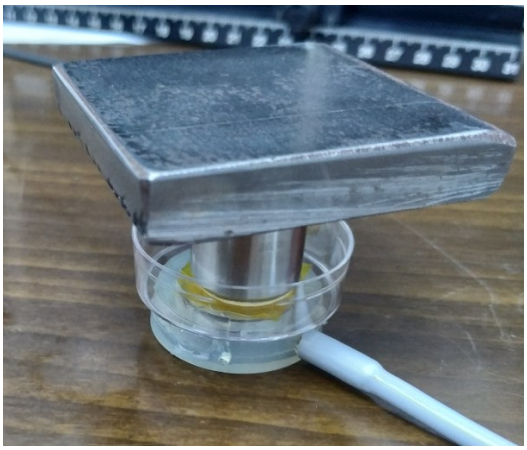

Figure 1.3.7. Setup realised to evaluate the ultrasound propagation through the bottom of a polystyrene dish.

We tested for 60 seconds and with 20 V voltage the following frequencies: 400 kHz, 700 kHz, 800 kHz, and 1,000 kHz. In this case, the transducer registered the same frequencies but with a lower amplitude than without dish.

Finally, we verified what is transmitted, in terms of ultrasound frequency and energy, through the dish. For this reason, we filled a 60 mm dish with water, than we put the Mistral transducer on the bottom on the dish and the KP-S20 probe on the top of the dish.

[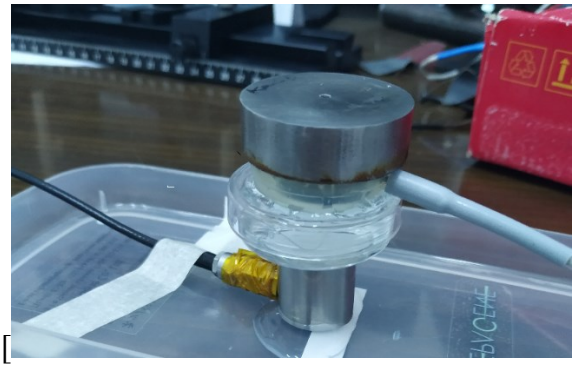

Figure1.3.8. Setup realised to evaluate the ultrasound propagation through a dish filled with water.

Even in this case, we tested for 60 seconds and with 20 V voltage the following frequencies: 400 kHz, 700 kHz, 800 kHz, and 1,000 kHz. Results showed that the transducer registered the same frequencies but with higher amplitude than without dish.

In conclusion, compared to the transducer placed directly on the probe configuration, results show that when dish and water are interposed, the amplitude and the energy are higher, due to resonant effects of the water, while, when only dish is interposed, the amplitude is lower and the energy is bigger.

1.3.3 Experimental study on low-intensity ultrasound effects on MG-63 cells

Osteosarcoma (OS) is the most common malignant primary bone tumour in children and adolescents with a 5-year survival of 68% [36]. OS has a bimodal age distribution, having the first peak during adolescence and the second peak in older adulthood with a male predominance [37]. Surgical tumour

resection and multi-agent chemotherapy based upon the backbone of cisplatin, doxorubicin and methotrexate (MTX) treatment are the main current therapeutic strategies for OS [38, 39]. Chemotherapeutic agents can overcome inherent tumour resistance, but considerable side effects are common and represent a major obstacle to effective treatment of OS [40]. In addition, patients with unrespectable primary tumours or clinically evident metastases have a poor prognosis, even in chemotherapy-responsive cases of osteosarcoma [41, 42]. The above discussion confirms the urgency of developing more effective and less toxic therapeutic protocols that can selectively act on cancer cells. Low-intensity pulsed ultrasound is a non-invasive ultrasound medical technology used to trigger bone formation and accelerate bone maturation in bone fractures [43, 44] or delayed fracture healing [45]. Literature data on the effects of low-intensity ultrasound on osteosarcoma cells appear to be limited. Matsuo et al. [46] demonstrated the positive effects of low-intensity ultrasound on cell viability, induction of apoptosis, modification of mitochondrial membrane potential and intracellular signaling molecules in the LM8 osteosarcoma cell line. This suggests that low-intensity ultrasound stimulation might be one of the treatments of metastatic bone tumor because of its non-invasiveness. The following paragraphs present the effects of low intensity ultrasound on the MG-63 osteosarcoma cell line.

The MG-63 cells were cultivated in Dulbecco's Modified Eagle Medium (DMEM) containing 10% Fetal Bovine Serum (FBS). $8x10^4$ cells/ml were seeded in T25 flasks and stored in an incubator at 37°C, under a standard mixture of 95% air and 5% CO_2. Upon reaching confluence, cells were detached with trypsin/EDTA, re-plated in six 60 mm Petri dishes, and stored in the incubator. Cell confluence was checked by a Nikon Eclipse Ti-U inverted microscope including a C1 Digital Eclipse modular confocal system.

The number of living cells was measured with a TC20 cell counter. Cells were detached from a 60 mm Petri dish again using trypsin/EDTA. Five µl of cultured cells treated with trypan blue were then put on a cell counting slide. Trypan blue selectively colors dead cells by permeating their membrane. With this method we found 100% living cell and a total count of 1.52×10^6 cells/ml. TC20 also allows to measure cell diameter which was found to vary between 10 and 15 µm.

Cells were sonicated at fixed frequencies for 180 s, using 10 Hz pulse repetition frequency, 50% duty cycle and a constant voltage of 60 V. The selected sonication frequencies were 400, 510, 582, 800 and 1.000 kHz. Ultrasounds were generated by a SonoPore K-TAC 4000 device, which has been presented in the previous paragraph.

Tests were executed introducing the KP-S20 probe in the Petri dish. The probe, in contact with the liquid solution but not immersed in it, was supported by an ad hoc designed structure. All experiments were executed directly on 60mm Petri dishes come to confluence, thus leaving cells in the attached configuration.

Figure 1.3.9. Experimental setup used for sonicating cells.

After each sonication, cells were detached with trypsin/EDTA and a 5 µl sample was put on a cell counting slide and treated with trypan blue. The trypan blue colored the dead cells. Each slide was put inside the TC20 cell counter. The cell counter evidenced information such as: total count (i.e. total of cells evaluated cell/ml); post test cells number (i.e. the number of cells presents at the end of sonication, this data was evaluated as percentage of cell counted at the end of test too).

Experimental data are reported in the following table. The following values were recorded for each sonication: frequency (kHz), total cell count (cells/ml) and cell count (cells/ml). The killing rate is calculated as the untreated live cells minus the treated live cells, divided by the number of total untreated cells.

Table 1.3.2. Results of experimental data and cell killing calculation.

Frequency (kHz)	Total count (cell/ml)	Live count (cell/ml)	Killing rate
0	1.520.000,00	1.520.000,00	-
400	989.000,00	962.000,00	0,35
510	1.180.000,00	1.160.000,00	0,22
582	1.080.000,00	1.050.000,00	0,29
800	831.000,00	831.000,00	0,45
1000	603.000,00	581.000,00	0,60

Killing rate significantly increases with frequency, especially at higher frequencies than 600 kHz. The 400 kHz is an outlier as there are much more dead/undetected cells than at higher frequencies. The following figure shows the variation of cell mortality with respect to sonication frequency.

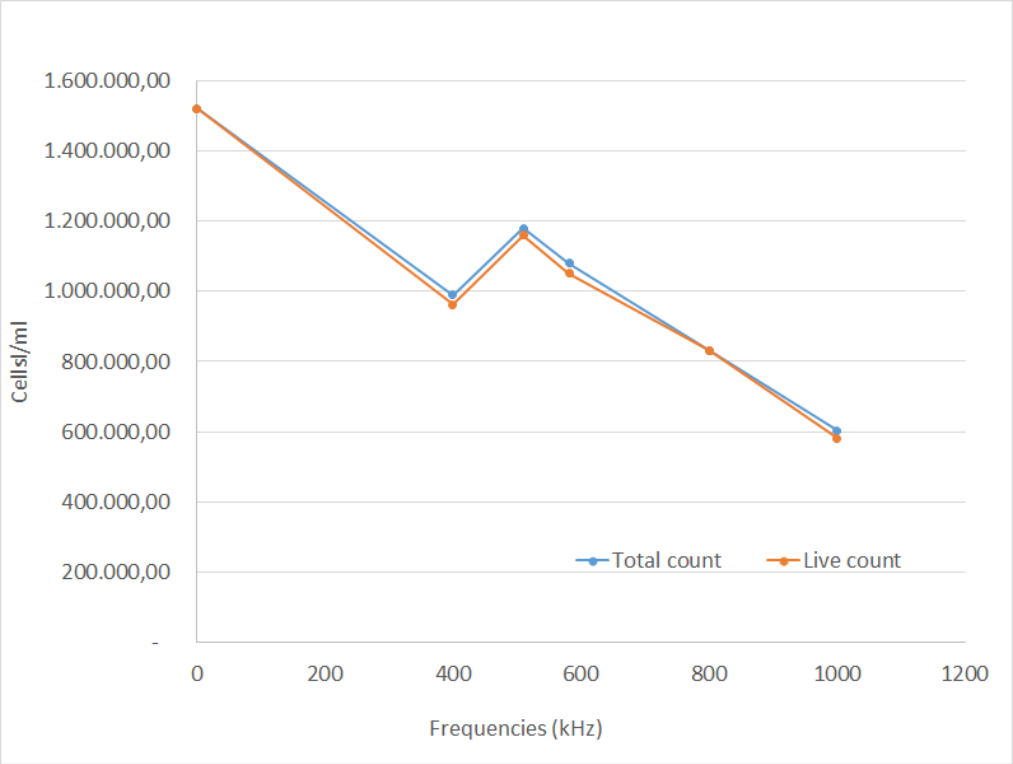

Figure 1.3.10. Variation of live cell concentration with the sonication frequency.

These experiments indicate that MG-63 cell mortality tends to increase with sonication frequency. However, several aspects remain to be explored. First, the variability of data obtained from Cell Counter requires more accurate investigations on cell killing rate. Moreover, it is important to evaluate cell proliferation after ultrasound treatment. Finally, it is necessary to evaluate possible presence of live cells in the culture medium, which could have been only detached and not killed by ultrasound treatment.

A first evaluation concerned the behaviour of the adherent cells in the period following the sonication. Researchers realised a time lapse video using an EVOS FL Microscope. Some cells were focused and their behaviour was recorded for an hour. It has been observed that cells, initially of elongated shape as they were attached, progressively assumed a round shape, temporarily losing their adhesion capacity.

Other important observations on the behaviour of cells after sonication were performed thanks to the Xcelligence instrument. The xCELLigence® RTCA DP instrument uses electrical impedance monitoring to quantify cell proliferation, morphology change, and attachment quality in a real-time

manner. The three cradles enable three separate electronic 16-well plates to be controlled and monitored.

Figure 1.3.11. The Xcelligence instrument with its three cradles.

Each well of the plate presents a set of gold microelectrodes fused to the well bottom. When submersed in an electrically conductive solution such as culture medium, the application of an electric potential across these electrodes causes an electron flow. The presence of adherent cells at the electrode-solution interface impedes electron flow.

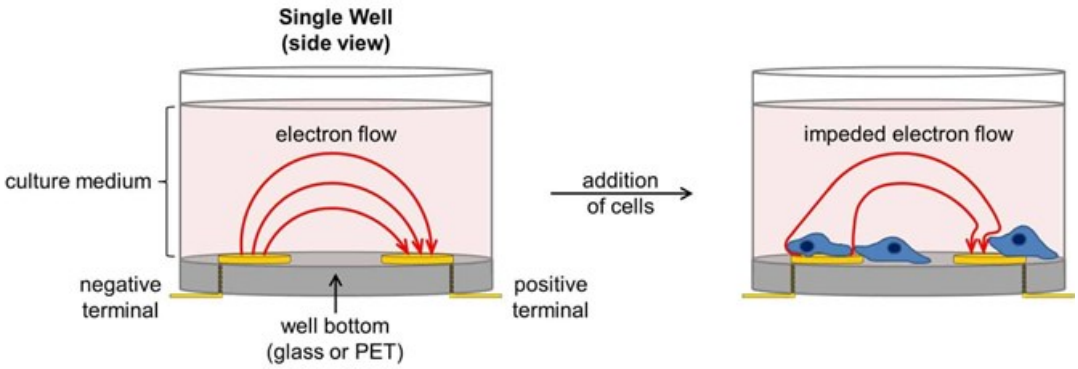

Figure 1.3.12. Representation of a single well of the E-plate used for Xcelligence measurement.

The impedance of electron flow caused by adherent cells is reported using a unitless parameter called Cell Index (CI):

$$\mathbf{CI} = \frac{(\mathbf{impedance\ at\ time\ point\ n} - \mathbf{\ impedance\ in\ the\ absence\ of\ cells})}{\mathbf{nominal\ impedance\ value}}$$

For the first few hours there is a rapid increase in impedance. This is caused by cells falling out of suspension, depositing onto the electrodes, and forming focal adhesions. When cells reach confluence the CI value plateaus, reflecting the fact that the electrode surface area that is accessible to bulk media is no longer changing.

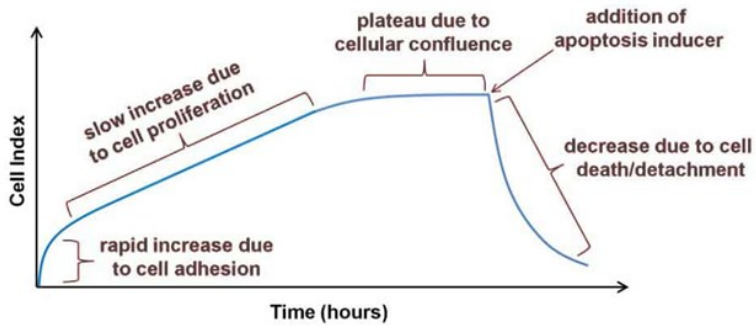

Figure 1.3.13. Typical trend of Cell Index for an apoptosis experiment.

Tests with Xcelligence were performed on MG-63 cell culture for the two ultrasound frequency values which gave the higher cell killing rate, 800 kHz and 1,000 kHz. Ultrasound were generated by the K-TAC 4000 device and emitted by the KP-S20 probe. Cells were cultured in 60 mm dishes and brought to confluence. Each dish was sonicated at fixed frequency, performing the test for 180 sec, with 60 V voltage, duty rate equal to 50% and burst rate equal to 10 Hz. We observed the variation of Cell Index for five different conditions:

- cells sonicated at 800 kHz (blue curves);
- cells sonicated at 1,000 kHz (brown curves);
- non-sonicated cells (red curves);
- cells suspended in the culture medium after sonication at 800 kHz (light blue curves);
- cells suspended in the culture medium after sonication at 1000 kHz (orange curves).

We tested two dishes for each condition, taking from each of them 3 samples. Each sample were subsequently cultured in the Xcelligence E-plate wells, and the Cell Index trend was registered for the following 72 hours.

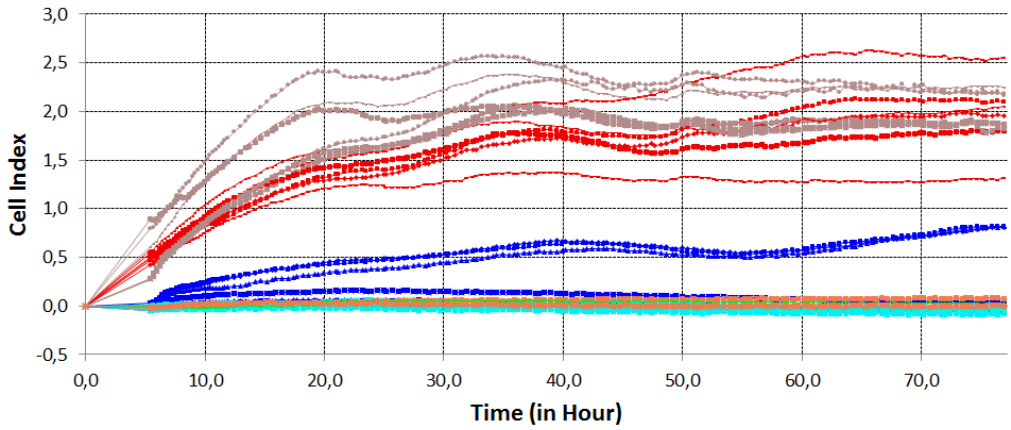

Figure 1.3.14. Cell index trend during 72 hours after sonication for: cells sonicated at 800 kHz (blue curves) and at 1,000 kHz (brown curves), non-sonicated cells (red curves), cells suspended in the culture medium after sonication at 800 kHz (light blue curves) and at 1000 kHz (orange curves).

The analysis of cell index trend for the conditions we evaluated allows to make several considerations. First, cells sonicated at 1 MHz have a high cell index, in some cases even greater than the non-sonicated cells. This data shows that cells not killed by sonication presents after the treatment high levels of cell proliferation. A second important result is the low level of cell index for cells sonicated at 800 kHz, equal to 0 for some well. This result shows that the treatment has some effects on cell proliferation. Finally, it is important to notice that cells suspended in the culture medium after sonication, both for 800 kHz and 1,000 kHz, present a cell index value equal to 0. This result allows to affirm that cells detached during ultrasound treatment have a cell proliferation equal to 0 and therefore these cells are irreversibly damaged or killed by the ultrasound waves.

1.3.4 Experimental study on low-intensity ultrasound effects on U937 cell line

U937 cell line is derived from malignant cells of a pleural effusion of 37-year-old Caucasian male with diffuse histiocytic lymphoma. In the previous chapter, several studies on low-intensity

ultrasound effects on U937 cell line were presented [23, 30], showing that it is possible to alter normal cellular behaviour by treating cells with ultrasound.

Previous experiments on U937 cells, performed by Polytechnic of Bari researchers in collaboration with Fukuoka University researchers [34], show that sonication at decreasing frequency in a range between 620 and 400 kHz, duty cycle 50%, burst rate 10 Hz, induces 80% cell killing rate after 180 s duration and another 13% apoptosis and 11% late apoptosis after 6-h incubation.

Further tests were carried out to evaluate the effects of fixed frequency ultrasound on U937 cell line. Cells were cultured in RPMI 1640 medium, supplemented with 10 % heat-inactivated foetal bovine serum, at 37°C in humidified air with 5 % CO2. Before starting the experiments, cells were centrifuged at 1500 rpm for 5 min and suspended in fresh medium at a final concentration of 10^6 cells/mL. Subsequently 2 mL were aliquoted in each well of a 12-well plate, in order to have $2 \cdot 10^6$ cells per well. We chose these plates because the diameter of each well is 20 mm, equal to the diameter of the KP-S20 probe. Ultrasounds were generated by a SonoPore K-TAC 4000 device, as for the MG63 cell line experiments. For each test, the probe was put on the basis of the well under treatment, coupled with a layer of gel.

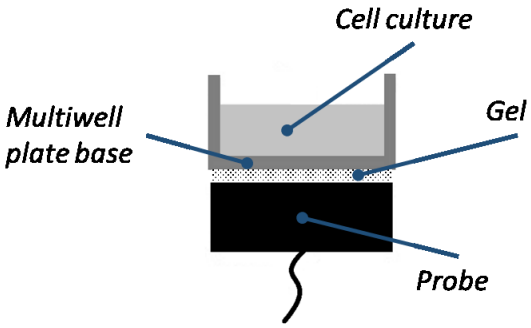

Figure 1.3.15 Representation of the sonication setup.

Moreover, for each set of parameters, tests were performed twice on the same day (biological double) and repeated on three different test days. Before starting tests, live cell count was equal to 97% and the medium diameter of cells was about 11µm, distributed as shown in the following figure.

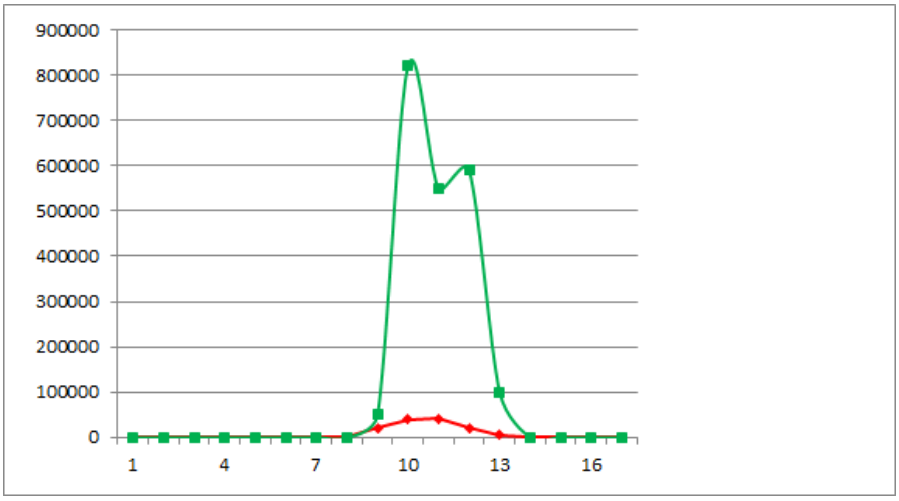

Figure 1.3.16. Number of U937 live (green) and death (red) untreated cells for each diameter (µm)

A first group of experiments was carried out to investigate the effects of different ultrasound frequency treatments for 180 seconds, 60 Volts, duty cycle equal to 50% and burst rate 10 Hz. The ultrasound frequency chosen were: 400 kHz, 600 kHz, 800 kHz and 1 MHz.

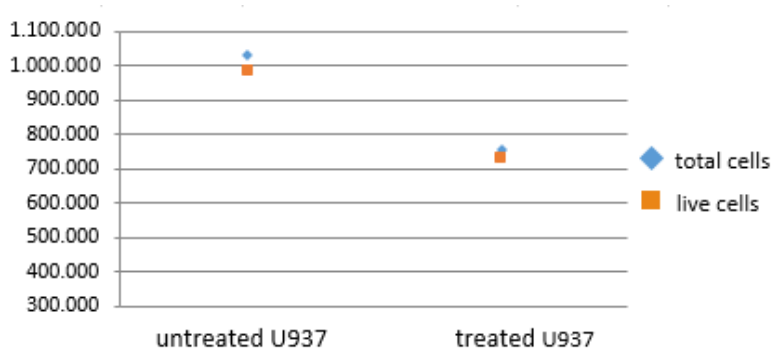

Figure 1.3.17. Number of total and live cells before and after treatment for 180 s with 400 kHz ultrasound, 60 V, 50% Duty cycle, 10 Hz burst rate.

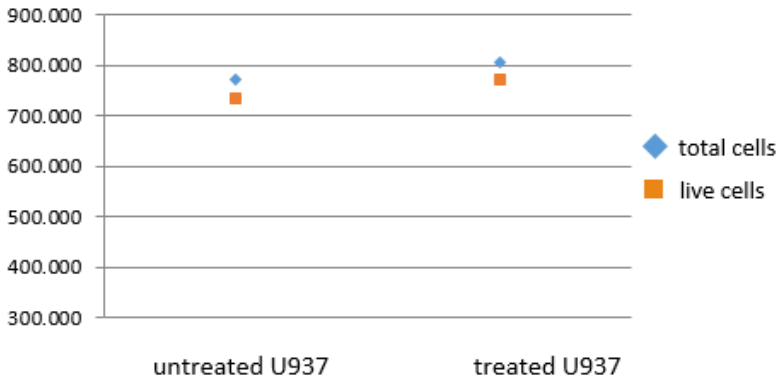

Figure 1.3.18. Number of total and live cells before and after treatment for 180 s with 600 kHz ultrasound, 60 V, 50% Duty cycle, 10 Hz burst rate.

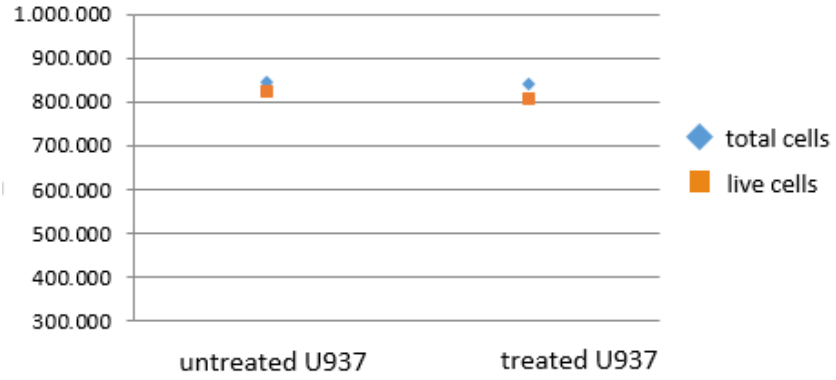

Figure 1.3.19. Number of total and live cells before and after treatment for 180 s with 800 kHz ultrasound, 60 V, 50% Duty cycle, 10 Hz burst rate.

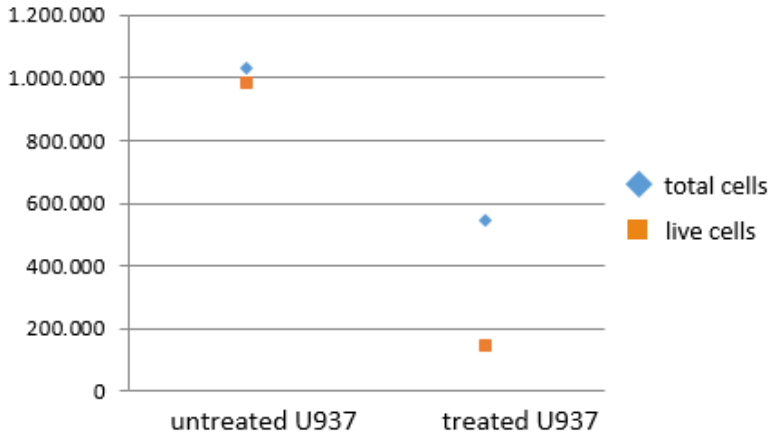

Figure 1.3.20. Number of total and live cells before and after treatment for 180 s with 1,000 kHz ultrasound, 60 V, 50% Duty cycle, 10 Hz burst rate.

For each treatment, the Cell mortality (%) was calculated as follows:

$$Cell\ mortality\ (\%) = \frac{(Number\ of untreated\ live\ cells) - (Number\ of\ treated\ live\ cells)}{(Number\ of\ untreated\ total\ cells)} \cdot 100$$

As shown in previous figures, only 1 MHz frequency presents high level of cell mortality, with a medium value of about 80%. Moreover, looking to the number of total cells counted by the TC20 instrument before and after sonication, we saw a drastic reduction of this number. This could mean that cells hit by ultrasonic waves fragment until they become undetectable by the TC20. We observed also that the medium diameter is reduced after sonication, as shown in the following picture, becoming about 4 micrometre.

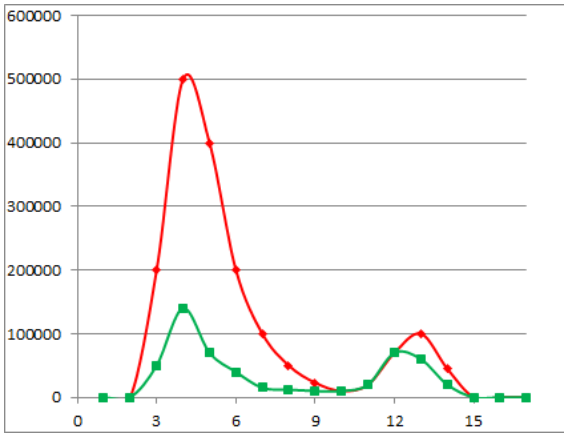

Figure 1.3.21. Distribution of the medium diameter (µm) for U937 live (green) and death (red) cells sonicated at 1 MHz.

It is important to notice that after sonication the temperature inside the wells treated at 1,000±50 kHz frequencies (180 s, 60 V, 50% duty cycle, 10 Hz burst rate) increase of about 10 ° C, accompanied by high levels of ultrasound intensity (> 7W / cm^2). To investigate the set of parameters able to maximize cell mortality without producing thermal effects, other experiments were conducted with lower values of voltage, keeping the frequency at 1 Mhz, with 50% duty cycle and 10 Hz burst rate. Different voltage values were evaluated: 30 V, 40 V and 50 V. With these voltage values, no thermal effects were found and ultrasound intensity was found to decrease considerably (<4 W/cm^2).

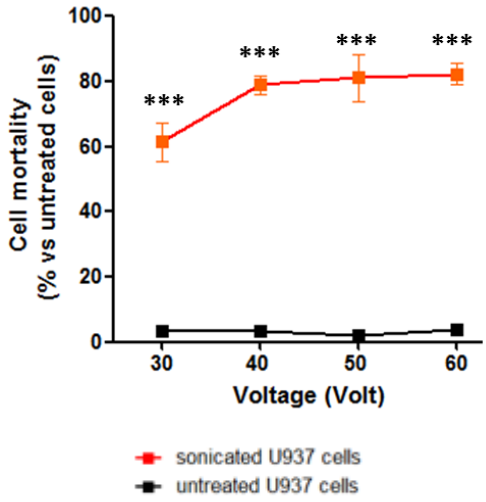

***p< 0.001, * p< 0.05 Two-Way ANOVA with Bonferroni post-test.

Figure 1.3.22. Trend of cell mortality as a function of ultrasound voltage.

Figure 1.3.22 shows that, sonication executed with 50 V and 40 V voltage values, the value of Cell mortality remains close to 80%, while sonication executed with 30 V voltage presents a considerable reduction of Cell mortality, which becomes equal to 60 %. Moreover, analyzing the temperature values after sonication at 40 and 50 V, it was found that sonication at 40 V determines the lowest temperature rise, so that it can be considered as the Voltage value which determined the best overall results.

After identifying the voltage that can maximize mortality without producing thermal effects, another group of experiments was conducted to investigate frequency values close to 1 Mhz, keeping all other parameters unchanged. The frequency values chosen were: 950 kHz, 1,000 kHz, 1,050 kHz, 1,100 kHz, 1,150 kHz, 1,200 kHz.

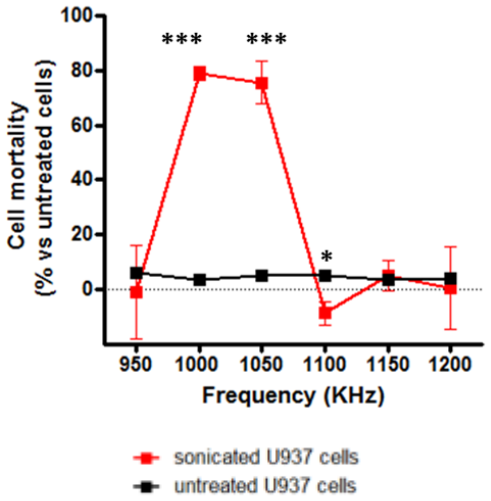

***p< 0.001, * p< 0.05 Two-Way ANOVA with Bonferroni post-test.

Figure 1.3.23. Trend of cell mortality as a function of ultrasound fixed frequency

As shown in Figure 1.3.23, the best values of Cell mortality were found for 1,000 kHz and 1,050 kHz. Moving away from this range, cell mortality decreases drastically.

After identifying the best frequency and voltage values, other tests were performed to investigate the effect of the duty cycle on Cell mortality. Therefore, tests were performed with duty cycle values equal to 75% and 100%, 1 Mhz frequency, 40 V, 10 Hz burst rate and 180 s duration.

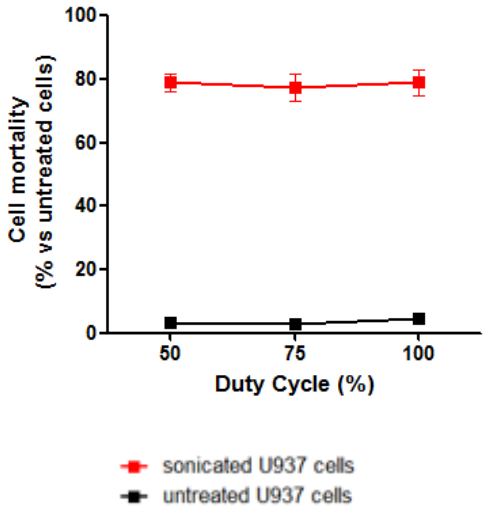

Figure 1.3.24. Trend of cell mortality as a function of ultrasound duty cycle.

Results shows that Cell mortality increase with duty cycle, with a 2 percentage point increase from 50% to 100%. However, increasing the duty cycle also causes the temperature inside the dish to increase.

Some considerations were also made regarding the duration of the treatment. In particular, the variation in Cell mortality was assessed when the duration of treatment doubled.

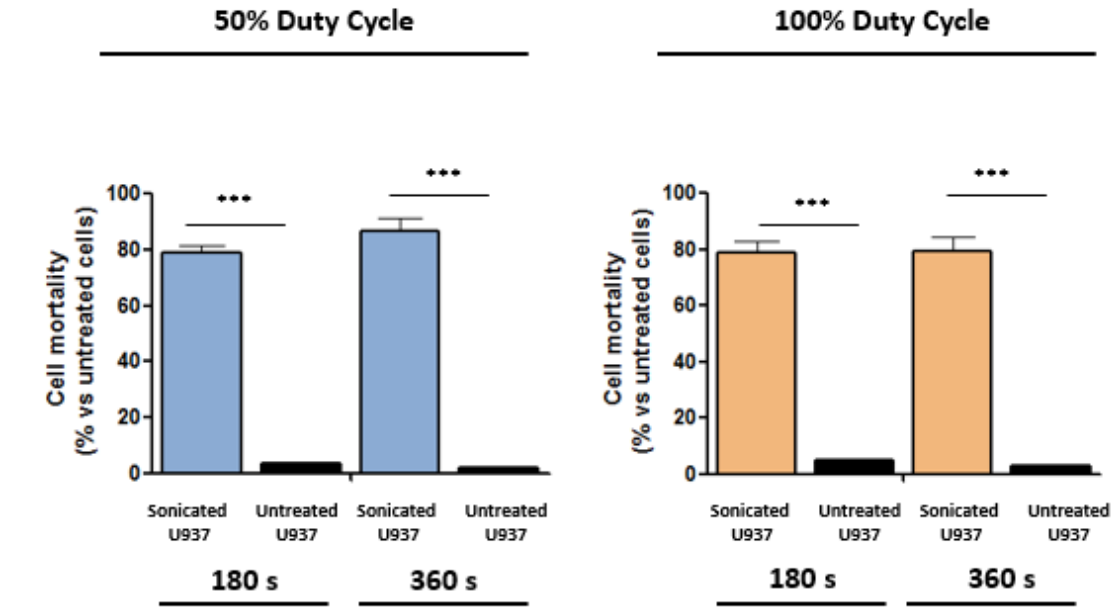

Figure 1.3.25. Dependence of cell mortality on Duty Cycle and Duration.

Results show that the increase in duration causes an increase in Cell mortality. This increase is bigger when the duty cycle is equal to 50% than when it is equal to 100%, as shown in Figure 1.3.25.

The following Table resume all the sonication conditions that allowed obtaining the best results in terms of Cell mortality.

Table 1.3.3. Mean and Standard Deviation of Cell Mortality (%) for the best sonication parameters.

	CELL MORTALITY (%)	
	Mean	**Standard Deviation**
Frequency: 1 MHz Voltage: 60 Volt Duration: 180 seconds Burst Rate: 10 Hz Duty cycle: 50%	82,26950612%	3,237793032
Frequency: 1 MHz Voltage: 50 Volt Duration: 180 seconds Burst Rate: 10 Hz Duty cycle: 50%	74,9778586%	7,713639922
Frequency: 1 MHz Voltage: 40 Volt Duration: 180 seconds Burst Rate: 10 Hz Duty cycle: 50%	76,817487%	4,874223523
Frequency: 1 MHz Voltage: 30 Volt Duration: 180 seconds Burst Rate: 10 Hz Duty cycle: 50%	61,47360889%	5,899174949
Frequency: 1 MHz Voltage: 40 Volt Duration: 180 seconds Burst Rate: 10 Hz Duty cycle: 75%	77,38996829%	4,141727535
Frequency: 1 MHz Voltage: 40 Volt Duration: 180 seconds Burst Rate: 10 Hz Duty cycle: 100%	78,97892107%	3,96143607

Frequency: 1,05 MHz Voltage: 40 Volt Duration: 180 seconds Burst Rate: 10 Hz Duty cycle: 50%	75,66687088%	7,91546518
Frequency: 1 MHz Voltage: 40 Volt Duration: 360 seconds Burst Rate: 10 Hz Duty cycle: 50%	84,37773934%	3,231104619
Frequency: 1 MHz Voltage: 40 Volt Duration: 360 seconds Burst Rate: 10 Hz Duty cycle: 100%	83,37443364%	1,79638697

Finally, some considerations were made on the ability of cells to proliferate after ultrasound treatment. Proliferation assay was performed for five sonication conditions and the number of live cells was measured using the TC20 instrument 48 hours, 120 hours and 168 hours after the treatment. For each of the considered sonication conditions, the proliferation test was performed in triplicate, on three different days. The following table shows the four sets of parameters considered and the relative results of the proliferation test.

Table 1.3.4. Proliferation assay for different sonication conditions.

1 MHz, 50 Volt, 180 seconds, 50% D.C., 10 Hz burst rate:				
	0 hours	**48 hours**	**120 hours**	**168 hours**
Number of live treated cells (Mean values, Cells/ml)	199.333,33	153.800,00	168.366,67	134.000,00

1 MHz, 40 Volt, 180 seconds, 50% D.C., 10 Hz burst rate:				
	0 hours	**48 hours**	**120 hours**	**168 hours**
Number of live treated cells (Mean values, Cells/ml)	239.000	152.000	160.967	97.933
1,05 MHz, 40 Volt 180 seconds, 50% D.C., 10 Hz burst rate:				
	0 hours	**48 hours**	**120 hours**	**168 hours**
Number of live treated cells (Mean values, Cells/ml)	231.667	130.600	143.000	77.900
1 MHz, 40 Volt, 180 seconds, 75% D.C., 10 Hz burst rate:				
	0 hours	**48 hours**	**120 hours**	**168 hours**
Number of live treated cells (Mean values, Cells/ml)	215.667	92.500	452.667	529.500
1 MHz, 40 Volt, 180 seconds, 100% DC, 10 Hz burst rate:				
	0 hours	**48 hours**	**120 hours**	**168 hours**
Number of live treated cells (Mean values, Cells/ml)	175.667	157.500	77.900	257.333
1 MHz, 40 Volt, 360 seconds, 50% DC, 10 Hz burst rate:				
	0 hours	**48 hours**	**120 hours**	**168 hours**
Number of live treated cells (Mean values, Cells/ml)	135.700	141.333	197.267	139.333

1 MHz, 40 Volt, 360 seconds, 100% DC, 10 Hz burst rate:				
	0 hours	**48 hours**	**120 hours**	**168 hours**
Number of live treated cells (Mean values, Cells/ml)	199.000	201.000	304.000	166.300

Results show that cells sonicated for 180 seconds with 50% duty cycle, frequency ranging between 1.00-1.05 MHz, voltage ranging between 40-50 V and 10 Hz burst rate have a significant reduction in cell proliferation. In particular, with 1.05 MHz ultrasound frequency, 40 Volt, 180 seconds, 50% duty cycle, 10 Hz burst rate sonication parameters, the average number of live cells 168 hours after treatment becomes one third of the number of living cells measured immediately after sonication. Finally, doubling the duration, the proliferation assay shows an initial increase in the number of living cells after 120 hours, which begins to decrease in the last 48 hours.

In conclusion, it was demonstrated that U937 cell culture sonicated for 180 s at frequency ranging between 1.00 – 1.05 MHz, 40 V, duty cycle 50% and burst rate 10 Hz induces more than 84% cell mortality immediately after treatment. Moreover, it has been shown that the increase in the duty cycle (>50%) leads to an increase in cell mortality after sonication, but does not give good results in terms of proliferation assay. Even the increase in duration leads to an increase in cell mortality after sonication, but does not give good results in terms of proliferation assay.
In the next studies, apoptosis will be evaluated for this cell line and the same experiments will be performed on the corresponding healthy cell line.

PART 2

ORTHODONTIC ALIGNERS AND THEIR MECHANICAL PROPERTIES

2.1 INVISIBLE ALIGNERS AND THEIR MECHANICAL BEHAVIOUR

Orthodontic therapy concerns the application of light and continuous forces to the teeth [47]. Every orthodontic treatment is based on the principle that prolonged application of pressure on a tooth determine its movement through a remodelling of the surrounding alveolar bone. The bone is reabsorbed on one side and selectively reconstructed on the other side, provoking tooth movement inside the bone. Since the bone response is mediated by the periodontal ligament, we could define tooth movement as a phenomenon primarily determined by this structure. The orthodontic forces applied on teeth can influence not only bone reconstruction and resorption, but also interfere with the action of skeletal structures distant from the teeth.

2.1.1 Biological response to the application of continuous orthodontic forces

Periodontal ligament (PDL) is a collagen support structure, which allows the attachment of the tooth to the surrounding alveolar bone, ensuring at the same time its isolation. PDL occupies a space of about 0.5 mm around the root of the tooth and it is composed principally by a set of parallel collagen fibres arranged next to root cement. These supporting fibres present an oblique pattern in the apical direction near tooth surface, in order to offer greater resistance to the forces occurring during normal masticatory activity.

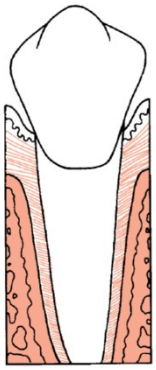

Figure 2.1.1. Schematic representation of periodontal structures.

In addition to the tangle of fibres, there are two other components of the periodontal ligament: the cellular component consisting of undifferentiated mesenchymal cells and tissue fluids. Both play an important role both during normal activity than in the orthodontic movement. Mesenchymal cells can differentiate in fibroblasts and osteoblasts. Osteoblasts and cementoclast can form new bone, while osteoclasts and cementoclasts can remove respectively alveolar bone and cement. Finally, fibroblasts produce new connective matrix, while fibroclasts destroy collagen previously deposed. The collagen in the periodontal ligament is constantly subjected to remodelling and renewal processes during normal activity, together with a continuous remodelling of the alveolar process and of the root cement. PDL presents cells of the blood system, nerve endings of amyelinic type and pressure receptors. Finally, it is important to note that the periodontal space is filled with a fluid able to absorb shocks under normal conditions.

During normal chewing activity, teeth are subject to heavy and intermittent forces, which range from 1 to 2 kg, for soft foods, up to 50 kg for harder foods. When the tooth is subjected to these loads, its rapid displacement in the PDL space is prevented by the presence of the fluid, which is incompressible. However, if a strong pressure is exerted on the tooth for a long time, the PDL fluid is released, and pain, necrosis of PDL cellular elements and “root resorption” occur. Lighter forces are compatible with the survival of PDL cells and induce painless remodelling of the dental alveolus through "frontal resorption". The orthodontic movement is possible thanks to the application of such forces.

The biological effect of an orthodontic force depends on its intensity and on the area of PDL on which it is exercised. Forces distribution on PDL depends on the type of orthodontic movement. There are types of orthodontic movement: tipping, body movement (translation), root straightening, rotation, extrusion and intrusion.

The simplest form of dental movement is tipping. This movement occurs when a single force is applied directly to the tooth crown. In this case the tooth rotates around its own "centre of resistance" located approximately at the middle of its root. When the tooth rotates in this direction, the PDL is compressed near the radicular apex and at the alveolar bone crest. Therefore, the maximum pressure is observed in these two areas and it gradually decreases moving towards the centre of resistance of the tooth.

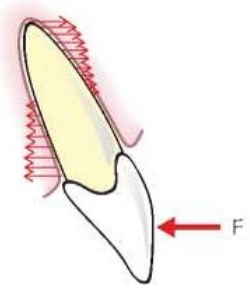

Figure 2.1.2. Representation of the tipping movement.

Body movement (translation) occur applying simultaneously two forces (couple) to the crown of the tooth. In this case the PDL area is compressed uniformly. In this case, to have the same pressure on the PDL and to induce the same biological answer, in the translation movement it is necessary to apply a force twice than in tipping movement.

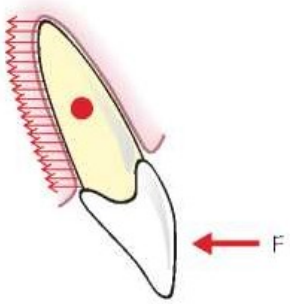

Figure 2.1.3. Representation of the translation movement.

Rotation movement is practically impossible to reproduce, as the force should be distributed over the entire surface of the PDL. Finally, extrusion and intrusion represent special cases of orthodontic movement.

The orthodontic movement of the teeth involves a remodelling of the alveolar bone and a real reorganization of the PDL. Depending on the intensity of the orthodontic forces, different unwanted biological effects could occur:

- excessive mobility and pain associated with orthodontic treatment;
- modest and transient pulp inflammation;

- effects on the root structure with particular regard to root shortening, which can occur in three different forms: moderate generalized reabsorption, severe generalized reabsorption, severe localized reabsorption.
- effects on the alveolar bone level.

The analysis of forces, moments and pressure points has long been of great interest in orthodontics. Wolf [48], Moss [49] and Von Limbourg [50] explained how pressure models the bone, directs its growth, and orients the trabeculae, and that anomalous pressure from the lips and cheeks is a determining factor in the genesis of malocclusion. Indeed, the surrounding soft tissues influence tooth position, in particular, the resting equilibrium established by the perioral muscles and tongue. Once this equilibrium is affected by external factors such as bad habits or orthodontic forces, the position of the teeth is altered. The literature informs us that an optimal system of forces produces an optimal reaction in the periodontal ligament [51]. However, there are different opinions regarding the nature of the force that is translated into optimal mechanical conditions within the periodontal ligament for orthodontic tooth movement, and the concept of optimal force has changed considerably over the years. For example, Schwarz [52] defined an optimal continuous force, which provokes a change in tissue pressure similar to the blood pressure in the capillaries in the periodontal ligament, thereby impeding their occlusion. However, optimal force is more commonly defined as that which generates a maximum rate of orthodontic movement, without damaging the surrounding tissues or causing patient discomfort. This force, however, will vary among both patients and individual teeth [47]. In fact, in 2003, a review by Kuijpers-Jagtman highlighted four fundamental obstacles to defining the concept of optimal force: the difficulty in precisely calculating the distribution of forces in the periodontal ligament with respect to the forces applied; the type of movement and the rate at which this is achieved; the variability in the stress distribution in function of uncontrolled tooth movement; the confusion regarding the relationship between force and rate of tooth movement (considering that orthodontic tooth movement can be divided into several phases (Burstone)) [53]; and the great inter-individual variability in both animals and humans (Von Bohl et al. and Maltha et al.) [53, 54].

4.2 Orthodontic devices

Orthodontic forces are explained by specific devices designed by the orthodontist. These medical devices allow the straightening and realignment of the teeth, with consequent aesthetic and functional improvement of problems such as irregular or crooked teeth, or malocclusions. It is important to

design orthodontic devices able to produce a system of forces neither too high nor too variable over time. Forces must not diminish too quickly, due to a loss of elasticity of the material used or to an excessive change in the amount of force expressed after tooth movement. In designing an orthodontic system, it is necessary to consider both the behaviour of the material and the mechanical factors involved in the dental response.

There are several fixed, mobile or even transparent orthodontic devices. The fixed appliances presents different shapes depending on the needs and the corrective actions to be implemented. They can be vestibular or lingual, depending on whether they are installed on the external or internal surface of the teeth. Today there are aesthetic orthodontic devices [55, 56, 57], as the brackets can also be manufactured in ceramic or transparent materials. Mobile devices can be inserted or removed independently by the patients, and they are used to improve dental occlusion or to "maintain" the position of already straightened teeth after removal of the fixed device.

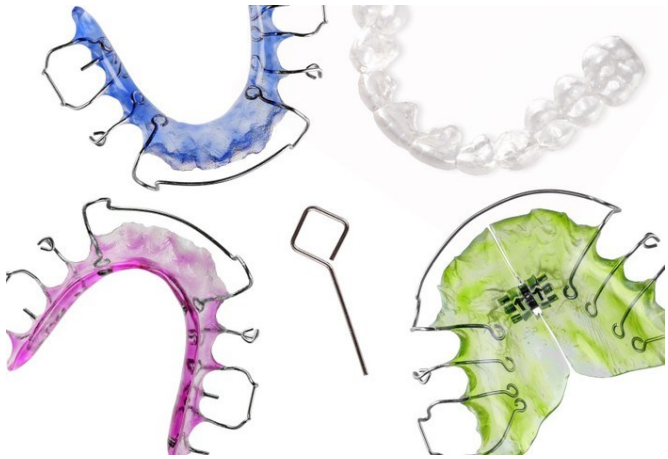

Figure 2.1.4. Several fixed, mobile or even transparent orthodontic devices.

More recently, invisible orthodontic devices were designed and marketed, called clear aligners [58]. These devices are especially suited for aesthetic orthodontic treatment in adult patients. They are used for orthodontic treatment in many types of malocclusion [59-62]. Ideally, aligners are worn for 22 h per day, being removed only for eating and for oral hygiene procedures. They are generally replaced every 7 or 14 days, with the consequent application of new pressures on the teeth [63]. This type of treatment is hygienic [64], reduces the perception of pain [65] and for this reason, generates more collaboration from the patients [66]. Moreover, they may be used also in combination with composite

attachments on some teeth [67, 68], in order to direct and concentrate the forces in certain areas of the dental arch. Nowadays, there are various types of aligners, and their characteristics are strongly influenced by their construction material, thickness and fit [69]. These devices are produced in various materials: Polyurethane (SmartTrack®) [70], Polyethylene Terephthalate Glycol-modified (PET-G), Polycarbonate (PC), Thermoplastic Polyurethanes (TPU), Ethylene Vinyl Acetate, Polyethylene Terephthalate (PET), and other materials [71].

Many studies evaluated the clinical effectiveness of clear aligner, but some aspects remain to be investigated [72-74]. In the following chapter, studies on two specific aspects not yet completely known will be presented: the dimensional modification and stability of clear aligner during the 15 days wear period and the maximum value of force exerted by an aligner.

2.2 EXPERIMENTAL STUDY ON INVISIBLE ALIGNERS

2.2.1 Experimental Studies of the Pressures and Points of Application of the Forces Exerted between Aligner and Tooth

In this study [75] we evaluated the specific pressures exert by invisible aligners on teeth, and the areas where these are applied. A secondary objective of this study was to evaluate reproducibility of the pressures exerted, taking into consideration manufacture-related variables.

We performed intraoral scans (TRIOS-3Shape) on a patient with molar and canine Class I and optimal alignment and levelling before (T0) and after (T1) 2º vestibularisation of the right upper central incisor with a centre of resistance 10 mm from the alveolar crest. Six digital models in STL format were generated using 3Shape OrthoAnalyzer® software (TRIOS 3Shape, Copenhagen, Denmark), 3 at T0 and 3 at T1.

Figure 2.2.1. T0 and T1 models. The white arrows indicate the analysed element, before and after moving with aligners.

These were in turn used to 3D print low-viscosity resin casts (E-Denstone Material) with a resolution of 35 microns, in a controlled environment at a constant temperature of 140 °C, by means of an

EnvisionTEC 3D printer (Desktop XL, PixCera, Perfactory® 4DDP4 Series- Gladbeck, Germany-Dearborn, Michigan, MI, USA). Before making the aligners, a 180-micron housing for the pressure sensor was created on the surface of the 1.1 and the corresponding gingival area on the casts. This procedure was carried out using a dedicated and extremely precise software (SINERGIA, Nobil-Metal®) in order to allow subsequent recordings to be as realistic and faithful as possible. The modified casts were then used as moulds for six aligners, three identical active (A1, A2, A3) for the prescribed movement, and three passive (P1, P2, P3) for calibration purposes. The aligners used in this study were F22 (Sweden and Martina Due Carrarae, Padua, Italy), made of thermoplastic polyurethane (TPU) with 0.75 mm thickness.

In order to measure the pressures transmitted by the aligners to the tooth, we inserted Fuji Prescale Film[76-79], a chemically treated PET film which is very sensitive to applied pressure, into the housing previously created. The film responds to pressure by turning from white to different shades of red and the colour density indicates the amount of pressure applied, thereby providing a kind of pressure map of the tooth surface. In order to optimise this technology for different operational pressures, Fuji Film has defined three measurement fields with specific ranges of action. In this study we used the Low Pressure (LP) film (2.5–10 MPa) for the active phase and Super Low Pressure (SLP) film (0.5–2.5 MPa) for the passive phase.

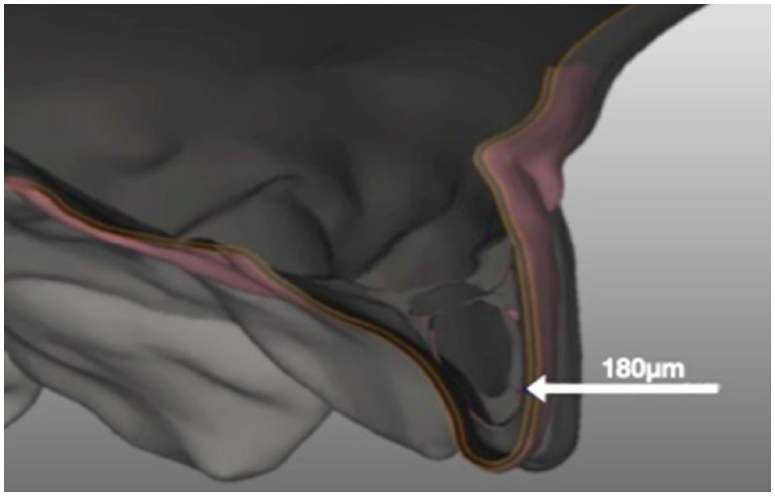

Figure 2.2.2. Sinergia software images generated to create the 180-micron pressure-film housing. The bright lines indicate exactly the thickness of 180 µm eliminated from the 3D model.

Films were removed 15 s after their application and subsequently analysed. The minimum area that can be measured is 0.1 mm^2, as the relative distribution of the uniform Fuji Prescale Film microcapsules is 0.1 mm^2 [76]. However, an accurate analysis of exposed Prescale film was carried out using an FPD-8010E analysis system (Fuji Film, Tokyo, Japan). This method involves scanning the exposed Prescale films, digitising the resulting scans, and storing the images prior to analysis [76, 77]. This system is accurate and repeatable, and enabled us to measure both the area and the degree of pressures exerted simultaneously [76].As in this study we focused on an aligner programmed to exert an active vestibulo-lingual force on the right upper central incisor, we examined the pressure map of the vestibular surface of the same tooth in all cases. Indeed, the upper central incisor has the flattest and most regular vestibular surface, making it suitable for this experiment, which was comprised of two major phases: calibration with three passive aligners (P1, P2 and P3) and analysis of the active phase with three active aligners (A1, A2 and A3). Calibration was carried out for all three passive aligners (P1, P2 and P3) on the cast at T0. The Super Low Pressure Film (SLP—0.5 to 2.5 MPa) was positioned in the 180-micron housing in the vestibular surface of the cast, and the aligner was fitted and kept in place for 15 s, before removing the aligner and mapping the film. In total, ten pressure films were obtained for each aligner in order to obtain mean and maximum calibration values to later be subtracted from the active pressure values subsequently obtained. Thus, all measurements were performed ten times, each by a sole operator on three aligners with identical programmed movements on a single cast (cast A at T0). The maximum pressure recorded during the passive phase was 1.46 ± 0.50 MPa. The calibration areas were 1.5 × 1.5 mm^2 each.

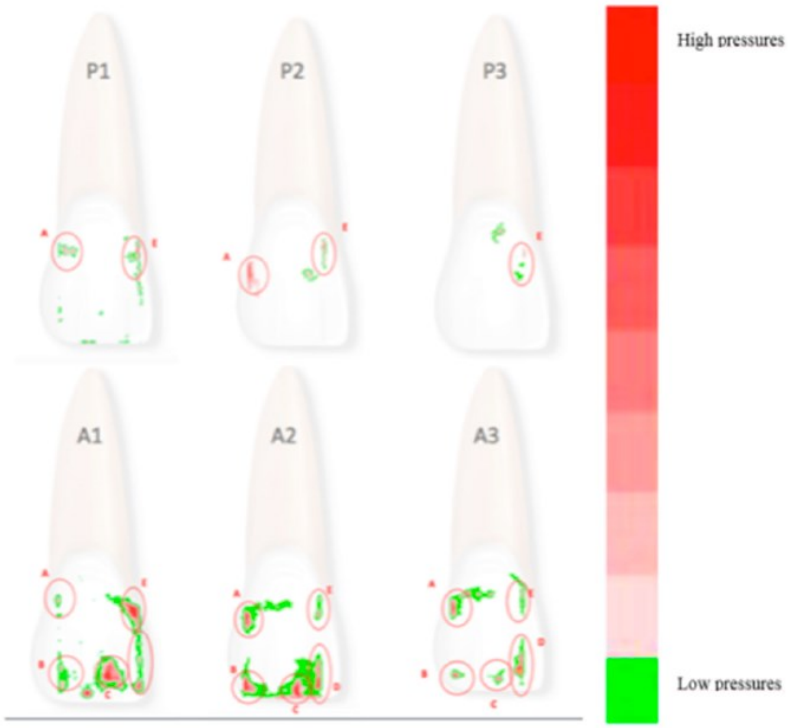

Figure 2.2.3. P1, P2 and P3: areas of pressure revealed by Super Low Pressure (SLP) film with passive aligners. A1-A2-A3: areas of pressure revealed by Low Pressure (LP) film with active aligners. The different colours correspond to different pressure values.

Table 2.2.1. Mean and maximum pressure obtained for the three passive aligners (P1, P2 and P3) during the calibration phase.

	P1					**P2**					**P3**				
Pressure areas	**A**	**B**	**C**	**D**	**E**	**A**	**B**	**C**	**D**	**E**	**A**	**B**	**C**	**D**	**E**
Mean pressure (MPa)	0.64	0.00	0.00	0.00	0.66	0.78	0.00	0.00	0.00	0.00	0.00	0.00	0.00	0.00	0.51
Maximum pressure (MPa)	1.29	0.00	0.00	0.00	1.34	1.46	0.00	0.00	0.00	0.00	0.00	0.00	0.00	0.00	1.01

The active analysis was carried out in the same way, ten times for each of the three identical active aligners (A1, A2 and A3) on a single cast (model A in T0) by a sole operator, but this time using a film able to register greater pressures, i.e., Prescale Low Pressure Film (LP—2.5 to 12.75 MPa).

Table 2.2.2. Pressure values obtained for the three active aligners (A1, A2 and A3), raw data.

	A1					A2					A3				
Pressure areas	A	B	C	D	E	A	B	C	D	E	A	B	C	D	E
Mean pressure exerted (raw data)(MPa)	3.43	2.65	3.43	3.26	2.96	1.56	3.05	3.91	3.48	2.63	2.06	5.58	4.05	2.43	4.53
Maximum pressure exerted (raw data)(MPa)	8.03	5.03	6.66	8.06	5.54	3.36	8.13	10.82	10.11	7.05	4.41	8.86	7.89	5.83	8.90

We then compared the coordinates of the active and passive pressures to ensure that the calibration areas were perfectly superimposed (with reference to Cartesian axes corresponding to the mesial surface and incisal margin of tooth 1.1). Using FPD-8010E software, we then calculated the mean and maximum pressures exerted by the active aligners on these areas with respect to the passive calibration data. Not all of the active areas of pressure were associated with areas of pressure exerted during the passive phase.

Table 2.2.3. Mean values calibrated of the three active aligners. Active areas did not always have corresponding passive areas.

	A1					**A2**					**A3**				
Pressure areas	**A**	**B**	**C**	**D**	**E**	**A**	**B**	**C**	**D**	**E**	**A**	**B**	**C**	**D**	**E**
Mean values calibrated (MPa)	2.79	2.65	3.43	3.26	2.90	0.78	3.05	3.91	3.48	2.63	2.06	5.58	4.05	2.43	4.02

Hypothesising that the vestibular surface of the tooth examined was flat (i.e., that the tooth was a parallelepiped), and that the forces exerted by the aligner are parallel and perpendicular to the tooth surface, the total net force exerted by each of the three aligners was calculated; areas of pressure measuring 1 × 1 mm2 were considered, using the adjusted mean pressure (i.e., the mean active pressure minus the mean passive pressure) calculated for each. The modulus of the resulting force was then calculated using Equation (1), assuming that the force was applied at the centre of the area of pressure.

$$F = PxA \qquad (1)$$

The point of application of the net force exerted on the entire surface of the tooth was determined by calculating the net force from the first two forces, and adding each of the net forces identified in turn. The net of two parallel forces was found to be applied at a certain point, P, which was identified via the following proportion:

$$d1: d2 = F1: F2 \qquad (2)$$

where, d1 and d2 indicate, respectively, the distance from point P to the points of application F1 and F2. If the forces are in agreement, point P will be located on the straight line that joins the points of application F1 and F2, and the net force modulus will be given by the sum of the force moduli for F1 and F2 as follows:

$$FTot = F1 + F2 \qquad (3)$$

As the Tables show, there was variability among the aligners studied, despite all efforts to standardise the study protocol. Indeed, the pressure distribution displayed by the three aligners was similar, but not identical, even in the calibration phase. However, the mean net pressure exerted across the entire tooth surface by the active aligners remained constant at roughly 15 MPa. The coordinates of the 5 areas of pressure were also almost identical, and coincide when superimposed (Figure 3). The overall similarity between aligners is confirmed by visual comparison of their respective pressure maps, but the numerical values obtained show that there were differences between the three. In particular, the following table reveals the differences between the three aligners in terms of net force and its point

of application (with reference to a Cartesian grid whose origin is at the junction of the surface and incisal margin of the tooth). It should be noted that the net force calculated in this way is based on an idealised (i.e., flat) coronal surface (Figure 4), and that the crown itself is not a free parallelepiped, but, together with its root, is part of a system containing supporting structures (i.e., the periodontal ligament and underlying bone).

Table 2.2.4. Values for resulting force and their points of application on the three active aligners studied.

	POINT OF APPLICATION OF NET FORCE	**MODULUS OF NET FORCE**
Aligner 1	(3; 3.11)	13.96 N
Aligner 2	(2.93; 2.15)	13.87 N
Aligner 3	(2.87; 2.44)	17.49 N

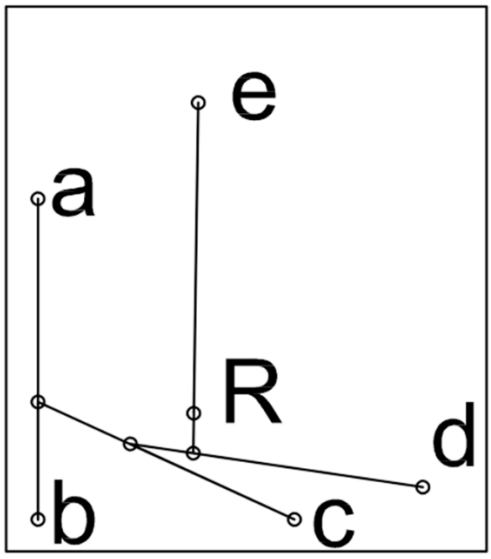

Figure 2.2.4. Calculation of the resulting force exerted by Aligner 2 on the vestibular surface of the tooth.

The letters a, b, c, d, e, respectively indicate the points of application of the forces exerted by the pressure areas A, B, C, D, E, while the letter R indicates the point of application of the resulting total force exerted by the aligner on the tooth. A power analysis to evaluate the sample size was performed by using the G*Power software. The hypothesis that net force experienced by active aligners 1 and 2 is equal was analysed with a confidence level of 0.95, and the effect size of the sample was found to be $d = 0.82$ corresponding to a power of the test equal to $p = 0.99$. A post hoc power analysis was performed on the comparison between aligners 2 and 3 as well; an effect size of $d = 2.248$ was found, corresponding to a power $p = 0.997$ for the hypothesis that the net force between the two aligners is different. If a priori analysis on the sample size is performed, a minimum sample dimension equal to 9 is found. These considerations justify, from a statistical point of view, the proper choice of the sample size. The difference in the response among the three passive aligners was tested from a statistical point of view. Figure 3 and Table 1 show some differences in several regions of the specimen. In fact, while no pressure is observed in areas B, C and D for all three of the specimens, differences are observed for that which concerns areas A and E. To test if the difference of observed pressure in area A in the P1 and P2 sample, a t-student analysis was performed on the set of ten measurements obtained for each sample. The t-value was found to be 4.16, so the recorded pressures can be considered different with a significance level $p < 0.01$. Analogously, if area E is compared for passive aligners P1 and P3, a t student value $t = 6.65$ is found, showing that recorded pressures in those areas can be considered different at a significance level $p < 0.01$. Results about mean pressure recorded in the five regions of interest for the three active aligners are summarised in Table 2. The level of significance for all of the regions was tested for A1, A2 and A3, considering the ten measurements performed on the three specimens. For all of the three specimens, the t student test demonstrated a significant difference ($p < 0.05$) among the values observed in the three specimens, with the only exception of region C. As a further analysis, the test was repeated, with reference to region A and C, to calibrated values, as obtained by subtracting the passive aligner values from the active aligners. Additionally, in this case a significant difference ($p < 0.05$) was observed. Finally, a statistical comparison was performed on the calculated net force. Ten values of net force were compared for each active aligner. When the net force was compared for aligners A1 and A2, a t-student value $t = 1.85$ was found with a significance level $P = 0.08$. This shows that, even if a different distribution of the forces is present, it corresponds to the same level of net force. A different result is found if the third aligner is compared; in this case, a statistically significant difference ($p < 0.01$) can be observed.

Although the literature presents several articles on in-vitro and in-vivo studies of the forces exerted by orthodontic appliances, it is difficult to compare our analysis with any of these, due to the innovative methodology we employed. Furthermore, the majority of studies considered the force applied, but not the pressure exerted. For example, Elkholy [80, 81] studied the forces applied during palatal or labial movement of a central incisor (upper jaw model Frasaco, Tettnang, Germany) using a force/moment sensor (Nano 17, ATI Industrial Automation, Apex, NC, USA). The aligners studied by Elkholy were made of Duran® of thickness 0.50, 0.625 and 0.75 mm. These yielded different force values, especially as regards the measurements of movements from the palatal side. Li [82] conducted a study using aligner materials and sensors different to ours, and even if we compare their results with those reported for the same thickness of the same aligner material at the same time-point by Elkholy, there are no similarities; indeed, the numerical variation is as high as 5 units. Although the sensors they used were different, this cannot entirely explain the discrepancies between their respective results. Another study that we could consider is that by Hahn [83]. They focused on central incisor torque, but reported values on three spatial planes, thereby allowing conversion of angular parameters into millimetres. As their torque measurements were expressed as palatal, vestibular and vertical intrusion forces, it is theoretically possible to compare the values they reported for vestibularisation and palatalisation with those reported by the abovementioned authors. However, even though the same sensor and unit of measurement were used, Hahn took measurements at time 0, while the others reported measurements taken after 30 min, 1 h or several days from aligner fitting, with obvious ramifications for the measurement of forces. Furthermore, the orthodontic movement considered by Hahn was 0.15 mm, while in the other studies it was 0.25 mm. The study which is most similar to ours was reported in an article by Barbagallo [84] in 2007. They calculated the force exerted by an aligner during 0.5-mm vestibulo-lingual movement of a first premolar. They also used a pressure-sensitive film, Fuji Pressurex, but not the scanner we used to reveal the pressure values exerted on the film itself. Instead, they relied on a light microscope (SZ-FO Dissecting Microscope, Olympus, Japan) connected to a digital camera (Color View Soft Imaging System, Olympus, Japan), and the resulting images were then analysed by means of a spectrophotometer. Moreover, their study was conducted in-vivo, and they reported results as forces rather than pressure. Barbagallo et al. [84] reported a mean force exerted by the aligner on the premolar was 28.09 ± 5.64 N at 15 s from its application. However, the authors subtracted from this raw figure a series of variables associated with the sensor, the anatomy of the analysed tooth and its anatomical location (although the details of this process were not fully specified). Pressure films are extremely sensitive. Using them directly inside the oral cavity (without counting the thickness of the film itself) would have led to the creation of

strengths that were not really present. Our intent is to describe the areas of applications and maximum pressures. Therefore, we know the perfect areas and we know that the pressures in the oral cavity, thanks to the periodontal ligament, will certainly be lower than those obtained. Hence, the historical concept of low and continuous forces in orthodontics. Moreover, it should be considered that, to avoid performing approximations of purely mathematical value and to focus instead on the raw measured data, our final values are reported in relation to the coronal area of the tooth analysed, which we treated as a parallelepiped. The net force on the tooth crown we calculated does therefore not wholly correspond to the force exerted by the aligner on a real tooth, which is supported by the surrounding soft and hard tissues. Indeed, the ultimate aim of our analysis was not so much to calculate the final force, but rather to determine whether "identical" aligners exerted the same force on the same tooth while performing the same movement. It should be observed that, when comparing aligners A1 and A2 a different distribution of the solicitations can be observed when the five regions of interest are considered. However, if the net force is analysed, the two samples behave in a similar way. Different observations should be made for sample A3, wherein a statistically significant difference is observed. This can be attributed to variations in the 3D printing and manufacturing of the aligners. Despite this, it should be noted that difference is nonetheless acceptable according to the orthodontics practice.

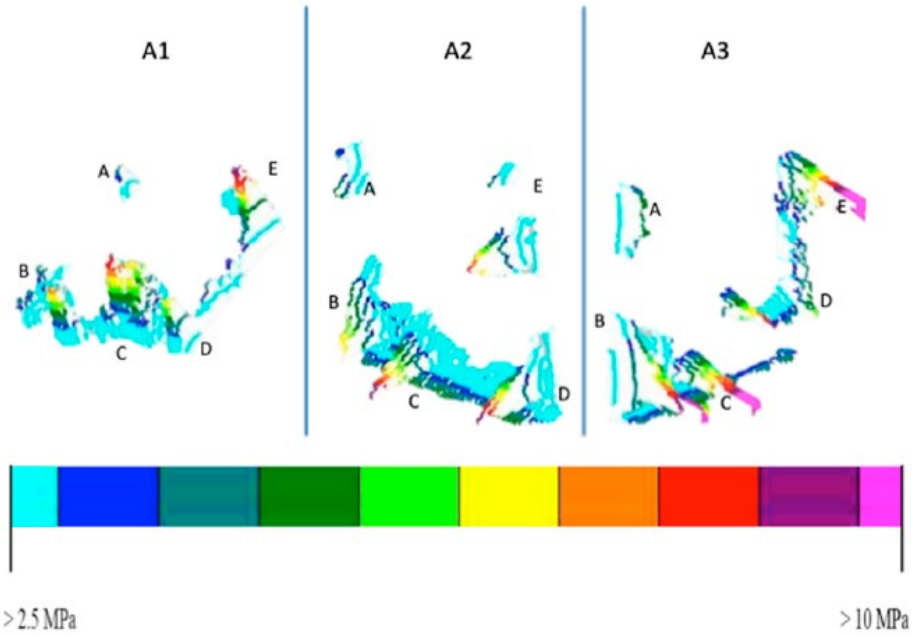

Figure 2.2.5. The 3D images of the 3 aligners, analysed as if they exerted pressure on the surface of parallelepiped. The colours shown in the figure indicate the various pressure variations. Green indicates lower pressures while yellow and red indicate higher pressures.

This study, having been performed in vitro and not in vivo, has limitations due to the difficulty of reproducing the environment present in the oral cavity. This has always been dictated by the fact that the sensor is extremely sensitive and therefore its direct application in the oral cavity would have considerably reduced the level of precision in the measurements.

The areas of pressure exerted by the three aligners analysed were similar, but not perfectly superimposable and therefore not entirely reproducible, likely due to manufacturing and methodological variables. That being said, the pressure exerted on the tooth to be moved was almost identical across all tests conducted. On the whole, the pressure, and hence the forces exerted during orthodontic aligner treatment, appear to be controlled and reproducible, and have a mean value of roughly 15 MPa.

2.2.2 Comparison of the Stress Strain Capacity between Different Clear Aligners

The aim of the present study [85] was to evaluate the dimensional stability of clear aligners after two types of stresses: in-vivo stress during 15 days wear-time, and in-vitro compressive strain.

One patient (male, 29 years of age) at the Orthodontic department of University of Foggia was selected and enrolled in the present study. The participant provided written informed consent to be involved in the study. The patient presented a moderate crowding of upper and lower incisors, no prosthetic rehabilitation, no fillings, no oral parafunctions, no Temporo- Mandibular Joint disorders, no periodontal infection and good oral hygiene.

Patient's impressions were taken with Polyvinilsylossane material and sent to three different CA manufacturers to obtain a clinical setup and a set of aligners. This allowed to obtain three different sets of CA made of different materials: the SmartTrack® (Align Technology), PET-G, and PET. No attachments were used to increase the aligner's stability. The thermoforming procedures in the present study were performed under the respective manufacturer's recommended conditions, and all the aligners had the same thickness of 0.8 mm. The first aligner of each set was programmed as a passive aligner, without any tooth movement. Three copies of the first aligner were requested to each manufacturer, to have three samples of each material: One to be used in-vivo, one to be tested in-vitro, and one to be used as a control.

One aligner of each material was worn by the patients for 15 days, 22 hours per day. A wash-out period of two-weeks was used between each use with different aligners of a different manufacturer. The patient was instructed to wear the aligner for the recommended time, and to remove it during meals, during oral-hygiene procedures, and during the assumption of any liquids except water. The aligners were cleaned using only cold water and a soft toothbrush.

An additional set of patient's impressions was used to produce a dental cast used for in-vitro testing. Dental casts were poured on a custom-made resin base, designed to be easily secured to the Instron machine.

Figure 2.2.6. Resin models secured to the Instron machine.

One aligner of each material was set on the dental cast, then the casts were settled into occlusion and secured to an Instron 3343 universal testing machine with a loading cell of 1kN. A compressive force of 50N was applied during a 6 seconds increase, then applied constantly for 15 minutes.

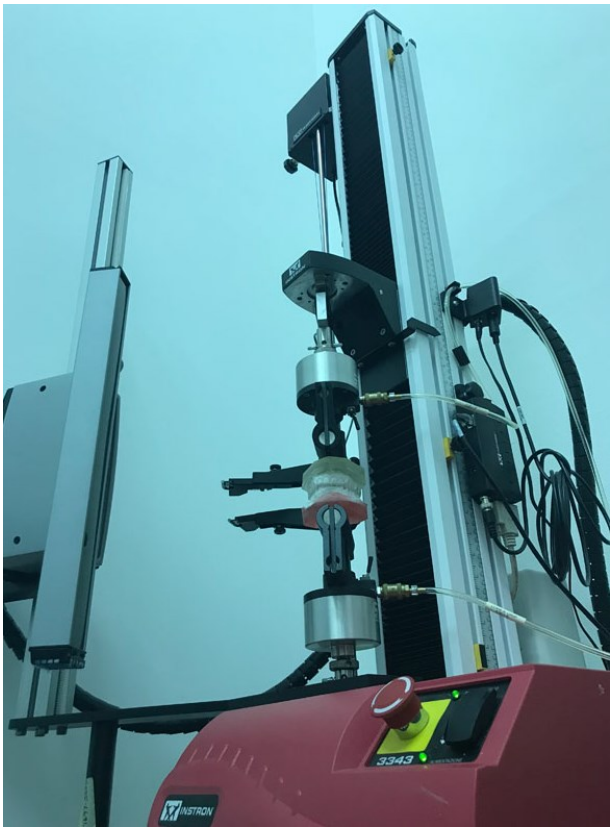

Figure 2.2.7. Instron machine used for static stress.

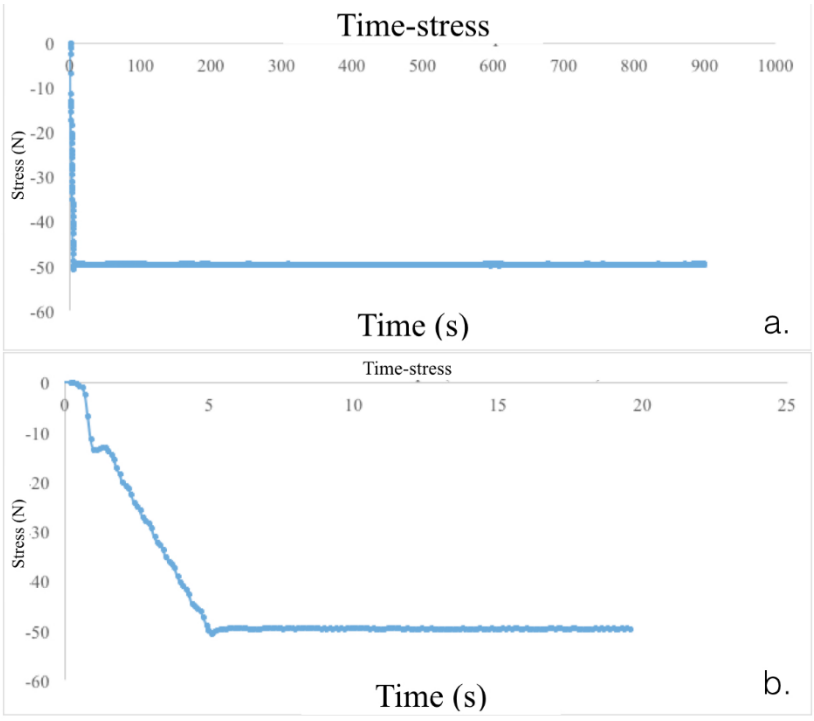

Figure 2.2.8. Stress-Time diagram.

At the end of the test, the tested and control aligners were covered with a 3D scan spray (Helling 3D Spray) then scanned using a laboratory scanner (3 Shape Scanlt Manager tps .Ink, 3Shape, Copenhagen, Denmark). The scanned aligners were evaluated with a dedicated software (3 Shape Orthoviewer, 3 Shape, Copenhagen, Denmark). Two points were identified on right and left first molar (posterior area), first premolar (middle area), and canine (anterior area): vestibular apical point of dental crown, defined as "base of the tooth point" (BoT point), and the intersection point of vertical and horizontal axis, defined "facial axis point" (FA point). The authors measured the distance between right and left BoT points on first molar, first premolar, and canine, and the distance between right and left FA points for the same teeth. These measurements were used to compare the dimensional stability of CA after in-vivo dynamic stress and invitro static stress within each material, and between different CA materials. To have a summary value for every material, the distances at the anterior, middle, and posterior parts for both in-vivo and in-vitro tested aligners were pooled and mean and standard deviation were calculated.

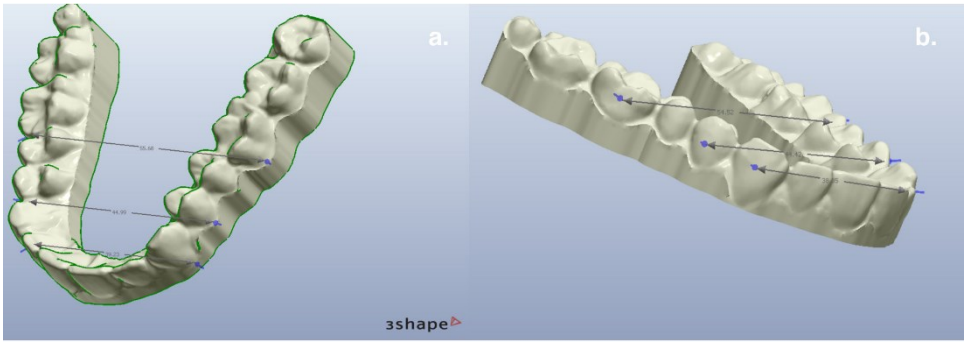

Figure 2.2.9. Clear aligners scanned in Ortho Viewer.

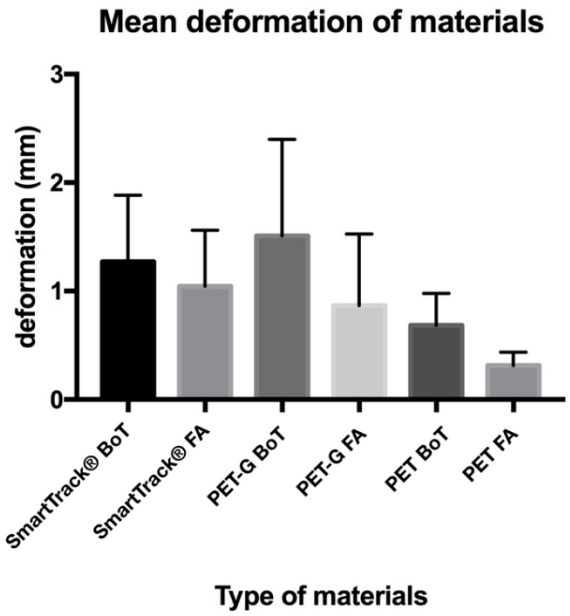

Figure 2.2.10. Mean deformation of materials.

The differences at the BoT point and at the FA point are shown in Tables 5.5 and 5.6. Both Smart track® and PET-G presented at the BoT point the same deformation in dynamic and static stresses. PET had the lowest deformation at the BoT point and at FA point than the PET-G and Smart Track®. The difference was higher in the posterior part than the anterior part. SmartTrack® showed higher deformations than the PET in the static and dynamic test. PETG had less deformation in the anterior area than the other materials. Examining the summary values of each material, in general PET showed the smallest deformation, followed by SmartTrack® and PET-G (Tables 5.8 and 5.9).

Table 2.2.5. Evaluation of BoT point of teeth distance in upper first molar, upper first pre-molar and upper first canine subject a dynamic (patient) and static (instron) stress with different materials.

Teeth Distance	Upper First Molar (16-26)			Upper First Pre-Molar (14-24)		Upper First Canine (13-23)	
Base-line distance in BoT point (mm)	54,5			43,8		38,3	
Smart Track®	Test	Patient Stress	Instron Stress	Patient Stress	Instron Stress	Patient Stress	Instron Stress
	Value (mm)	56.66	55.69	45.47	45.02	38.97	38.84
	Difference	+ 2,16	+1,19	+1,67	+1,4	+0.67	+0.54
PET-G	Test	Patient Stress	Instron Stress	Patient Stress	Instron Stress	Patient Stress	Instron Stress
	Value (mm)	57.46	56.27	45.43	45.30	38.66	39.13
	Difference	+2,96	+1.77	+1,63	+1,5	+0,36	+0.83

Teeth Distance	Upper First Molar (16-26)			Upper First Pre-Molar (14-24)		Upper First Canine (13-23)	
PET	Test	Patient Stress	Instron Stress	Patient Stress	Instron Stress	Patient Stress	Instron Stress
	Value (mm)	55.02	55.38	44.60	44.90	38.81	38.59
	Difference	+0,52	+0.88	+0,8	+1.1	+0,51	+0.29

Table 2.2.6. Evaluation of FA point of teeth distance in upper first molar, upper first pre-molar and upper first canine subject a dynamic (patient) and static (instron) stress with different materials.

-	Upper First Molar (16-26)			Upper First Pre-Molar (14-24)		Upper First Canine (13-23)	
Base-line distance in FA point (mm)	54,1			43,8		37,7	
Smart Track®	Test	Patient Stress	Instron Stress	Patient Stress	Instron Stress	Patient Stress	Instron Stress
	Value (mm)	56.11	55.20	44.84	44.66	38.21	38.51
	Difference	+ 2,01	+1,1	+1,04	+0,8	+0.51	+0.81
PET-G	Test	Patient Stress	Instron Stress	Patient Stress	Instron Stress	Patient Stress	Instron Stress
	Value (mm)	56.21	54.73	44.86	44.44	38.12	38.04
	Difference	+2,11	+0.63	+1,06	+0,64	+0,42	+0.34
PET	Test	Patient Stress	Instron Stress	Patient Stress	Instron Stress	Patient Stress	Instron Stress
	Value (mm)	54.89	54.59	44.04	44.07	38.00	38.26
	Difference	+0,79	+0.49	+0,24	+0,27	+0,3	+0.56

Table 2.2.7. Static and Dynamic evaluation of the differentials obtained on tested materials.

-	BoT Point						FA Point					
-	Upper First Molar		Upper First Pre-Molar		Upper First Canine		Upper First Molar		Upper First Pre-Molar		Upper First Canine	
-	Dynamic	Static	Dynamic	Static	Dynamic	Static	Dynamic	Static	Dynamic	Static	Dynamic	Static
SmartTrack®	+ 2,16	+1,19	+1,67	+1,4	+0.67	+0.54	+ 2.01	+1,1	+1,04	+0,8	+0,51	+0,81
PET-G	+2,96	+1.77	+1,63	+1,5	+0,36	+0.83	+2,11	+0,63	+1,06	+0,64	+0,42	+0,34
PET	+0,52	+0.88	+0,8	+1.1	+0,51	+0.29	+0,24	+0,27	+0,3	+0,56	+0,24	+0,27

Table 2.2.8. Summary values of pooled data for dimensional measurements at BoT point.

BoT Point	SmartTrack®	PET-G	PET
Mean (mm)	1,27	1,51	0,68
Std. Deviation	0,6	0,9	0,3
Std. Error of Mean	0,2	0,4	0,1

Table 2.2.9. Summary values of pooled data for dimensional measurements at FA point.

FA Point	SmartTrack®	PET-G	PET
Mean (mm)	1,04	0,87	0,31
Std. Deviation	0,5	0,7	0,1
Std. Error of Mean	0,2	0,3	0,1

The first set up dental movement was described by Kesling [86] in 1945. The use of occlusal splint in the upper and lower arch with a sequence of aligners induce a tooth movement which solves a malocclusion. The first aligners used were too stiff and thus produced hard forces on teeth; double-layer foils replaced the single-layer foils featuring a highly elastic layer on the inner side of the aligner [87]. One of the greatest advantages is better oral hygiene during orthodontic treatment for both adults and adolescents. On the other hand, the level of patient compliance is the greatest disadvantage. For this reason, many manufacturers introduced a compliance indicator on aligners [88], to evaluate the effective use of the CA. The dental movement may not be adequate for three reasons: the lack of patient's compliance, the planning of an excessive amount of dental movement, the inadequate transfer of the dental movement from the aligners to the tooth [89].

The planning of an excessive amount of dental movement is one of the causes of CA failure. Some manufacturers apply an amount of tooth movement ranging from 0,5 to 1 mm with a single step [90], while others plan tooth movements of 0.1-0,2 mm with a single aligner [91]. The use of smaller tooth movement steps is proven to increase the efficacy of the CA treatment and to provide a reduction of the relapse tendency [92]. As many studies have shown, the efficacy of CA treatment depends also on the type of the programmed tooth movements, since rotations and torquing movements are less predictable than others, although additional mechanics can be used to overcome such limitations of CA, like the use of miniscrews [93, 94], elastics, or cantilever mechanics [95]. The efficacy of the aligner treatment may be also influenced by the deformation of the CA during the 15 days treatment period. In the present paper, the authors evaluated the CA structure deformation following in-vivo stress (the patient worn the CA for 15 days) and in-vitro static stress with a force of 50 N for 15 minutes. The deformation was evaluated at the posterior part of the CA (i.e. at the first molars of BoT point and FA point), in the middle part (i.e. at the first premolars of BoT point and FA point) and in the anterior part (i.e. at the canine of BoT point and FA point). The best performance evaluated was that of the Polyethylenterephthalat (PET). All materials presented a reduction of deformation passing from the posterior part to the anterior part both at the BoT point and FA point. The mean deformation at the BoT point was of 1.27 mm (SmartTrack®), 1.51 mm (PET-G) and 0.68 mm (PET); at the FA

point, the mean deformation was of 1.04 mm (SmartTrack ®), 0.87 mm (PET-G) and 0.31 mm (PET). Barbagallo et al., suggest that the deformation of the CA is related to a possible change in the mechanical properties of the aligner foils due to hygroscopic expansion caused by the presence of saliva and the different elastic rebound behavior of the displacement teeth due to their elastic anchorage to the Periodontal Ligament (PDL) [84]. The present experimental setup allowed to isolate the effects of the oral cavity environment (i.e. the oral temperature and the saliva adsorption) from the effects of pure mechanical stress (i.e. the effects of biting force, simulated by an Instron machine). Previous studies tried to simulate the saliva contact with artificial saliva spray [96]. Ryokawa et al [97] measured the changes in thickness of the thermoplastic materials with thermoforming and water adsorption. The range of modification after thermoforming and water absorption was: thickness change from 74.9% to 92.6%, linear expansion from 100.3% to 119.9%. In the present study, the materials showed a higher deformation following the 15 days contact with saliva. The deformation decreased from the posterior to the anterior part both in dynamic test (with human saliva contact) and in static test (i.e. static stress test). PET showed an opposite behavior, with an increase of deformation from the posterior to the anterior part. The difference was higher from the posterior part to the middle part. A contraction of PET was evaluated following the dynamic test, suggesting that PET had a volume reduction following the contact with human saliva, rather than an expansion.

Investigations about aligners must continue to find the best compromise between chemical properties, mechanical properties, aesthetics, and patient comfort. The balance between mechanics and aesthetics must also increase the reliability of these intraoral devices in order to improve the predictability of dental movement.

BIBLIOGRAPHY

1. Turner W. The cell theory, past and present. J Anat Physiol. 1890, Vol. 24, pp. 253-87.
2. Kim-Campbell N., Gomez H., Bayir H. Cell Death Pathways: Apoptosis and Regulated Necrosis. *Critical Care Nephrology* 2019, pp. 113-121.
3. Tang S.K.Y., Marshall W.F. Self-repairing cells: How single cells heal membrane ruptures and restore lost structures. *Science* 2017, Volume 356, pp. 1022–1025.
4. Streuli C. Extracellular matrix remodelling and cellular differentiation. *Current Opinion in Cell Biology* 1999, Vol. 11, pp. 634–640.
5. Weinberg R.A. The biology of cancer. *Garland Science* 2006.
6. D. Hanahan, R.A. Weinberg. The Hallmarks of Cancer. *Cell* 2000, Vol. 100, pp. 57–70.
7. L. Luzzatto. The mechanisms of neoplastic transformation. *European Journal of Cancer* 2001, Vol. 37, pp. 114–117.
8. S.E. Cross, Y. Jin, J. Rao, J.K. Gimzewski. Nanomechanical analysis of cells from cancer patients. *Nature Nanotechnology* 2007, Vol. 2, pp. 780-783.
9. Xu W., Mezencev R., Kim B., Wang L., McDonald J., Sulchek T. Cell Stiffness Is a Biomarker of the Metastatic Potential of Ovarian Cancer Cells. PLoS ONE 7(10): e46609. doi:10.1371/journal.pone.0046609
10. Luo Q., Kuang D., Zhang B., Song G. Cell stiffness determined by atomic force microscopy and its correlation with cell motility. BBA - General Subjects 2016, doi: 10.1016/j.bbagen.2016.06.010
11. https://www.cancer.gov/about-cancer/treatment/types
12. S. Sengupta, V.K. Balla. A review on the use of magnetic fields and ultrasound for non-invasive cancer treatment. *Journal of Advanced Research* 2018, Vol. 14, pp. 97-111.
13. F. Maman, Quando la musica guarisce. Amrita 2001.
14. Crocetti S., Beyer C., Schade G., Egli M., Fröhlich J., Franco-Obregón A. Low intensity and frequency pulsed electromagnetic fields selectively impair breast cancer cell viability. PLoS One. 2013;8(9):e72944.
15. P. Meleady, R. O'Connor. General Procedures for Cell Culture. Cell Biology (Third Edition) 2006, Vol. 1, pp. 13-20.

16. G. Kossoff. Basic Physics and Imaging Characteristics of Ultrasound. *World J. Surg*. 2000, Vol.24, pp. 134–142.
17. Bushberg, et al. The Essential Physics of Medical Imaging. *Williams & Wilkins,* 2001.
18. Fowlkes J.B. American Institute of Ultrasound in Medicine consensus report on potential bioeffects of diagnostic ultrasound: Executive summary. *J. Ultrasound Med.* 2008, Volume 27, pp. 503–515.
19. Krasovitski B., Frenkel V., Shoham S., Kimmel E. Intramembrane cavitation as a unifying mechanism for ultrasound-induced bioeffects. Proceedings of the National Academy of Sciences of the United States of America 2011, Volume 108, pp. 3258-3263.
20. Zhang T., Chen L., Zhang S., Xu Y., Fan Y., Zhang L. Effects of high-intensity focused ultrasound on cisplatin-resistant human lung adenocarcinoma in vitro and in vivo. *Acta Biochim. Biophys. Sin.* 2017, pp. 1–7.
21. Lentacker I., De Cock I., Deckers R., De Smedt S.C., Moonen C.T.W. Understanding ultrasound induced sonoporation: Definitions and underlying mechanisms. *Advanced Drug Delivery Reviews* 2014, Volume 72, pp. 49–64.
22. Zhao L., Feng Y., Shi A., Zong Y., Wan M. Apoptosis induced by microbubble-assisted acoustic cavitation in K562 cells: the predominant role of the Cyclosporin A-dependent mitochondrial permeability transition pore. *Ultrasound in Med. & Biol.* 2015, pp. 1–10.
23. Feril L.B., Kondo T. Biological Effects of Low Intensity Ultrasound: The Mechanism Involved, and its Implications on Therapy and on Biosafety of Ultrasound. *J. Radiat. Res.* 2004, Volume 4, pp. 479-489.
24. Mizrahi N., Zhou E.H., Lenormand G., Krishnan R., Weihs D., Butler J.P., Weitz D.A., Fredberg J.J., Kimmela E. Low intensity ultrasound perturbs cytoskeleton dynamics. *Soft Matter* 2012, Volume 8, pp. 2438-2443.
25. T.M. Louw, G. Budhiraja, H.J. Viljoen, A. Subramanian. Mechanotransduction of ultrasound is frequency dependent below the cavitation threshold. Ultrasound in Med. & Biol. 2013, Vol. 39, pp. 1303–1319.
26. Sato M., Nagata K., Kuroda S., Horiuchi S., Nakamura T., Karima M., Inubushi T., Tanaka E. Low-Intensity Pulsed Ultrasound Activates Integrin-Mediated Mechanotransduction Pathway in Synovial Cells. *Annals of Biomedical Engineering* 2014, Vol. 40, pp. 2156–2163.
27. Miller A.D., Chama A., Louw T.M., Subramanian A., Viljoen H.J. Frequency sensitive mechanism in low-intensity ultrasound enhanced bioeffects. PLoS ONE 2017, Volume 12, e0181717.

28. Furusawa Y., Kondo T. DNA Damage Induced by Ultrasound and Cellular Responses. *Mol. Biol.* 2017, Volume 6, pp. 1-6.
29. Feril L.B., Kondo T., Ogawa R., Zhao Q. Dose-dependent inhibition of ultrasound-induced cell killing and free radical production by carbon dioxide. *Ultrasonics Sonochemistry* 2003, Volume 10, pp. 81–84.
30. Feril L.B., Kondo T. Major factors involved in the inhibition of ultrasound-induced free radical production and cell killing by pre-sonication incubation or by high cell density. *Ultrasonics Sonochemistry* 2005, Volume 12, pp. 353–357.
31. Kinoshita M., Hynynen K. Key Factors That Affect Sonoporation Efficiency in in vitro Settings; The Importance of Standing Wave in Sonoporation. *Biochem Biophys Res Commun*. 2007, Vol. 359(4), pp. 860–865.
32. Hensel K, Mienkina M.P., Schmitz G. Analysis of ultrasound fields in cell culture wells for in vitro ultrasound therapy experiments. Ultrasound Med Biol. 2011, Vol. 37(12), pp. 2105-15.
33. Hrazdira, I., J. Skorpikova, and M. Dolnikova, Ultrasonically induced alterations of cultured tumour cells. *Eur J Ultrasound*, 1998. 8(1): p. 43-9.
34. Ivone, M., Pappalettere C., Tachibana K. Study of cellular response induced by low intensity ultrasound frequency sweep pattern on myelomonocytic lymphoma U937 cells. *J Ultrasound*, 2016. 19(3), pp. 167-74.
35. Lagneaux, L., et al., Ultrasonic low-energy treatment: a novel approach to induce apoptosis in human leukemic cells. Exp Hematol, 2002. 30(11): p. 1293-301.
36. Chou, A.J. and R. Gorlick, Chemotherapy resistance in osteosarcoma: current challenges and future directions. *Expert Rev Anticancer Ther*, 2006. 6(7): p. 1075-85.
37. Ottaviani G., J.N. The Epidemiology of Osteosarcoma.Pediatric and Adolescent Osteosarcoma. . Norman Jaffe, Øyvind S. Bruland, Stefan Bielack. Springer, 2009.
38. Longhi, A., et al., Primary bone osteosarcoma in the pediatric age: state of the art. *Cancer Treat Rev*, 2006. 32(6): p. 423-36.
39. Marina, N., et al., Biology and therapeutic advances for pediatric osteosarcoma. *Oncologist*, 2004. 9(4): p. 422-41.
40. Dasari, S. and P.B. Tchounwou, Cisplatin in cancer therapy: molecular mechanisms of action. *Eur J Pharmacol*, 2014. 740: p. 364-78.
41. Ham, S.J., et al., Historical, current and future aspects of osteosarcoma treatment. *Eur J Surg Oncol,* 1998. 24(6): p. 584-600.

42. Durfee, R.A., M. Mohammed, and H.H. Luu, Review of Osteosarcoma and Current Management. *Rheumatol Ther*, 2016. 3(2): p. 221-243.
43. Heckman J.D., R.J.P., McCabe J., Frey J.J., Kilcoyne RF. Acceleration of tibial fracture‐healing by non‐invasive, low‐intensity pulsed ultrasound. *J Bone Joint Surg Am* 1994. 76: p. 26‐34.
44. Harrison, A., et al., Mode & mechanism of Low Intensity Pulsed Ultrasound (LIPUS) in fracture repair. *Ultrasonics*, 2016. 70: p. 45-52.
45. Rutten S, N.P., Guit GL, Bouman DE, Albers GH. J Trauma, Use of low-intensity pulsed ultrasound for posttraumatic nonunions of the tibia: A review of patients treated in the Netherlands. *J Trauma* 2007. 62: p. 902-908.
46. Matsuo, T., et al., Inhibitory effects of low-intensity pulsed ultrasound sonication on the proliferation of osteosarcoma cells. *Oncol Lett*, 2017. 14(3): p. 3071-3076.
47. Proffit W., Fields H. Contemporary Orthodontics; St Louis, Calif: Mosby-Year Book Inc, 1999; pp. 296–325.
48. Wolff J. Das Gesetz der transformation der knochen; Hirschwald: Berlin, Germany, 1892.
49. Moss M.L., Salentijn L. The primary role of functional matrices in facial growth. A.J.O. 1969, Volume 55, pp. 566-577.
50. Von Limbourg J. The role of genetic and local environmental factors in the control of postnatal craniofacial morphogenesis, Acta Morphol. Neerl. Scand. 1972; Volume 10, pp. 37-47.
51. Burstone C.J. The biophysics of bone remodeling during orthodontics — optimal force considerations. In The Biology of Tooth Movement, Norton L.A., Burstone C.J., Eds; CRC Press, Inc.: Boca Raton, Florida, 1989; pp. 321–334.
52. Schwarz A.M. Tissue changes incident to orthodontic tooth movement. Int J. Orthod. 1932; Volume 18, pp. 331–352.
53. Pilon J.J., Kuijpers-Jagtman A.M., Maltha J.C. Magnitude of orthodontic force and rate of bodily tooth movement, an experimental study in beagle dogs. Am. J. Orthod. Dentofacial Orthop. 1995; Volume 107, pp. 16–23.
54. Dellinger E.L. A histologic and cephalometric investigation of premolar intrusion in Macaca speciosa monkey. Am. J. Orthod. 1967; Volume 53, pp. 325–355.
55. Russell JS. Aesthetic orthodontic brackets. *J Orthod* 2005; 32(2):146-63.
56. Filho HL, Maia LH, Araújo MV, Eliast CN, Ruellas AC. Colour stability of aesthetic brackets: Ceramic and plastic. *Aust Orthod J* 2013; 29(1): 13-20.

57. Waring D, McMullin A, Malik OH. Invisible orthodontics part 3 Aesthetic orthodontic brackets. *Dent Update* 2013; 40(7): 555-556, 559-561, 563.
58. Miller RJ, Derakhshan M. Three-dimensional technology improves the range of orthodontic treatment with esthetic and removable aligners. *World J Orthod* 2004; 5(3): 242-9.
59. Dupaix RB. B.M., Finite strain behavior of polyetylglycol (PETG). Polymer (Guildf) 2005; 46: 4827-38.
60. Giancotti A, Garino F, Mampieri G. Use of clear aligners in open bite cases: An unexpected treatment option. J Orthod 2017; 44(2): 114-25.
61. Harnick DJ. Using clear aligner therapy to correct malocclusion with crowding and an open bite. Gen Dent 2012; 60(3): 218-23.
62. Dallel I, Bergeyron P, Chok A, Tobji S, Ben Amor A. Intramaxillary devices of molar distalization on fixed appliance and with aligners. Orthod Fr 2017; 88(4): 355-66.
63. Boyd RL, Oh H, Fallah M, Vlaskalic V. An update on present and future considerations of aligners. J Calif Dent Assoc 2006; 34(10): 793-805.
64. Lin F, Yao L, Bhikoo C, Guo J. Impact of fixed orthodontic appliance or clear-aligner on daily performance, in adult patients with moderate need for treatment. *Patient Prefer Adherence* 2016; 10: 1639-45.
65. Allereau B, Sabouni W. Perception of pain in orthodontic treatment with thermoformed aligners. Orthod Fr 2017; 88(4): 383-9.
66. Abbate GM, Caria MP, Montanari P, et al. Periodontal health in teenagers treated with removable aligners and fixed orthodontic appliances. *J Orofac Orthop* 2015; 76(3): 240-50.
67. Miller KB, et al. A comparison of treatment impacts between Invisalign aligner and fixed appliance therapy during the first week of treatment 2007; 131:302 e 1-9. [http://dx.doi.org/10.1016/j.ajodo.2006.05.031]
68. Garino F, Castroflorio T, Daher S, et al. Effectiveness of composite attachments in controlling upper-molar movement with aligners. J Clin Orthod 2016; 50(6): 341-7.
69. Lombardo L., Martines E., Mazzanti V., Arreghini A., Mollica F., Siciliani G. Stress relaxation properties of four orthodontic aligner materials: A 24-hour in vitro study. *The Angle Orthodontist*, 2017; Volume 87, pp. 11-18.
70. Tuncay OC, Bowman SJ, Nicozisis JL, Amy BD. Effectiveness of a compliance indicator for clear aligners. J Clin Orthod 2009; 43(4):263-8.
71. Technology A. Invisalign introduces Smart Track Available at: http://invisalign.com.au/ doctor/ doc/brochures/ SmartTrack_ brochure.pdf.

72. Gomez JP, Peña FM, Martínez V, Giraldo DC, Cardona CI. Initial force systems during bodily tooth movement with plastic aligners and composite attachments: A three-dimensional finite element analysis. Angle Orthod 2015; 85(3): 454-60.
73. Tepedino M, Paoloni V, Cozza P, Chimenti C. Movement of anterior teeth using clear aligners: A three-dimensional, retrospective evaluation. Prog Orthod 2018; 19(1): 9.
74. Ercoli F, Tepedino M, Parziale V, Luzi C. A comparative study of two different clear aligner systems. Prog Orthod 2014; 15(1): 31.
75. Cervinara F., Cianci C., De Cillis F., Pappalettere C., Siciliani G., Lombardo L. Experimental study of the pressures and points of application of the forces exerted between aligner and tooth. *Nanomaterials*, 2019.
76. Fuji Prescale Film. Product's support. Available online: https://www.fujifilm.com/products/prescale/ (accessed on 04.07.2019)
77. Liggins A. B. The practical application of Fuji Prescale pressure-sensitive film. In Optical measurement methods in biomechanics; Shelton J.C., Orr J.F., Eds.; Springer, Boston, MA; pp.173-189
78. Daubs B. M., McLaughlin R. M., Silverman E., Rizon J. Evaluation of compression generated by self compressing Orthofix bone pins and lag screws in simulated lateral humeral condylar fractures. *Vet. Comp. Orthop. Traumatol*. 2007, Volume 20, pp. 175-9.
79. Ralphs G., Lunsford T.R., Greenfield J. Measurement of Plantar Pressure Using Fuji Prescale Film - A Preliminary Study. *Journal of Prosthetics & Orthotics* 1990, Volume 2, pp. 130-138.
80. Elkholy F., Panchaphongsaphak T., Kilic F., Schmidt F., Lapatki B.G. Forces and moments delivered by PET-G aligners to an upper central incisor for labial and palatal translation. *J. Orofac. Orthop.* 2015, Volume 76, pp. 460-475.
81. Elkholy F., Schmidt F., Jaeger R., Lapatki B.G. Forces and moments delivered by novel, thinner PET-G aligners during labiopalatal bodily movement of a maxillary central incisor: An in vitro study. *Angle Orthod.* 2016, Volume 86, pp. 883-890.
82. Li X., Ren C., Wang Z., Zhao P., Wang H., Bai Y. Changes in force associated with the amount of aligner activation and lingual bodly movement of the maxillary central incisor. Korean J. Orthod. 2016, Volume 46, pp. 65-72.
83. Hahn W., Zapf A., Dathe H., Fialka-Fricke J., Fricke-Zech S., Gruber R., Kubein-Meesenburg D., Sadat-Khonsari R. Torquing an upper central incisor with aligners—acting forces and biomechanical principles. *European Journal of Orthodontics* 2010, Vol. 32, Issue 6, pp. 607–613.

84. Barbagallo L.J., Shen G., Jones A.S., Swain M.V., Petocz P., Darendeliler M.A. A Novel Pressure Film Approach for Determining the Force Imparted by Clear Removable Thermoplastic Appliances. Ann. Biomed. Eng. 2008, Volume 36, pp. 335–341.
85. Ciavarella D., Cianci C., Laurenziello M., Troiano G., De Cillis F., Tepedino M., Montaruli G., Grassia V., Lo Muzio L., Pappalettere C. Comparison of the Stress Strain Capacity between Different Clear Aligners. *The Open Dentistry Journal*, 2019, Vol.13, 41-47.
86. Kesling H. The philosophy of the tooth positioning appliance. Am J Orthod Oral Surg 1945; 31: 297-304.
87. Torres FC, Jóias RP, Cepera F, Paranhos LR, Sanders D. A clinical case treated with clear aligners. Int J Orthod Milwaukee 2011; 22(3): 11-5.
88. Fernandez Sanchez J, Pernia Ramirez I, Martin Alonso J. Osamu active retainer for correction of mild relapse. J Clin Orthod 1998; 32(1): 26-8.
89. Schott TC, Göz G. Color fading of the blue compliance indicator encapsulated in removable clear Invisalign Teen® aligners. Angle Orthod 2011; 81(2): 185-91.
90. Elkholy F, Mikhaiel B, Schmidt F, Lapatki BG. Mechanical load exerted by PET-G aligners during mesial and distal derotation of a mandibular canine : An in vitro study. J Orofac Orthop 2017; 78(5):361-70.
91. Kim TW, Echarri P. Clear aligner: An efficient, esthetic, and comfortable option for an adult patient. World J Orthod 2007; 8(1): 13-8.
92. Barbagallo LJ, Jones AS, Petocz P, Darendeliler MA. Physical properties of root cementum: Part 10. Comparison of the effects of invisible removable thermoplastic appliances with light and heavy orthodontic forces on premolar cementum. A micro-computed tomography study. *Am J Orthod Dentofacial Orthop* 2008; 133(2): 218-27.
93. Tepedino M, Masedu F, Chimenti C. Comparative evaluation of insertion torque and mechanical stability for self-tapping and selfdrilling orthodontic miniscrews: An in vitro study. Head Face Med 2017; 13(1): 10.
94. Tepedino M, Cattaneo PM, Masedu F, Chimenti C. Average interradicular sites for miniscrew insertion: Should dental crowding be considered? Dental Press J Orthod 2017; 22(5): 90-7.
95. Rossini G, Parrini S, Castroflorio T, Deregibus A, Debernardi CL. Efficacy of clear aligners in controlling orthodontic tooth movement. A systematic review. Angle Orthod 2015; 85(5): 881-9.

96. Ciavarella D, Mastrovincenzo M, D'Onofrio V, et al. Saliva analysis by surface-enhanced laser desorption/ionization time-of-flight mass spectrometry (SELDI-TOF-MS) in orthodontic treatment: First pilot study. Prog Orthod 2011; 12(2): 126-31.
97. Ryokawa H, Miyazaki Y, Fujishima A, Takashi M, Koutaro M. The mechanical properties of dental thermoplastic materials in a simulated intraoral environment. Orthod Waves 2006; 65: 64-72.